PROCESS SYNTHESIS FOR MANUFACTURING MICROCELLULAR THERMOPLASTIC PARTS: A CASE STUDY IN AXIOMATIC DESIGN

by

Vipin Kumar

B.Tech., Indian Institute of Technology, Kanpur, India, 1970
M.S. , University of Rhode Isalnd, 1972
M.B.A. , University of Rhode Island, 1974

SUBMITTED IN PARTIAL FULFILLMENT
OF THE REQUIREMENTS FOR
THE DEGREE OF

DOCTOR OF PHILOSOPHY

at the

MASSACHUSETTS INSTITUTE OF TECHNOLOGY

May 1988

Signature of Author.....
Department of Mechanical Engineering

Certified by .....
Nam P. Suh
Thesis Supervisor

Accepted by .....
Chairman, Departmental Committee on Graduate Students
Ain A. Sonin

PROCESS SYNTHESIS FOR MANUFACTURING MICROCELLULAR THERMOPLASTIC PARTS: A CASE STUDY IN AXIOMATIC DESIGN

Vipin Kumar

Submitted to the Department of Mechanical Engineering on 29 April 1988 in partial fulfillment of the requirements for the degree of Doctor of Philosophy in Mechanical Engineering at the Massachusetts Institute of Technology.

Abstract

A case study of the design of a novel manufacturing process is presented. The objective was to synthesize a process to produce plastic parts with a given geometry and microcellular structure. Conventional means to impart deformation were found to be detrimental to the structure. Deformation had to be integrated in the foaming process in a way that met the requirements for both the part geometry and the microstructure.

The problem was cast in the axiomatic framework, which guided the design of key experiments. The basic idea was to *decouple* the cell nucleation and growth processes from deformation. The structure of microcellular foam was characterized and bounds were established on the process variables that control the cell nucleation and cell growth phenomena. The nature and extent of coupling between the process functional requirements was experimentally studied and strategies were sought to minimize such coupling where it existed. The final process achieved the design objectives and allowed independent realization and control of the functional requirements.

This process is based on the recognition that the amount of gas dissolved in the polymer is a function of both temperature and pressure (as expected from thermodynamics). Previously, gas supersaturation was believed to provide the sole driving force for bubble nucleation. We found that the reduction of nitrogen solubility in polystyrene with temperature provides a driving force for cell nucleation that is comparable to that provided by gas supersaturation. *A combined evaluation of the process in terms of the process physics and the design axioms yielded an uncoupled process.*

Thesis supervisor: Nam P. Suh
Title: Professor of Mechanical Engineering

To the loving memory
of my parents

Acknowledgements

I would like to express my deepest gratitude to Professor Nam P. Suh for his guidance, support, and criticism of this work. I thank him for constantly challenging me to do a thesis that will "not simply sit on a shelf." He has led by example, and given me a philosophy on science, engineering, and education; for that, I thank him most of all.

I thank the members of my thesis committee for many helpful discussions. I always came back with a rare insight after talking to Professor Robert C. Armstrong. Dr. Osman Gebizlioglu was a most patient listener and helped me understand the nature of the polymers I worked with. Dr. Lewis Erwin provided guidance throughout this work, both as a committee member and as a sponsor. I thank him for his encouragement and advice all these years. Finally, although not formally a member of my thesis committee, Professor Kenneth C. Russell always made himself available to discuss the nucleation phenomenon.

Special thanks are due Dr. Nannaji Saka for his friendship and guidance all these years. I frequently turned to him with all sorts of problems when Professor Suh was at NSF, and he was always there. The many late-night discussions with Dr. Saka, both technical and general, will remain a fond memory of these years.

A number of undergraduates have worked with me from time to time. Thanks to Brian Lasher, John Krusac, Thomas Pitten, Richard Lightburn, and Robert Pyle for their help in performing some of the experiments. Thanks also to Professor Timothy Gutowski, Director of the Program, for making UROP help available, for it has contributed significantly to progress on this project.

I am indebted to numerous people in the Laboratory for Manufacturing and Productivity. Thanks to fellow P^3 students for their friendship and cooperation in the laboratory. Thanks to my office mates, Joe, Mike and Neil, and my neighbours, Sue, Al, and Karl, for putting up with me and for all the laughs. Thanks to Fred Cote, Bob Kane, Steve Holmberg, Joe Pressing, and Wesley Cobb for their invaluable help. Special thanks to Victor Lerman for machining the mold, but especially for his friendship. I would also like to thank Doris Elsemiller and Dorothy Cavignano for their help throughout the course of this project.

This work was sponsored by the MIT-Industry Polymer Processing Program, whose member companies are Boeing, Du Pont, Kraft, Lockheed, and Lord. Special thanks to Paul Grabowski of Kraft for all his help and technical insights.

A number of friends and family members, too numerous to mention, supported my decision to leave industry and return to MIT; thank-you all. Special thanks to brothers Bishan, Krishna, Vinay, Ramesh, and Krishnamurari, and my friends Virendra and Dhiraj, for their encouragement and moral support. Special thanks also to Dr. Vijay Stokes of the General Electric Company, my former teacher in India, for some timely advice.

Kumud, thank you, I could not have done this without your love and support. Tulika and Tushar, thanks for your love and understanding when Dad was not available.

Table of contents

List of figures

List of tables

1.0 INTRODUCTION

1.1 Background

Microcellular thermoplastics refer to plastic foams with cell diameters on the order of 10 μm. This idea was originally conceived by Suh (1979) as a means of reducing the amount of plastic used in mass-produced items. The original rationale was that if voids smaller than the pre-existing critical flaw size in polymers can be nucleated, then the material cost could be reduced without compromising the mechanical properties. Such a process has been developed using a thermodynamic instability phenomenon to achieve cell nucleation (Martini, Waldman, and Suh, 1982; Martini, Suh, and Waldman, 1984). This process also provides the possibility of foaming thin-walled plastic parts with thickness in the 1 to 2 mm range which cannot be foamed by conventional means without excessive loss of strength.

Martini et al. (1982, 1984) produced polystyrene foams with cell diameters in the range 2 to 25 μm (hence the word "microcellular") and void fractions of 0.05 to 0.30. The basic procedure involves saturating the polystyrene sheet with high pressure nitrogen at room temperature. When the pressure is removed, a specimen supersaturated with nitrogen is produced since the excess nitrogen is unable to escape the glassy thermoplastic matrix. As this specimen is heated above the glass transition temperature, a very large number of bubbles nucleate. Since the number of cells nucleated is very large and the amount of excess gas

is limited, very small cells nucleate. The bubbles cannot expand quickly because of the extremely high viscosity of the material at the glass-transition temperature. Thus it was possible to obtain cell diameters on the order of 10 μm, showing the possibility of foaming thin-walled parts.

Figures 1.1-1 to 3 show some examples of microcellular foam produced by this method. Figure 1.1-1 shows overall view across thickness of a polystyrene sample that was saturated at 1500 psi (10.3 MPa) and foamed at 110 °C . The cell density and average cell size for this sample are 50 million cells per cm^3 and 25 μm, respectively. Note the general uniformity in the microstructure in Fig. 1.1-1. Figure 1.1-2 shows a close-up of the cell structure obtained from a sample saturated at 2000 psi (13.8 MPa) and foamed at 110 °C. The cell density for this sample is approximately 400 millio per cm^3 and the average cell diameter is 10 μm. In both examples, the unfoamed sample was 0.068 in. (1.7 mm) thick.

The polystyrene samples were prepared in the form of two inch diameter disks in an injection molding machine. In one experiment, the polystyrene flash from injection molding was foamed to see if the process works on extremely thin samples. The results are shown in Fig. 1.1-3. The flash, of original thickness 0.016 in.(0.4 mm), successfully foamed to a final thickness of 0.024 in. (0.6 mm). This demonstrates that the main promise of microcellular foam, namely the foaming of thin walled rigid plastic parts can indeed be realized.

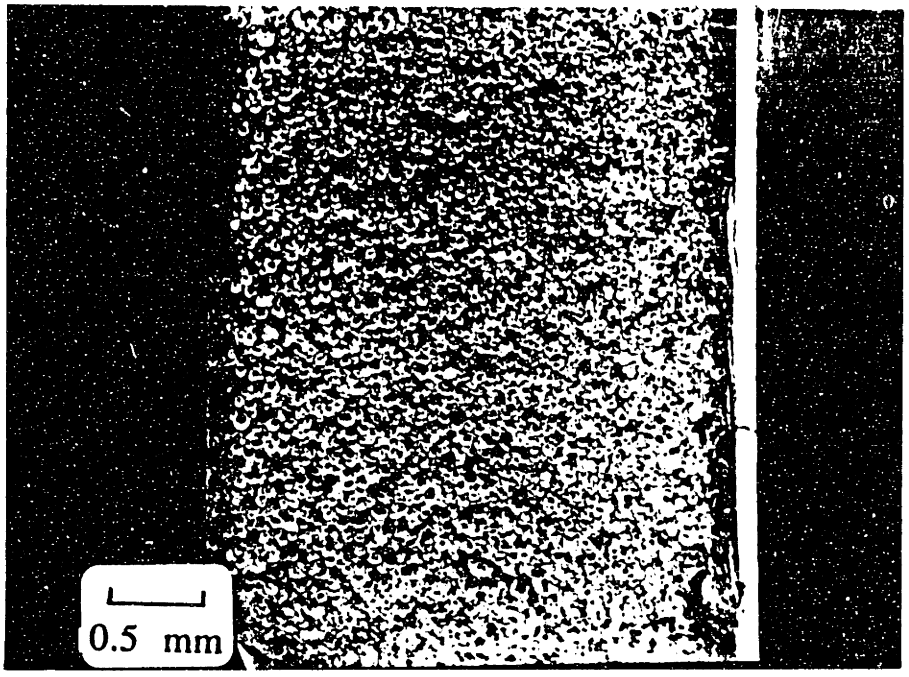

Figure 1.1-1. Scanning electron micrograph of a polystyrene disk foamed by the microcellular process, showing overall view across thickness.

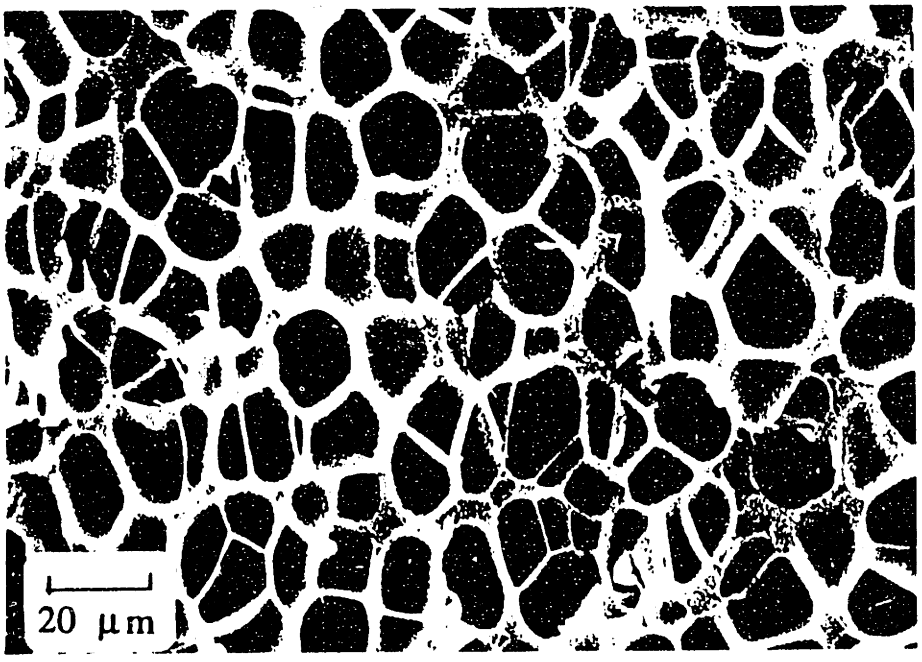

Figure 1.1-2. Scanning electron micrograph of microcellular foam showing structural details.

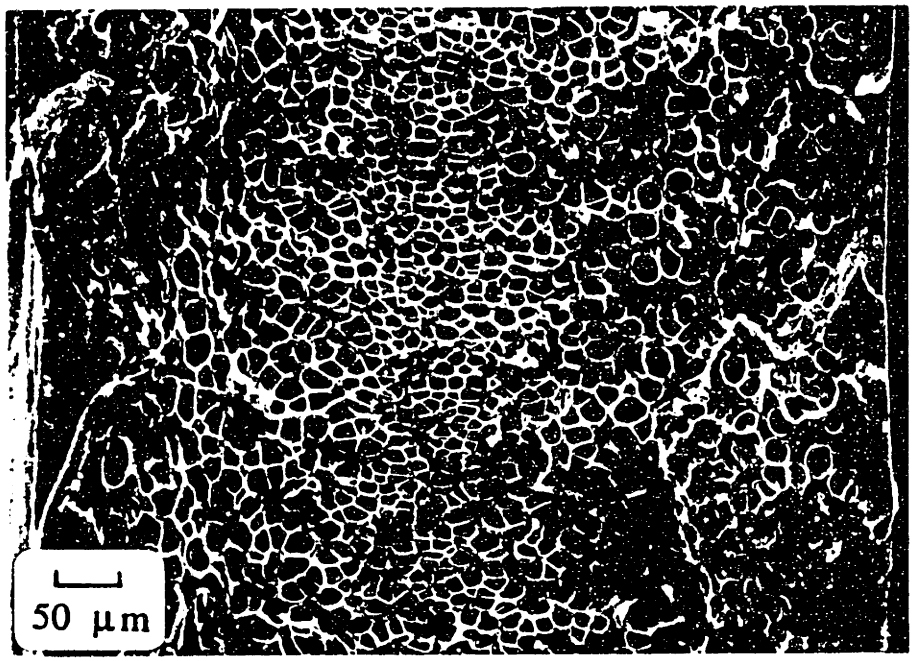

Fig.1.1-3 Scanning electron micrograph of a thin polystyrene sample ,of original thickness 0.016 in. (0.4 mm), showing full cross-sectional view. Thickness after foaming was 0.024 in. (0.6 mm).

1.2 Previous work

Waldman (1982) further characterized the conditions necessary to produce microcellular foam and studied its mechanical properties. He found that the tensile strength of this foam drops by no more than its reduction in density, which is a significant improvement over conventional structural foams. Fracture toughness of the microcellular foam was found to be four to seven times the unfoamed plastic (see Fig. 1.2-1). Waldman's work further showed the potential of microcellular foams as a new class of engineering materials.

The original microcellular foaming process developed by Martini(1981) was a batch process. Waldman (1982) attempted to produce microcellular foam continuously in a modified extrusion process. Polystyrene pellets were saturated with nitrogen at a high pressure and fed into the extruder. A high pressure chamber enclosed the die to suppress the nucleation of bubbles as a sheet of polystyrene saturated with nitrogen was extruded. At exit from the pressure chamber, the sheet was cooled to a temperature sufficiently below T_g to prevent bubble nucleation. In this manner, a supersaturated sheet of polystyrene was produced continuously. The sheet could now be foamed at the proper temperature. Unfortunately, there were problems in the implementation of this scheme, and a successful steady-state operation was not achieved. The idea to produce microcellular foam in a continuous process is important and should be explored further.

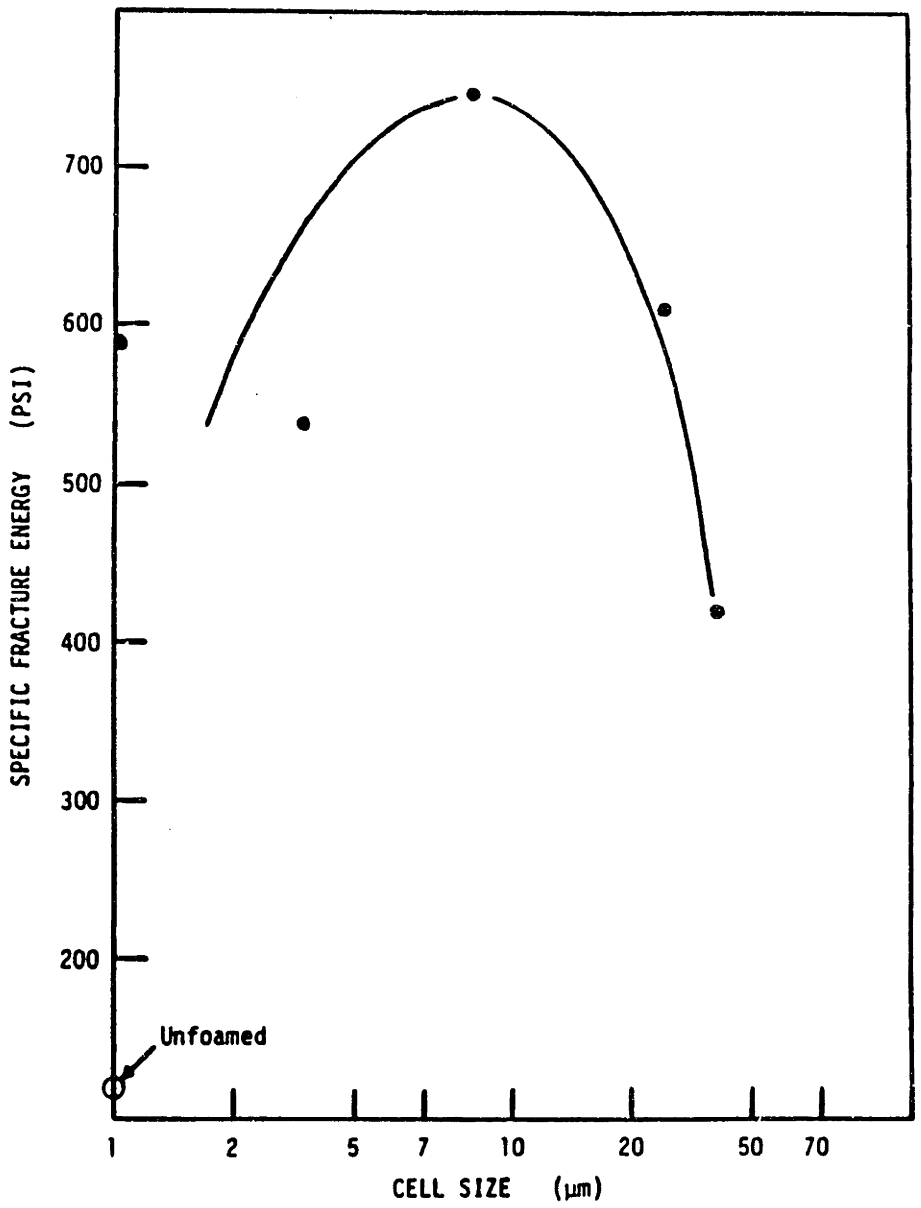

Figure 1.2-1. Impact strength of microcellular foam as a function of cell size (from Waldman, 1982)

Colton (1985, 1987) studied the phenomenon of nucleation in amorphous thermoplastics and proposed a model to predict the rate of nucleation in the presence of a nucleating agent. The nucleation process is complex and depends on the solubility, concentration, interfacial energy of any additives present, and the concentration of the foaming gas. Colton suggests that at very low concentrations, when the additives dissolve in the polymer to form a solution, homogeneous nucleation occurs within the free volume in the polymer. At concentrations above the solubility limit of the additive, particles of the additive are present in the matrix. As the activation energy for nucleation at the particle-matrix interface is smaller than that for homogeneous nucleation, the bubbles primarily nucleate heterogeneously when a large number of particles are present. This is the case, for example, when an additive well in excess of its solubility limit is present. In this case the number of bubbles nucleated is largely a function of the number of particles (nucleation sites) and the effect of saturation pressure on cell nucleation density is minimal. This suggests the possibility of using large amounts of nucleating agent and lower saturation pressures in the microcellular process. However, the effects of large amounts of nucleating agent (several percent by weight) on foam properties have not yet been evaluated.

The term 'microcellular foam' has been used to by other investigators in the literature in different contexts. Rand and Kraynik (1983) of Sandia National Laboratories have investigated the effect of cell size on drainage of aqueous foams. Jackson etal

(1986) have developed an image processing technique to determine cell size distributions in open-cell (porous) foams. The technique was used to characterize porous polystyrene foams with cells in the 10 to 100 μm range, and may be applicable to closed-cell foams described in this thesis. Since detailed information on cell size distributions was not needed in our work, a simple procedure to determine the average cell size was used (see Chapter 4).

The mechanical properties of foams have been related to the properties of the cell wall, and to the cell geometry (Gibson and Ashby, 1982). Deformation and energy absorption diagrams for foams have also been developed (Maiti, Gibson, and Ashby, 1984). These studies, however, rely on data on conventional polymeric foams with cells 0.1 mm or larger, and may not be directly applicable to microcellular foams.

1.3 Research objective

The potential of microcellular foam as a new class of engineering materials has been amply demonstrated in the above mentioned studies. However, a number of manufacturing issues have to be addressed before the promise of this idea can be realized. A key question is: how do we make a three dimensional part with microcellular structure? Integration of deformation in the process so as to obtain a desired geometry while preserving the microcellular structure has not been attempted in the past. This will be the object of this investigation.

Martini and others produced microcellular structure in a polystyrene sheet. If we try to impart deformation to a foamed sheet, the cell structure may be damaged. We attempted to thermoform a polystyrene sheet that was first foamed by the microcellular process. As expected, the cell structure was seriously damaged in regions of high deformation gradient or strain (see Fig. 1.3-1). If we form the part first, and then foam it, the dimensional accuracy of the part is lost. This is illustrated in Fig. 1.3-2, which shows a photograph of an injection molded polystyrene box that was microcellularly foamed. Heating the plastic part above the glass transition temperature during the foaming process causes residual thermal stresses to relax, resulting in gross distortions in the shape of the part.

In both processes discussed above, the functional requirements of producing a certain microstructure (i.e., a certain cell density and size) and a certain geometry are coupled. A coupled process is difficult to implement and control. The goal of this research is to decouple the process such that the microstructure and the geometry can be independently controlled by defining the conditions under which the polymer must be processed.

1.4. Organization of this thesis

Chapter 2 describes the fundamentals of the axiomatic design approach and the formulation of the design problem in this framework. In Chapter 3 we review the basics of the nucleation phenomenon in polymers. The experimental techniques and the

procedures used to characterize the microstructure are described in Chapter 4.

In Chapter 5 the question of controlling the microstructure of the foam is addressed. General features of the foam structure are first studied and a model is developed for predicting the skin thickness. Experimental results on controlling the cell density and the average cell size are then presented.

In Chapter 6 experimental results are presented on the extent of functional coupling that exists between the functional requirements established in Chapter 2. These experiments give new insights in the nucleation of microcellular foam, and help develop the processing strategy.

Chapter 7 describes the final phase of the development of a process concept in which the microstructure and geometry are decoupled. The concept is demonstrated on a conventional thermoforming machine.

Finally, conclusions and reccommendations for further work are presented in Chapter 8.

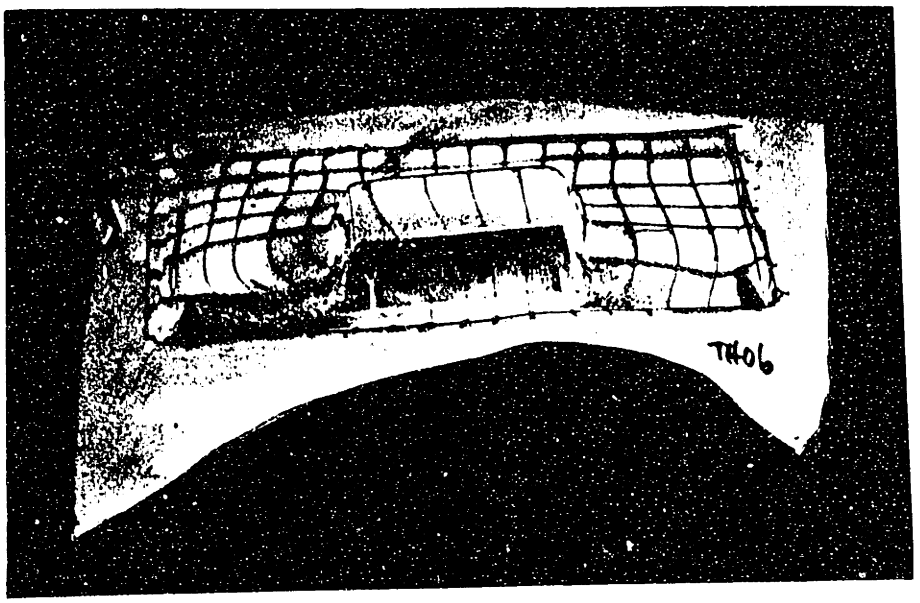

Figure 1.3-1. Photograph of a polystyrene sheet that was first foamed by the microcellular process and then thermoformed. Note the gross distortion in cell structure.

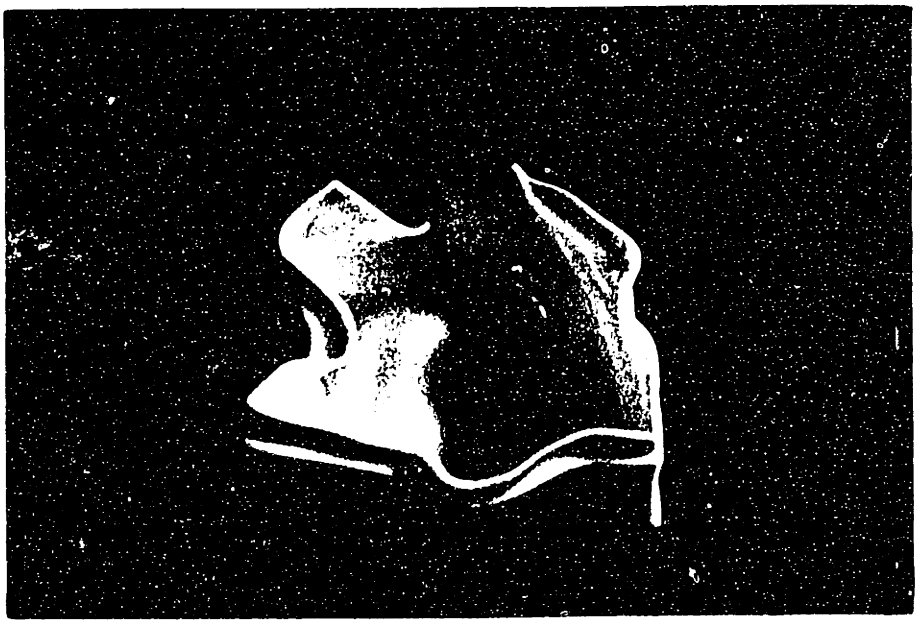

Figure 1.3-2. Photograph of an injection molded polystyrene box that was foamed by the microcellular process. Note the gross distortion in the shape of the box.

2.0 THE DESIGN AXIOMS AND THEIR APPLICATION

2.1 The axiomatic approach to design

A general theory and methodology that has been introduced to deal with the design of manufacturing process is called the axiomatic approach (Suh, Bell, and Gossard, 1978; Suh, 1984, 1988). This theory is applied to the present research so as to decouple the cell nucleation and deformation processes. The theory rests on two axioms:

- Axiom 1: The Independence Axiom.
  Maintain the independence of functional requirements.
- Axiom 2: The Information Axiom.
  Minimize the information content.

Functional requirements are defined as the minimum set of independent requirements for a product or process that completely characterizes the design objective. That is, each functional requirement can be stated without consideration of any other functional requirement. In Axiom 2, the information content is defined as a measure of complexity. It can be considered to be the minimum amount of information required to describe the system or process completely. The application of design axioms to a number of examples is discussed by Suh (1984). A detailed discussion of functional coupling and its measurement is beyond the scope of this

thesis (refer to Rinderle and Suh, 1982; also Suh, 1988). However, some of the key ideas are described below.

Design is considered as a mapping between the functional space characterized by the functional requirements (FR's), and the physical space characterized by process variables (PV's). (Note: PV's are sometimes replaced by DP's which are called design parameters.) Once the FR's are defined and the PV's identified, the relationship between the two can be expressed in the following form:

$$\{FR\} = \text{Function}\,(PV_1, PV_2, \ldots) \qquad (2.1\text{-}1)$$

For simplicity, the functional requirements are assumed to be a linear function of the process variables. Thus,

$$FR_1 = a_{11}PV_1 + a_{12}PV_2 + a_{13}PV_3 + \ldots$$
$$FR_2 = a_{21}PV_1 + a_{22}PV_2 + a_{23}PV_3 + \ldots \qquad (2.1\text{-}2)$$

Equations 2.1-2 can be written in a matrix form:

$$\{FR\} = [A]\ \{PV\} \qquad (2.1\text{-}3)$$

where {FV} and {PV} are vectors representing the functional requirements and process variables, respectively, and [A] is the design matrix. Equation 2.1-3 is called the Design Equation.

Equation 2.1-3 is an algebraic representation of the design problem. The coefficient a_{ij} represents the degree of coupling between FR_i and PV_j. One can also think of a_{ij} as representing the magnitude of effect of PV_j on FR_i. The main advantage of expressing

the problem in this form is that it allows quick evaluation of the degree to which a proposed process satisfies the independence requirement of the first axiom.

In an optimal design, the design matrix must be a square matrix. Since otherwise the design results either in a coupled or in a redundant design (Suh, 1988). In a truly independent process, the design matrix would be diagonal. In a quasi-coupled design, a triangular matrix is obtained. When the design matrix is neither triangular nor diagonal, the design is said to be a coupled design. The objective is to determine the extent of coupling that exists in the design, and then try to minimize it by eliminating the parameters that cause interdependence.

2.2 Formulation of the design problem

Our basic process design objective was: "starting with a polystyrene sheet saturated with nitrogen, produce a part with a given geometry and microcellular structure". In the final part, in order to achieve a certain void fraction, and satisfy the part geometry requirement, we want to ensure that cell size does not exceed a certain target value. To achieve both goals, we will need to independently control the number of cells nucleated and the cell size. The functional requirements for this process can therefore be stated as:

FR_1 = cell density (number of cells nucleated per unit volume)

FR_2 = cell size

FR_3 = part geometry

The main conditions that the functional requirements have to satisfy are that they be independent of each other, and be more or less equally important with respect to the design objective. Note that the third FR has been stated as 'part geometry' and may appear to be vague. The specific geometry, however, is not of concern at the level at which we are synthesizing this process. The main question is how to decouple the geometry from the microstructure. Therefore, a general geometry requirement would suffice.

In general, we would like to obtain a high cell density and small cell size to create the microcellular structure. The pressure at which polystyrene is saturated with nitrogen directly affects the number of cells nucleated -- the higher the saturation pressure, the higher the cell density. Cell size, on the other hand, can be controlled by the time and temperature to which the plastic is exposed during the foaming cycle. Thus the key process variables are:

PV_1 = saturation pressure

PV_2 = time-temperature exposure

PV_3 = deformation

Here the word deformation is used in a general sense. It is assumed that an appropriate method of deformation to achieve the desired part geometry can be used.

The design equation may now be written as

$$\begin{bmatrix} FR_1 \\ FR_2 \\ FR_3 \end{bmatrix} = \begin{bmatrix} a_{11} & a_{12} & a_{13} \\ a_{21} & a_{22} & a_{23} \\ a_{31} & a_{32} & a_{33} \end{bmatrix} \begin{bmatrix} PV_1 \\ PV_2 \\ PV_3 \end{bmatrix} \qquad (2.2\text{-}1)$$

To get some insight into the design equation, let us establish the design matrix for a particular process concept. We will set $a_{ij} = 0$ if PV_j has no significant effect on FR_i.

Consider the case where we first produce microcellular structure in the sheet, and then impose deformation on it by using a thermoformer. As mentioned previously, this procedure results in grossly distorted cells in regions of high deformation gradient. The realization of part geometry (FR_3) is thus coupled with cell density (FR_1) and cell size (FR_2) which are adversely affected by deformation. In this case, independence of the functional requirements is not maintained, violating the first axiom. The design matrix for this process is given below.

Process: Nucleate cells, grow cells, deform.

$$\begin{bmatrix} \text{cell density} & FR_1 \\ \text{cell size} & FR_2 \\ \text{geometry} & FR_3 \end{bmatrix} = \begin{bmatrix} a_{11} & a_{12} & x \\ a_{21} & a_{22} & x \\ a_{31} & a_{32} & a_{33} \end{bmatrix} \begin{bmatrix} \text{saturation pressure} & PV_1 \\ \text{time-temp. exposure} & PV_2 \\ \text{deformation} & PV_3 \end{bmatrix}$$

(2.2-2)

In the design matrix, x denotes the coupling discussed above.

Let us examine the other off-diagonal coefficients in the design matrix.

Coefficient a_{12} ($= \partial FR_1/\partial PV_2$) represents the effect of time-temperature exposure on cell nucleation. Bubble nucleation in plastics is a rate process; accordingly, the usual Arrhenius type dependence of cell density on temperature is expected. If nucleation occurs at a higher temperature, we would expect a higher cell density (see Section 6.2) Similarly, foaming for an extended length of time to achieve a certain cell growth may induce some secondary nucleation. In both cases, time-temperature exposure can affect cell nucleation, and coefficient a_{12} can not be set equal to zero.

Coefficient a_{21} ($= \partial FR_2/\partial PV_1$) represents the effect of saturation pressure on cell size. High saturation pressures are needed to get high cell nucleation rates (see Section 5.2). For a given concentration of gas, the bubble size will be smaller when the number of cells nucleated is large. On the other hand, high saturation pressures will also tend to create large bubbles since the dissolved gas volume increases with increase in saturation pressure.

Thus there is a possibility of coupling between the functional requirements of high cell density and small cell size. We will have to address this issue in our process design. At this point we shall leave a_{21} as undetermined.

Since saturation pressure (PV_1) has no effect on part geometry (FR_3), coefficient $a_{31} = \partial FR_3/\partial PV_1 = 0$.

Again, since time-temperature exposure has no effect on part geometry, coefficient $a_{32} = \partial FR_3/\partial PV_2 = 0$.

Equation (2.2-2) can now be written as:

$$\begin{bmatrix} FR_1 \\ FR_2 \\ FR_3 \end{bmatrix} = \begin{bmatrix} a_{11} & a_{12} & x \\ a_{21} & a_{22} & x \\ 0 & 0 & a_{33} \end{bmatrix} \begin{bmatrix} PV_1 \\ PV_2 \\ PV_3 \end{bmatrix} \qquad (2.2\text{-}3)$$

Equation (2.2-3) suggests that if $a_{21} = 0$, then we may be able to decouple the functional requirements by sequential application of the process variables. That is, if we vary PV_3 first, then PV_2 and finally PV_1, we can control the functional requirements independently. This sequence of process variables is, however, physically not possible, as it requires PV_2 (cell growth) to precede PV_1 (cell nucleation). We have to determine a new set of process conditions that will eliminate the coupling shown in equation (2.2-3).

Ideally, in order to fully decouple deformation from nucleation and growth of cells, we would like to accomplish deformation first, followed by nucleation and growth of bubbles. To achieve this, we will need to suppress nucleation during the deformation step. This could be done by maintaining sufficient external pressures during deformation. The external pressure would eliminate the thermodynamic instability that causes cell nucleation. In this scheme, cell nucleation occurs following deformation.when the external pressure is released. We need to investigate how deformation affects cell nucleation. Further, since deformation may induce molecular orientation, we will need to establish the effect such molecular orientation may have on cell nucleation, a primary functional requirement.

Research is conducted in three phases. In phase I the microcellular structure is characterized and bounds established on the process variables that control the microstructure. In phase II functional coupling is experimentally studied and ways to minimize such coupling explored. In particular, the effect of saturation pressure on cell size is studied in order to determine the nature of coupling between cell density and cell size. Further, in order to evaluate the scheme proposed above to decouple deformation and cell nucleation, experimental investigation of the effect of deformation on cell nucleation and growth is undertaken. The design matrix for the process is evaluated, and the process design is modified until a diagonal design matrix has been obtained. Finally in phase III, the process synthesized is demonstrated.

3.0 BUBBLE NUCLEATION IN POLYMERS

3.1 Introduction

In this chapter the classical nucleation theory will be applied to understand the nucleation phenomenon and to establish the critical parameters that control the cell nucleation in the microcellular process. This theory was primarily developed for condensation from vapor phase and has been subsequently extended to many different nucleation phenomena (Zeldovich, 1943; Frenkel, 1955; Wiedersich and Katz, 1979). Blander (1979) has reviewed nucleation in liquids, while an extensive review of the transient and steady state effects on nucleation rate in solids has been provided by Russell (1980). Youn and Suh (1985) have applied the classical nucleation theory to predict the rate of nucleation in production of microcellular polymer composites. Recently Colton and Suh (1987) have developed a model to predict the rate of nucleation in microcellular foam made from amorphous thermoplastics. Nucleation in crosslinked elastomers has been studied by Gent and Tompkins (1969).

The spontaneous nucleation of a large number of cells is a key requirement in producing a uniform distribution of micro-bubbles. This can be achieved by creating a thermodynamically unstable state prior to nucleation. In the microcellular process the thermodynamic instability is introduced by supersaturating the amorphous plastic below the glass transition temperature. Due to lack of thermal mobility in the polymer matrix, the only mechanism for excess gas

to leave is by slow molecular diffusion. When the supersaturated plastic is heated to its glass transition temperature, there is spontaneous nucleation of a large number of bubbles.

The driving force for nucleation is provided by the decrease in free energy that results from the phase transformation. The system being considered consists of a given amount of polymer that contains a certain concentration of gas molecules distributed in the matrix. A calculation for free energy of formation as a function of size of the bubble is shown in Fig. 3.1-1 for different saturation pressures. A critical free energy ΔG^* is needed to form a stable bubble of radius r^*. As the bubble grows further, the system free energy decreases since the gas present as a second phase has a lower free energy than the individually dispersed molecules. Before the critical bubble size is reached, however, the system free energy increases since energy is required to create the new interfaces of bubble embryos. Note from Fig. 3.1-1, also, that at a higher saturation pressure, smaller bubbles become stable, and correspondingly smaller activation energy is needed to create a stable embryo.

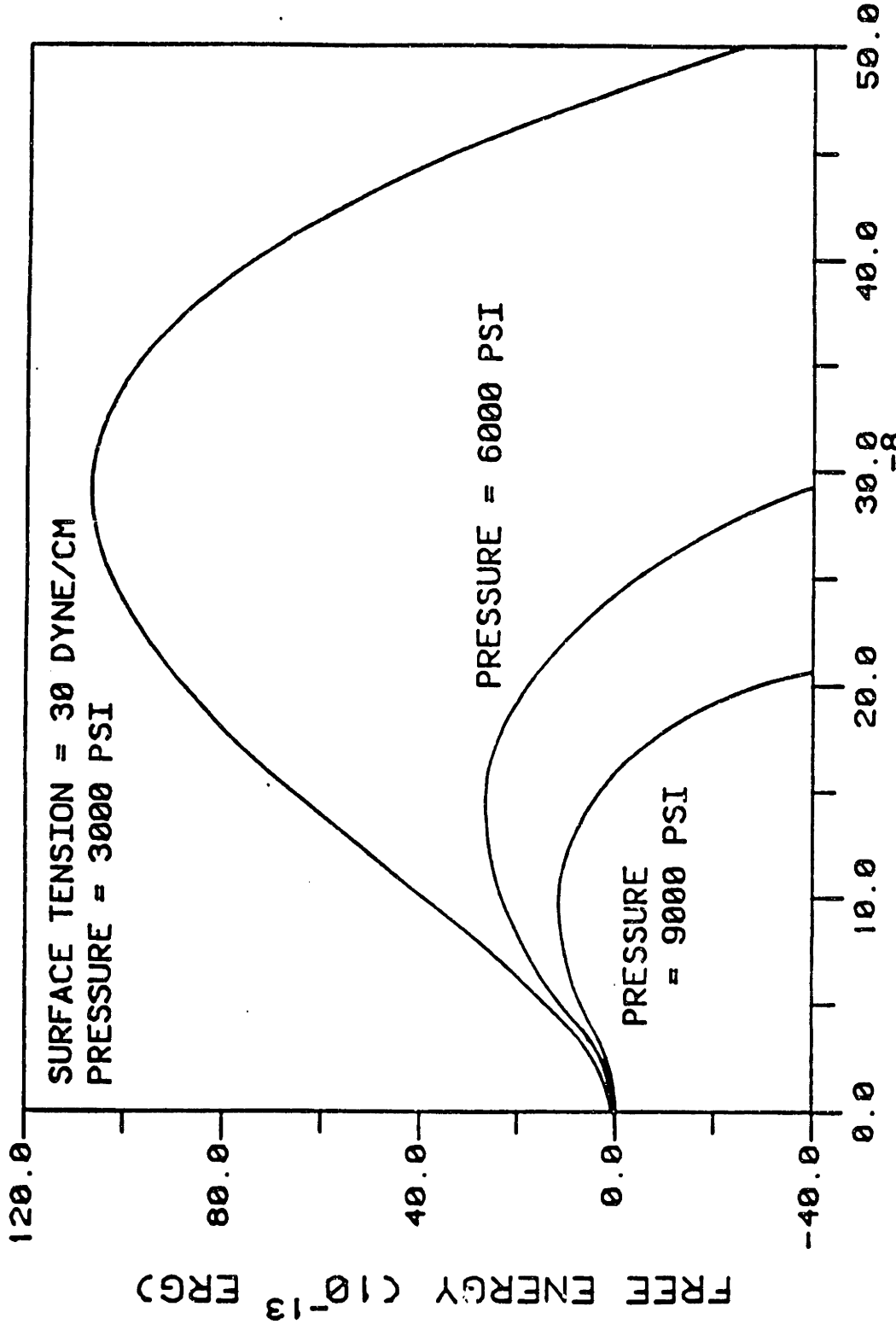

Figure 3.1-1. Free energy of formation as a function of bubble radius for homogeneous nucleation at different saturation pressures. (From Youn and Suh, 1985)

3.2 Basic Principles[1]

The various developments of nucleation theory appear at first to differ widely. With few exceptions, however, all may be developed from the following three basic principles:

1. The probability of nucleation is proportional to exp (-W*/ kT) where W* is the minimum work required to make the system unstable with respect to the transformation.

2. Fluctuations that lead to a stable nucleus form and decay by the same path.

3. Microscopic fluctuations decay, on the average, by macroscopic laws.

The exponential relationship between the fluctuation probability and W* in the first principle was derived by Einstein (1910). The second principle, also called the time reversal principle, follows from the symmetry with respect to time in the classical and quantum mechanical equations of motion. The third principle, due to Onsagar (1931), allows the application of macroscopic laws to microscopic entities such as a bubble embryo containing a few hundred molecules of a gas.

The steady state J_s and transient J(t) rates of nucleation (nuclei / cm^3-sec) can be written as

$$J_s = Z \beta^* N \exp\left[\frac{-\Delta G^*}{kT}\right] \qquad (3.2\text{-}1)$$

and

[1]This subsection has been strongly influenced by Russell (1980)

$$J(t) = J_s \exp\left[\frac{-t}{\tau}\right] \qquad (3.2\text{-}2)$$

where:

- Z = Zeldovich non-equilibrium factor ($\cong 10^{-2}$),
- β^* = Rate at which atoms or molecules are added to the critical nucleus,
- N = Number of atomic nucleation sites (of a particular type) per unit volume,
- ΔG^* = Gibbs free energy of forming a critical nucleus,
- kT = Boltzman's constant times absolute temperature,
- t = Isothermal reaction time, and
- τ = Induction period for establishing steady state nucleation conditions.

Although the form of the equations for J_s and $J(t)$ do not change, the quantities Z, β^*, N, ΔG^*, and τ are all specific to the system and to the type of the nucleation process considered. They must be developed on an individual basis according to the principles stated above.

3.3. Homogeneous Nucleation

Homogeneous nucleation refers to formation of a second phase (in our case, a gas bubble) in the primary phase (polymer matrix) from the dissolved second phase 'particles' in solution. This would require a sufficient number of gas molecules to come together to form a stable nucleus. Homogeneous nucleation in solids is rather rare since the activation energy barrier must be overcome without the aid of heterogeneities. It is, however, a convenient starting point for theoretical analysis.

The rate of homogeneous nucleation N_{HOM} is given by (Colton and Suh, 1987)

$$N_{HOM} = f_0 C_0 \exp\left[\frac{-\Delta G^*}{kT}\right] \qquad (3.3\text{-}1)$$

where f_0 is a frequency factor ($\cong 10^{-5}$ / sec) for the rate at which molecules join a critical nucleus; C_0 is the concentration of gas molecules. The activation energy for homogeneous nucleation ΔG^* is

$$\Delta G^* = \frac{16 \pi \gamma^3}{3 (\Delta p)^2} \qquad (3.3\text{-}2)$$

where γ = surface energy of the polymer; and $\Delta p = P_s - P_0$, the supersaturation pressure. Here P_s is the gas saturation pressure and P_0 the environmental pressure at which nucleation is to occur. Usually P_0 is the atmospheric pressure and ΔP can be taken to be equal to P_s.

The size of the critical nucleus is given by

$$r^* = \frac{2\gamma}{\Delta p} \qquad (3.3\text{-}3)$$

where r^* is the radius of the critical nucleus.

We can see from Eqs. (3.3-2) and (3.3-3) that as the supersaturation pressure is increased, both the critical radius and the critical free energy decrease. In Fig. 3.3-1, we have plotted ($\Delta G^*/kT$) as a function of Δp. The temperature 115°C was chosen

since a large number of foaming experiments were conducted at this temperature. The surface tension of polystyrene at 115°C is estimated to be 30 dynes / cm using a surface energy temperature coefficient $\partial\gamma / \partial T$ = -0.06 dynes/cm·°C (see Cherry, 1981, p.9). Figure 3.3-2 shows the size of the critical radius as a function of the supersaturation pressure. For Δp = 100 atm, the critical radius is approximately 50 Angstroms, and contains approximately five hundred gas molecules. Note from Figure 3.3-1 that the critical free energy drops rapidly as the saturation pressure is increased from, say 50 atm to 200 atm. For further increase in the saturation pressure, the drop in ΔG^* is smaller. Thus the saturation pressure should provide a means to control the activation energy, and hence the number of cells nucleated, especially in the 50 - 200 atm range for saturation pressure.

The homogeneous nucleation rate was computed as a function of the supersaturation pressure and is plotted in Figure 3.3-3. C_0 in Eq. (3.3-1) was estimated to be 1.8 x 10^{20} / cm^3 at a saturation pressure of 2000 psi (13.8 MN/m^2). We see from Fig. 3.3-3 that in order for homogeneous nucleation to proceed at the rate of one bubble per cm^3 per second, a saturation pressure of 500 atm (7500 psi) is needed.

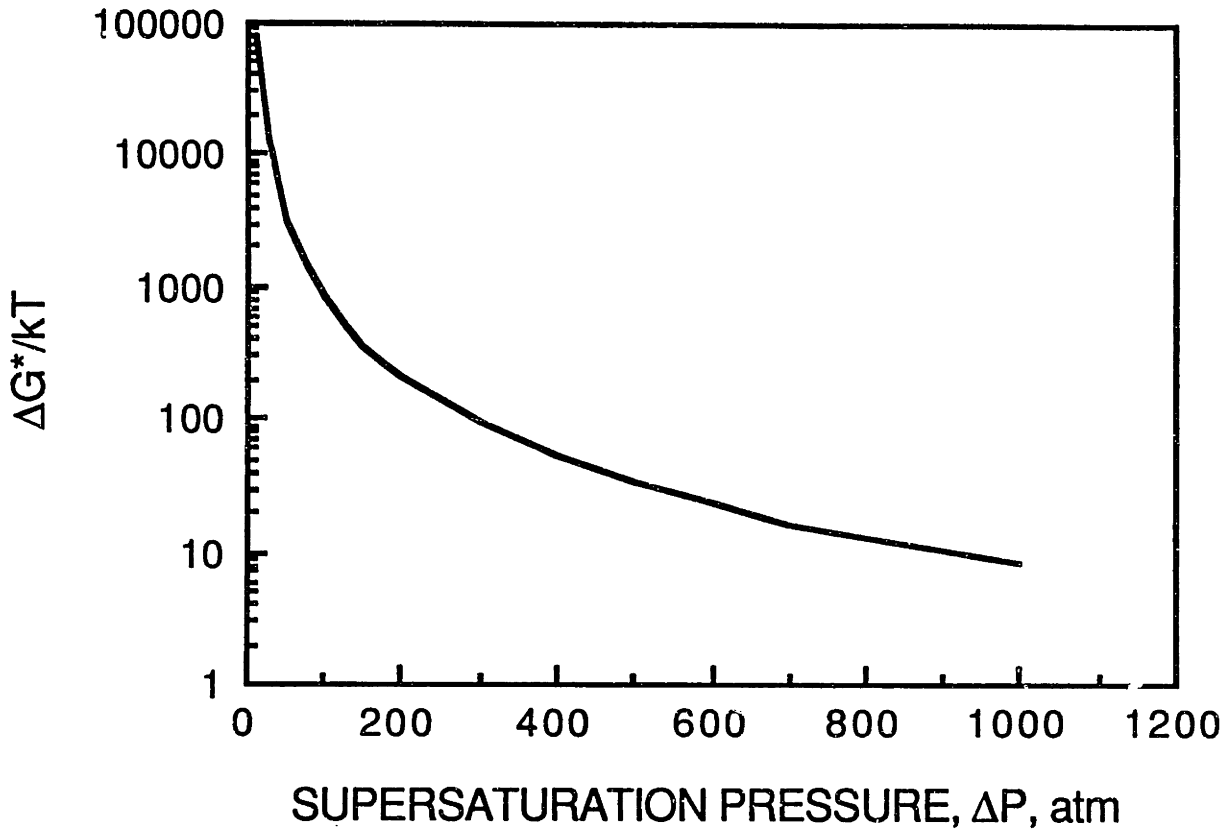

Figure 3.3-1. Plot of critical free energy as a function of supersaturation pressure for homogeneous nucleation. (surface tension 30 dynes/cm ; temperature 115 °C)

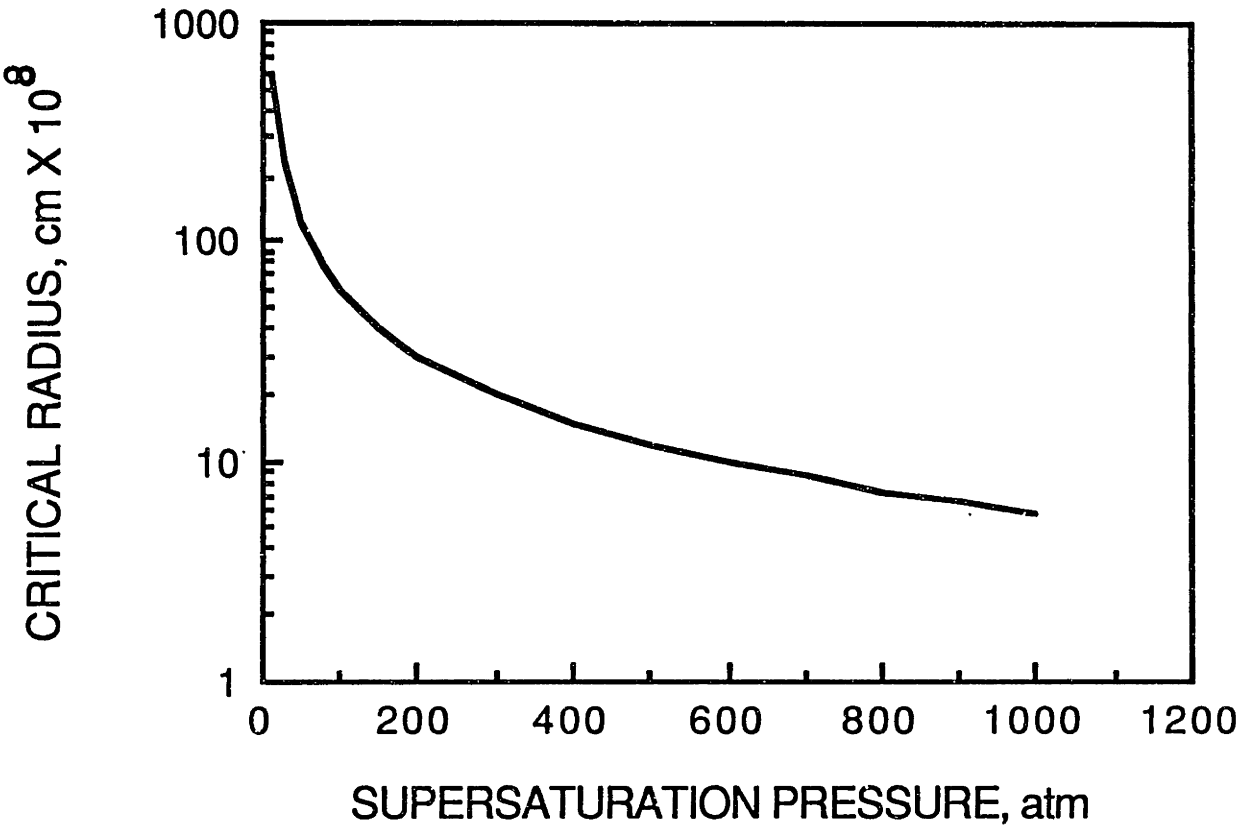

Figure 3.3-2. Plot of critical radius as a function of supersaturation pressure. (surface tension 30 dynes/cm)

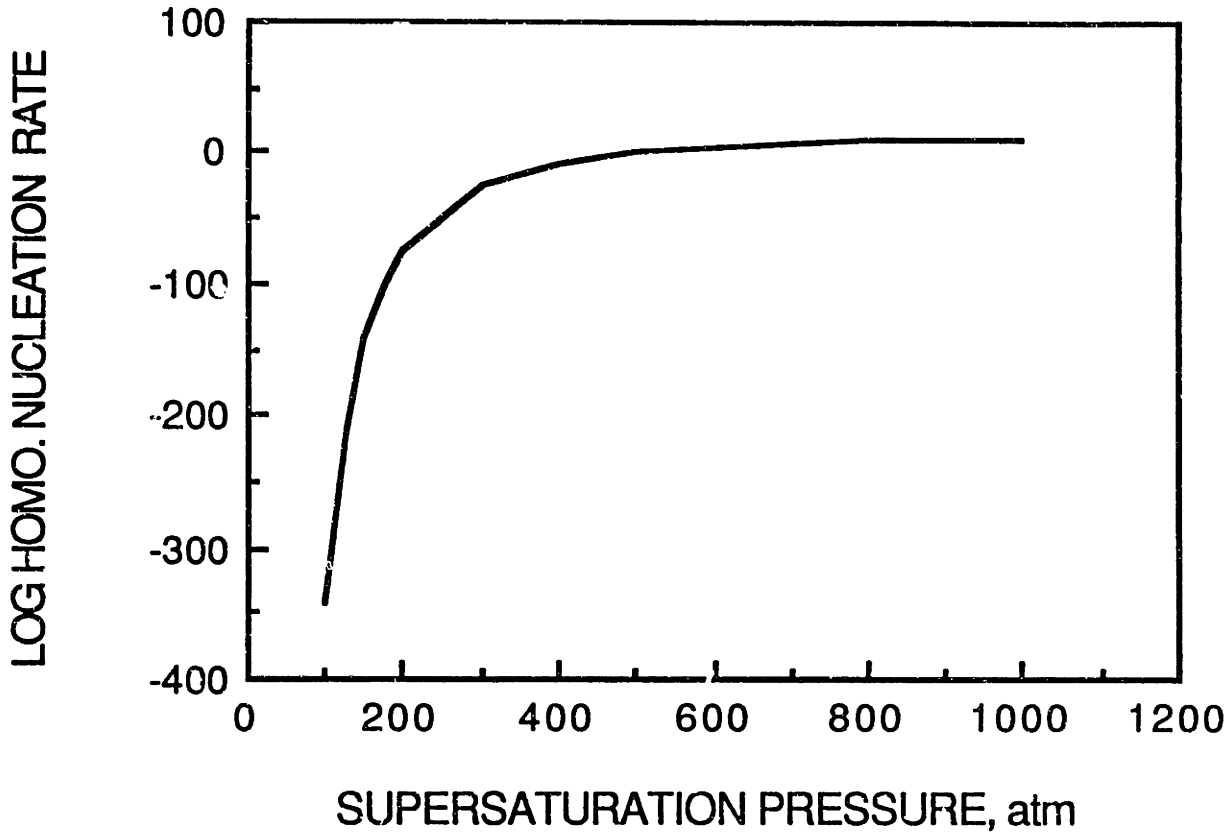

Figure 3.3-3. Plot of log homogeneous nucleation rate as a function of supersaturation pressure.
(surface tension 30 dynes/cm ; temperature 115 °C)

3.4. Heterogeneous Nucleation

Under most conditions bubbles are nucleated heterogeneously at the interface between two different phases. The conditions for heterogeneous nucleation depend on the properties of the surfaces (such as presence of cracks and cavities) and interfacial tensions.

Heterogeneous nucleation in liquids has been reviewed by Blander (1979). Several possibilities are considered: nucleation at plane rigid surface; at liquid-liquid surface; in a cavity, etc. In all cases interface acts as a 'catalyst' for nucleation by reducing the activation energy that must be surmounted to obtain a stable nucleus. In solids, Russell (1980) has provided an extensive review of heterogeneities that may affect nucleation. In addition to nucleation at interfaces and cavities, these include nucleation at dislocations and stacking faults in a solid. Wiedersich (1979) has analyzed the nucleation of voids in crystalline solids as a result of radiation. It appears that an effort to characterize heterogeneities that may affect nucleation in polymeric materials near the glass transition temperature has not been undertaken yet.

We will attempt to establish the extent to which heterogeneities affect nucleation in polymers near the glass transition temperature. We will first see, qualitatively, the effect of reducing the activation energy for homogeneous nucleation on the rate of nucleation. Consider Eq. 3.3-2 for the activation energy for homogeneous nucleation. Let K by a "heterogeneity factor", so that the effective activation energy for heterogenous nucleation is

$$\Delta G^*_{het} = K \Delta G^* \qquad (3.4\text{-}1)$$

where ΔG^* is the activation energy for homogeneous nucleation.

Let us examine the consequence of reducing the activation energy ΔG^* by allowing K to take different values. In Fig. 3.4-1 we have plotted log of the nucleation rate for the conditions of Fig. 3.3-3, for different values of K. K = 1.0 corresponds to the homogeneous nucleation rate of Fig. 3.3-3. For other values of K the same pre-exponential factors were used so as to clearly see the effect of varying the heterogeneity factor.

We see that as the degree of heterogeneity increases (i.e. K gets smaller), the sensitivity of the activation energy, and hence of the rate of bubble nucleation, to the supersaturation pressure decreases. For K = 0.01, we see that the rate of nucleation is essentially independent of the supersaturation pressure. In Fig. 3.4-2, we have re-plotted the calculations excluding K = 1, so that the variation of rate of nucleation with supersaturation pressure can be seen more clearly for smaller values of K. In addition, we have added a plot for K = 0.001 which shows that if the heterogeneities present reduce ΔG^* by three orders of magnitude, then the rate of nucleation is practically independent of the saturation pressure.

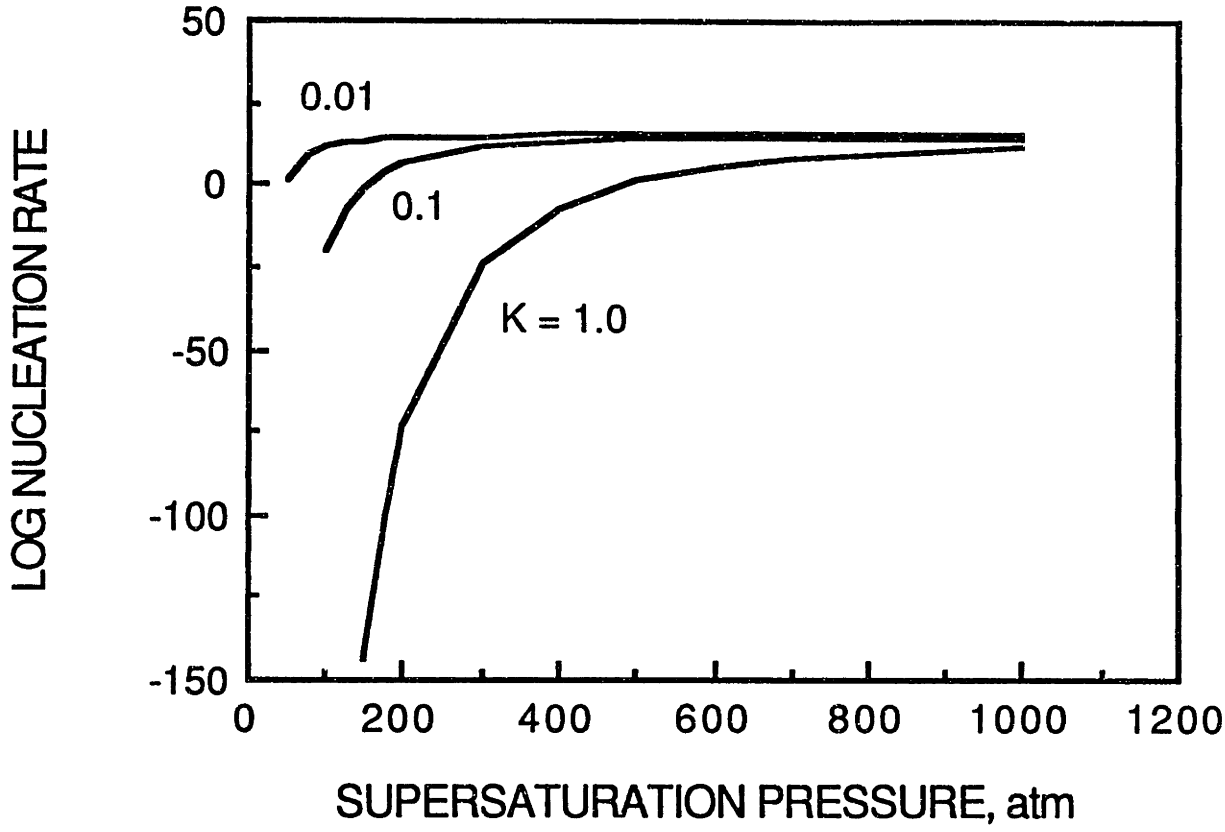

Figure 3.4-1. Plot of log nucleation rate as a function of supersaturation pressure for different values of the heterogeneity factor K.

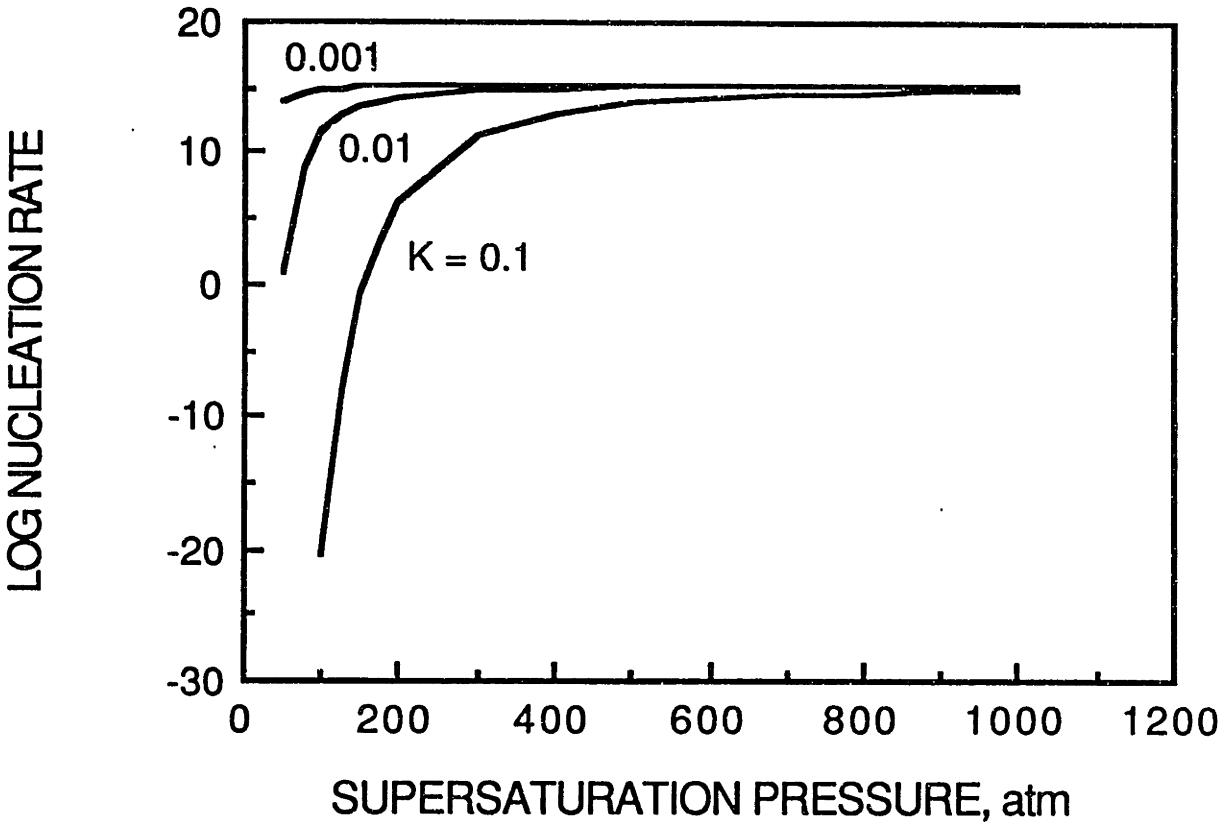

Figure 3.4-2. Plot of log nucleation rate as a function of supersaturation pressure for different values of the heterogeneity factor K. (A magnified view of Fig. 3.4-1)

4.0 EXPERIMENTAL PROCEDURES

4.1 Materials and equipment

All experiments were conducted on DOW XP6065 polystyrene with weight average molecular weight of 200,000. Circular disks 2 in. (50.8 mm) in diameter and 1/16 in. (1.55 mm) thick were injection molded from the resin. These disks were foamed using the microcellular process and the microstructure was studied using a Scanning Electron Microscope.

The basic foaming procedure calls for saturation of the disk with nitrogen at a high pressure (called the saturation pressure). A pressure vessel hooked to a compressed nitrogen cylinder was used to saturate the polystyrene disks as shown in Fig. 4.1-1. The nitrogen was diffused at room temperature and took three days to reach 98% of the limiting saturation. When the saturated disk was removed from the pressure vessel, it was "supersaturated" with nitrogen, as it contained more nitrogen (by a factor equal to the ratio of saturation pressure to atmospheric pressure) that can stay dissolved in polystyrene at atmospheric pressure.

Cell nucleation and growth occurred when the supersaturated disk was heated above the glass transition temperature. This was accomplished in a heated glycerin bath,shown in Fig. 4.1-2, usually maintained at 115°C-- about 15°C above the glass transition temperature. A Haake circulator/controller Model E3 was used to heat and circulate the glycerin. The bath temperature was

controlled to ± 0.2°C. After foaming for a certain time (depending upon the desired cell growth or void fraction) the disk was quenched in water. The foamed disk was then dipped in liquid nitrogen, removed after approximately one minute of cooling, and fractured to obtain a sample about 10 mm x 10 mm. Cooling with liquid nitrogen ensured a clean fracture with cell structure intact. The sample was then gold coated in order to make the surface conductive. Finally the microstructure exposed by fracture was studied under a Scanning Electron Microscope (SEM) and average cell density and cell size were determined from the micrographs.

For certain experiments gas saturation at an elevated temperature was required. A high pressure mold shown in Fig. 4.1-3 was built for this purpose. This mold was also used to study cell nucleation under hydrostatic external pressure.

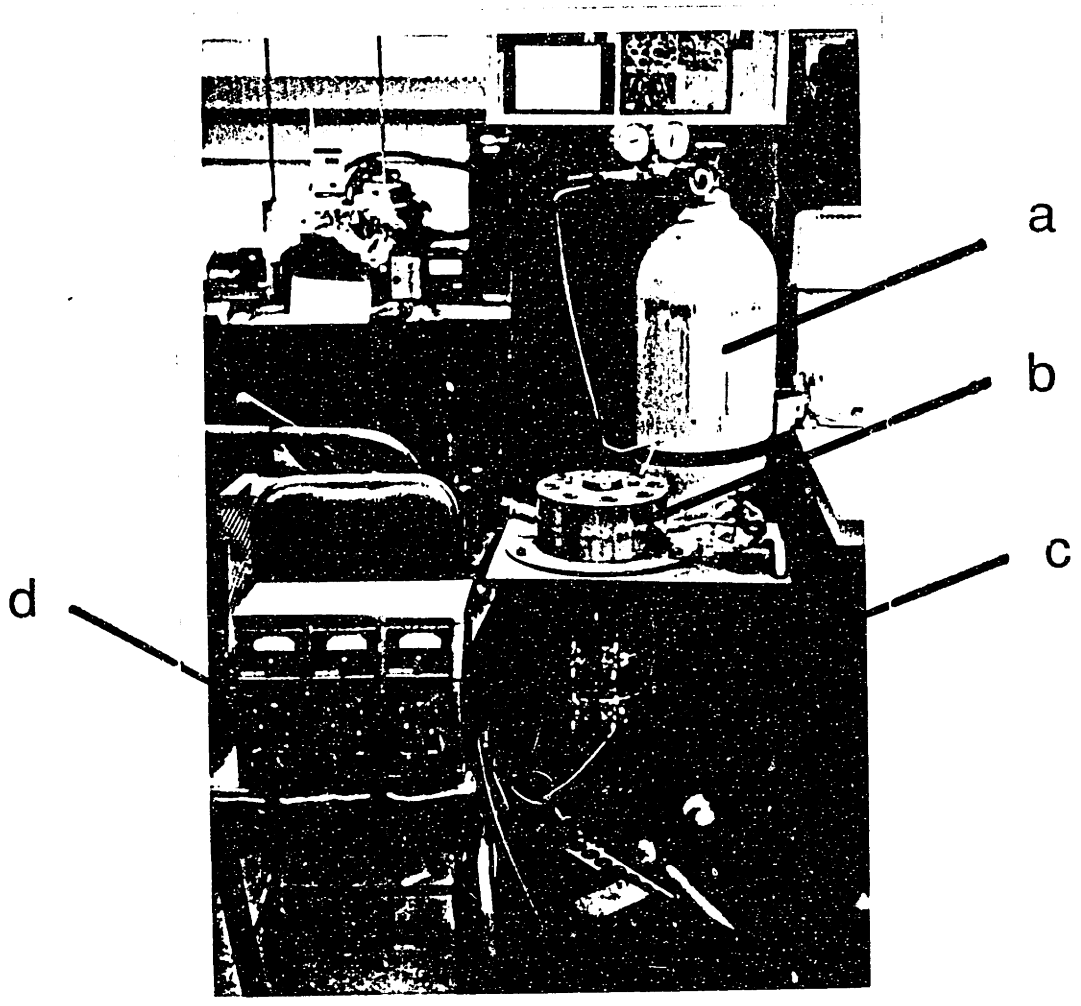

Figure 4.1-1. Photograph showing the setup for saturation of polystyrene with nitrogen.

a. 6000 psi nitrogen cylinder.
b. Pressure vessel.
c. Heating elements attached to the vessel.
d. Temperature controller.

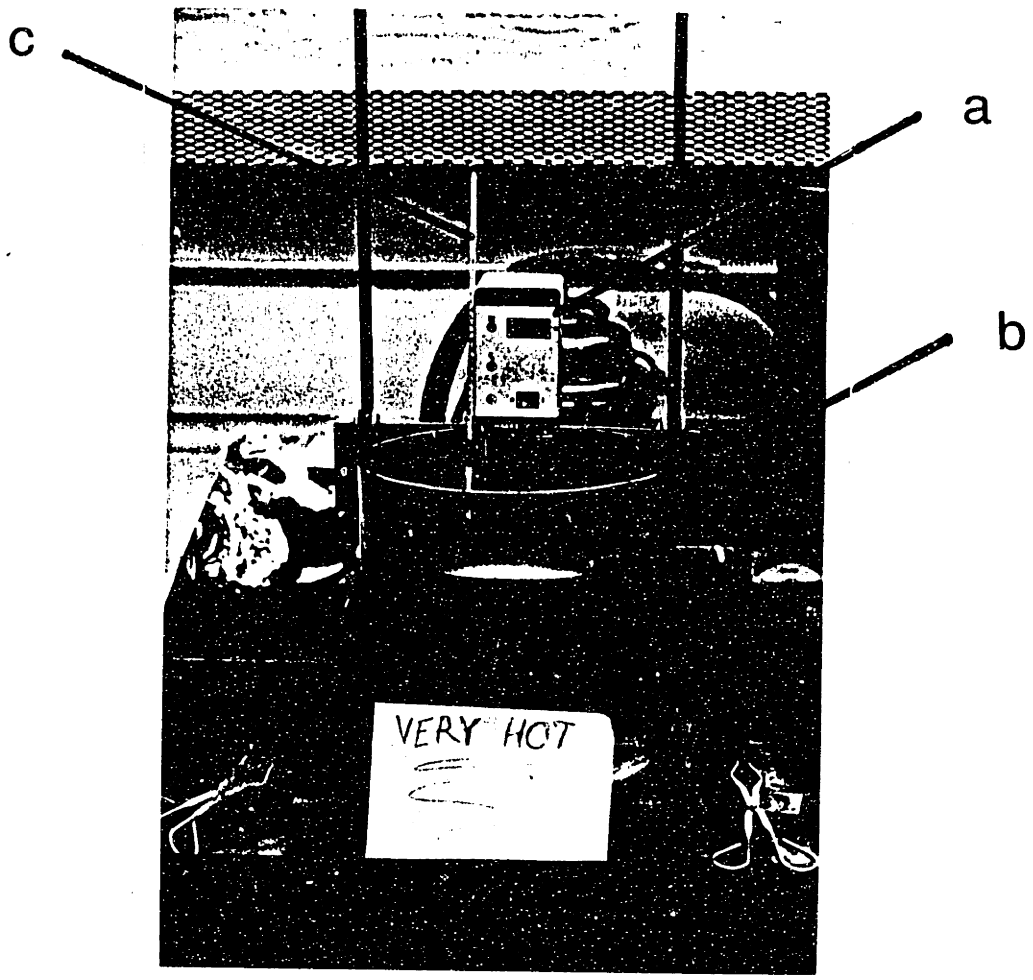

Figure 4.1-2. Photograph of the setup for foaming of samples.

a. Haake circulator-controller.
b. Pyrex vessel with glycerin.
c. Thermometer

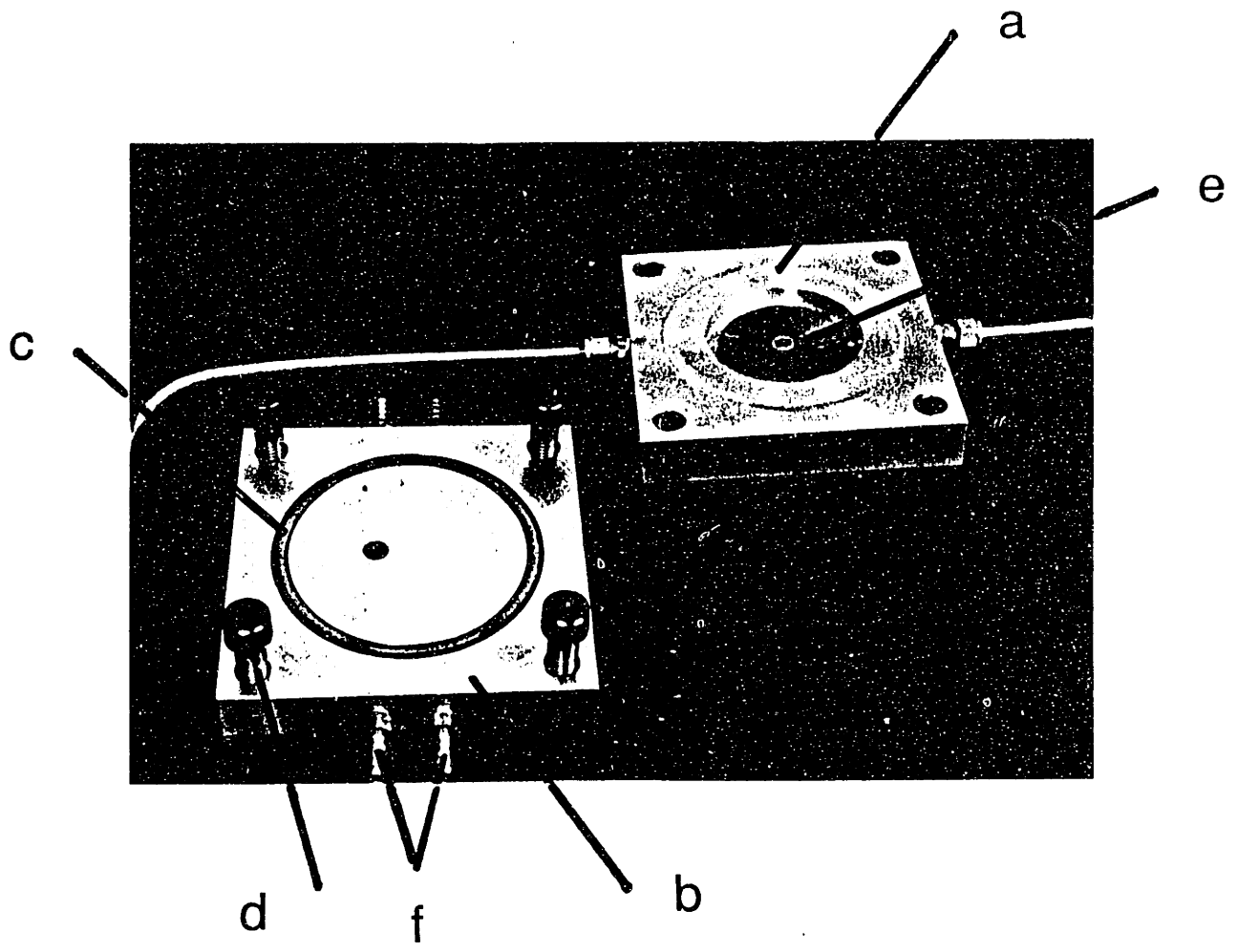

Figure 4.1-3. photograph showing components of the high pressure mold.

a. Top half of mold containing tubing connected to nitrogen cylinder.
b. Bottom half of mold. A thermocouple (not shown in picture) was located 1/16" below the surface to monitor the cavity temperature .
c. Silicon O-Ring.
d. Clamping bolts
e. A movable plate to adjust cavity height.
f. Plumbing for cooling water.

4.2 Determination of cell size and density

To determine the cell density, a micrograph that showed 100 to 200 bubbles was obtained and the exact number of bubbles was determined. Fig. 1.1-2 is typical of a micrograph used to determine cell density. Assuming isotropic distribution of bubbles the number of cells per cm^3 of foam, N_f, was determined. To determine average cell size, usually a second micrograph at a higher magnification was obtained. Average bubble diameter d over an area including 25 to 50 bubbles was determined. Void fraction V_f in the foam was estimated from

$$V_f = (\pi/6) \cdot d^3 \cdot N_f \qquad (4.2\text{-}1)$$

Note that in equation (1), N_f is the cell density in the foam. A more useful measure is the number of cells nucleated per unit of original unfoamed volume, N_o. N_o allows us to compare cell nucleation density in different samples which may have experienced different amounts of cell growth. Using the void fraction calculated from (1) we can estimate N_o from

$$N_o = N_f / (1 - V_f) \qquad (4.2\text{-}2)$$

Unless otherwise mentioned, all data on cell density shows N_o obtained from equation (4.2-2).

5.0 CONTROL OF MICROCELLULAR FOAM STRUCTURE

5.1 General features of microcellular foam

In this section we report on some general characteristics of the microcellular structure. We address such questions as: How homogeneous is the microcellular structure? How does the structure vary across the thickness? How reproducible are the cell size and cell density distributions? This basic understanding of the microcellular structure is necessary in order to properly interpret data obtained in later experiments.

5.1.1. Homogeneity of cell structure

In order to study local variability in cell structure, overlapping scanning electron micrographs were taken approximately 250 μm apart along the entire length of one SEM specimen (approximately 7 mm). The micrographs were taken at the center of the specimen so as to avoid any effect of location across the thickness on the measurements. The nature of structural variation across the foam thickness is discussed in the next subsection. The sample was saturated at 2000 psi (13.8 MPa) and foamed in a glycerin bath at 115°C for twenty seconds.

The results of cell density and cell size measurements are shown in Figs 5.1-1 and 2 respectively. The cell density ranges from 170 million to 400 million per cm^3 with an average of 280 million. The standard deviation of cell density measurements is 60

million/cm^3. Overall, the local variation in cell density is very similar to that found among different samples foamed under identical conditions shown in Fig. 5.1-3. This means that the structural factors responsible for variations at the local level are also the main cause of variations among different polystyrene samples.

The cell size measurements in Fig. 5.1-2 range from 6 to 11μm with an average of 8.3 μm and a standard deviation of 1.3 μm. Again, the local variation in cell size is comparable to the variation among different samples in Fig. 5.1-11.

A close look at the pattern of cell size and density variations in Figs 5.1-1 and 2 shows that when cell density goes up, there is a decrease in the corresponding cell size, and vice versa. To see this effect more clearly, the cell density data has been overlaid on the cell size data in Fig. 5.1-3. The out-of-phase character of the local cell density and cell size variations is now more evident. The cell size adjusts to the local cell density in such a way that the void fraction remains constant. This is clearly seen in Fig. 5.1-4, where the void fraction calculated from the data in Figs. 5.1-1 and 2 has been plotted. Void fraction represents the amount of nitrogen that must precipitate out of the polymer matrix depending on the saturation and foaming conditions. With a uniform nitrogen concentration in the plastic disk, and the uniform temperature in the glycerin bath, we expect a constant void fraction in our sample.

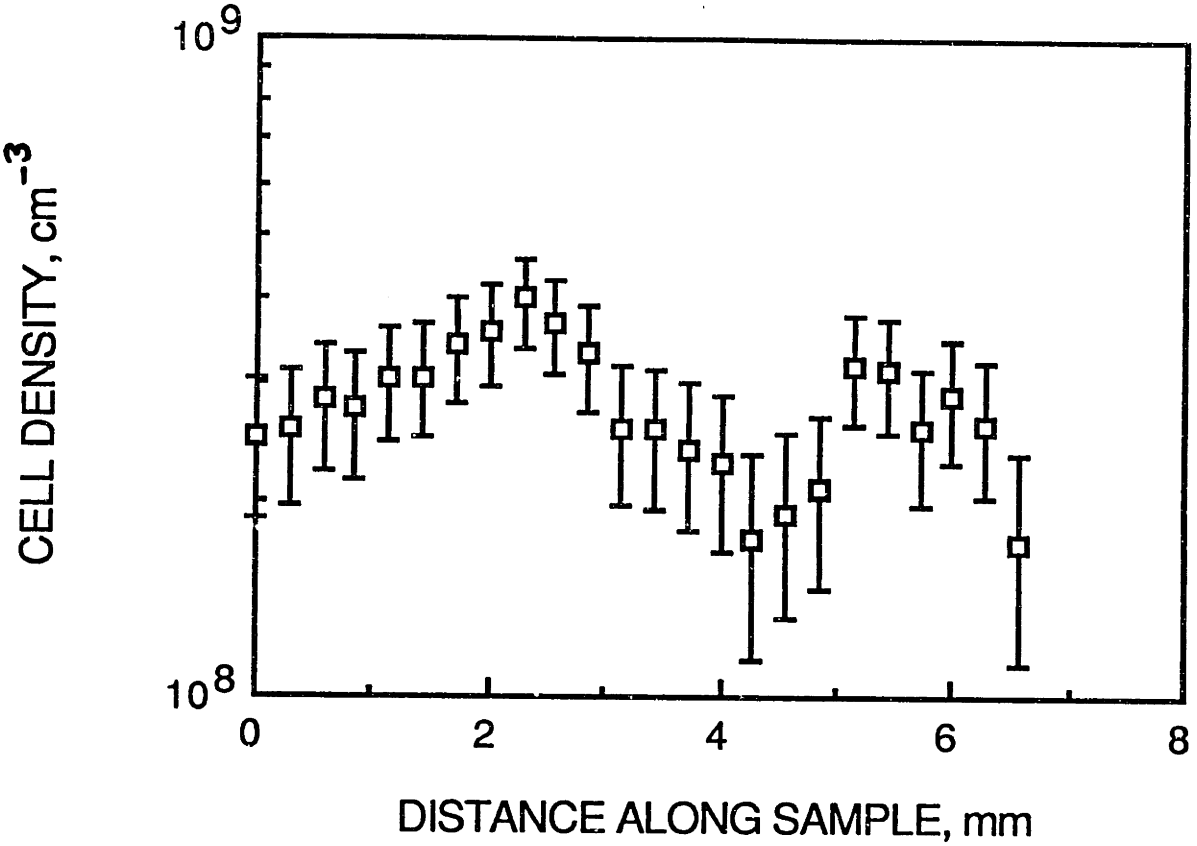

Figure 5.1-1. Local variation in cell nucleation density. The data was obtained from overlappling scanning electron micrographs approximately 250 μm apart.

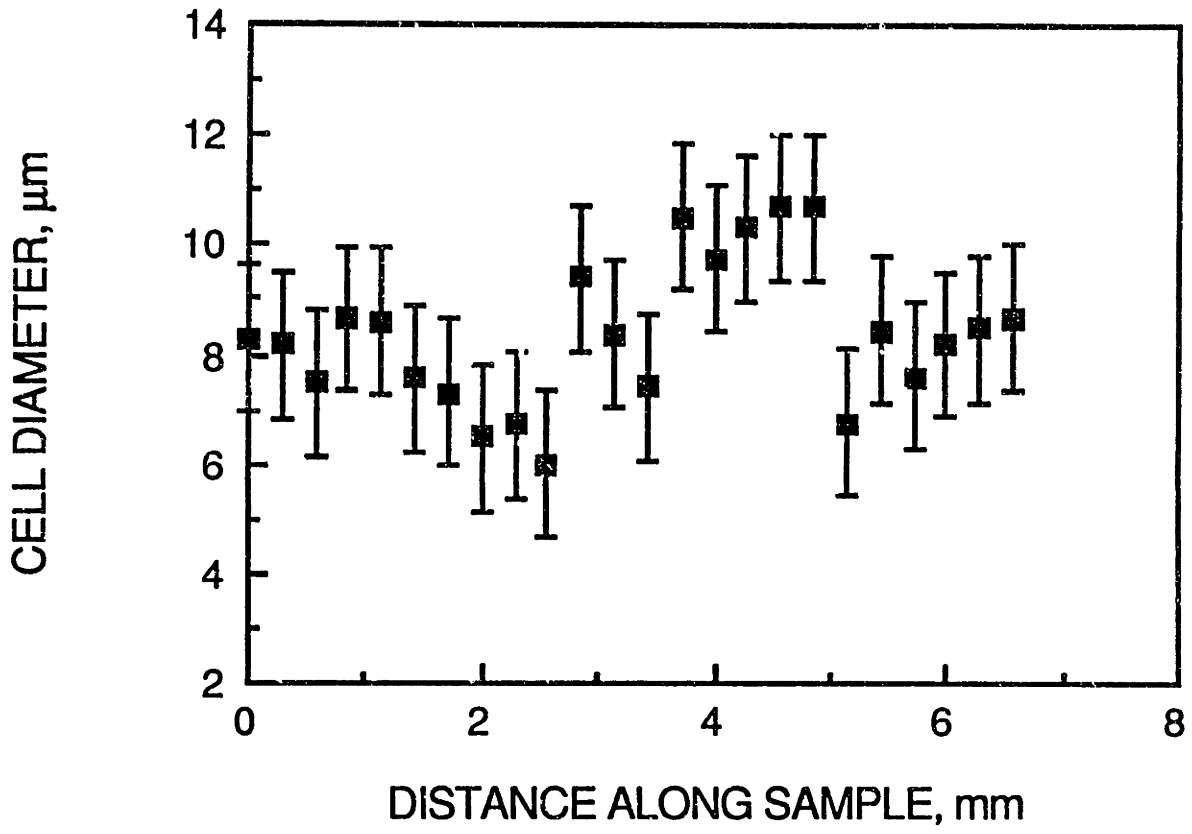

Figure 5.1-2. Local variation in cell size.The data was obtained from overlappling scanning electron micrographs approximately 250 μm apart.

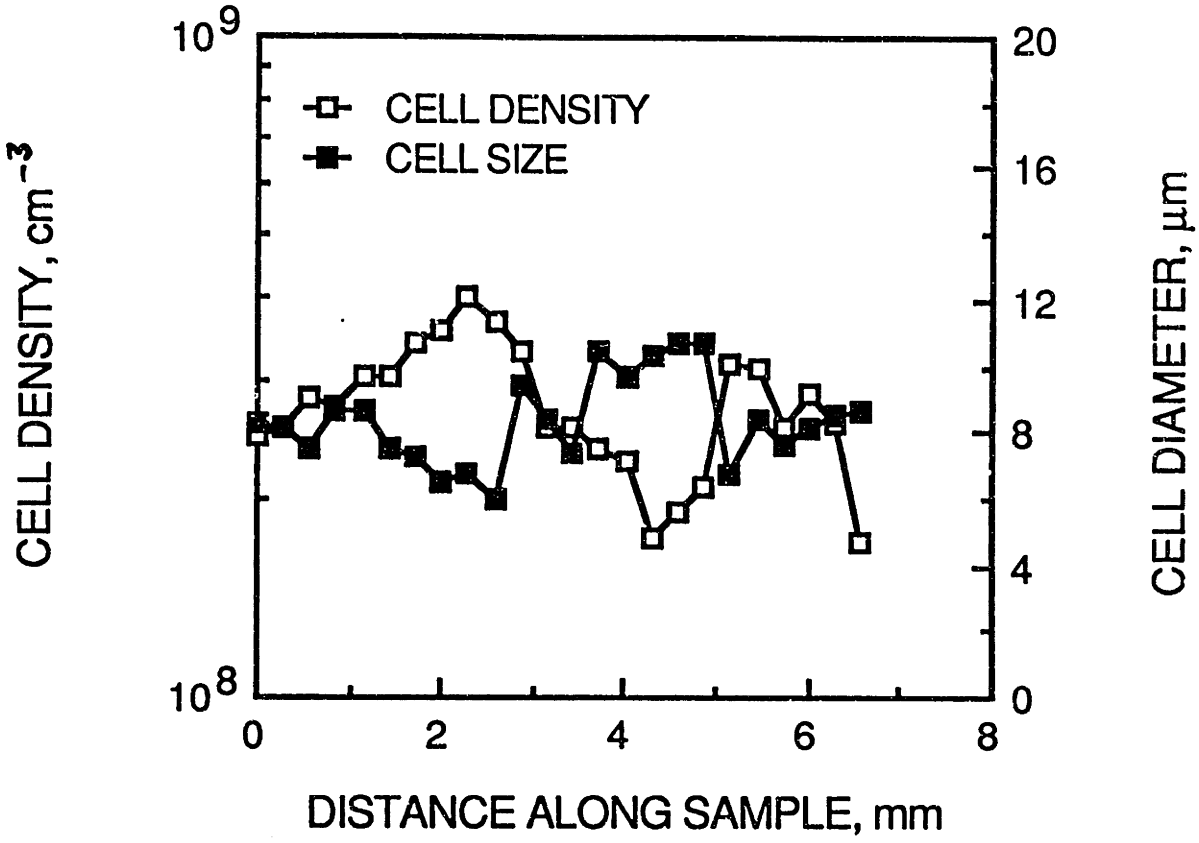

Figure 5.1-3. Local variation in microstructure. In this plot, Figs. 5.1-1 and 2 have been overlapped. Note the out-of-phase character of the cell size and cell density variations.

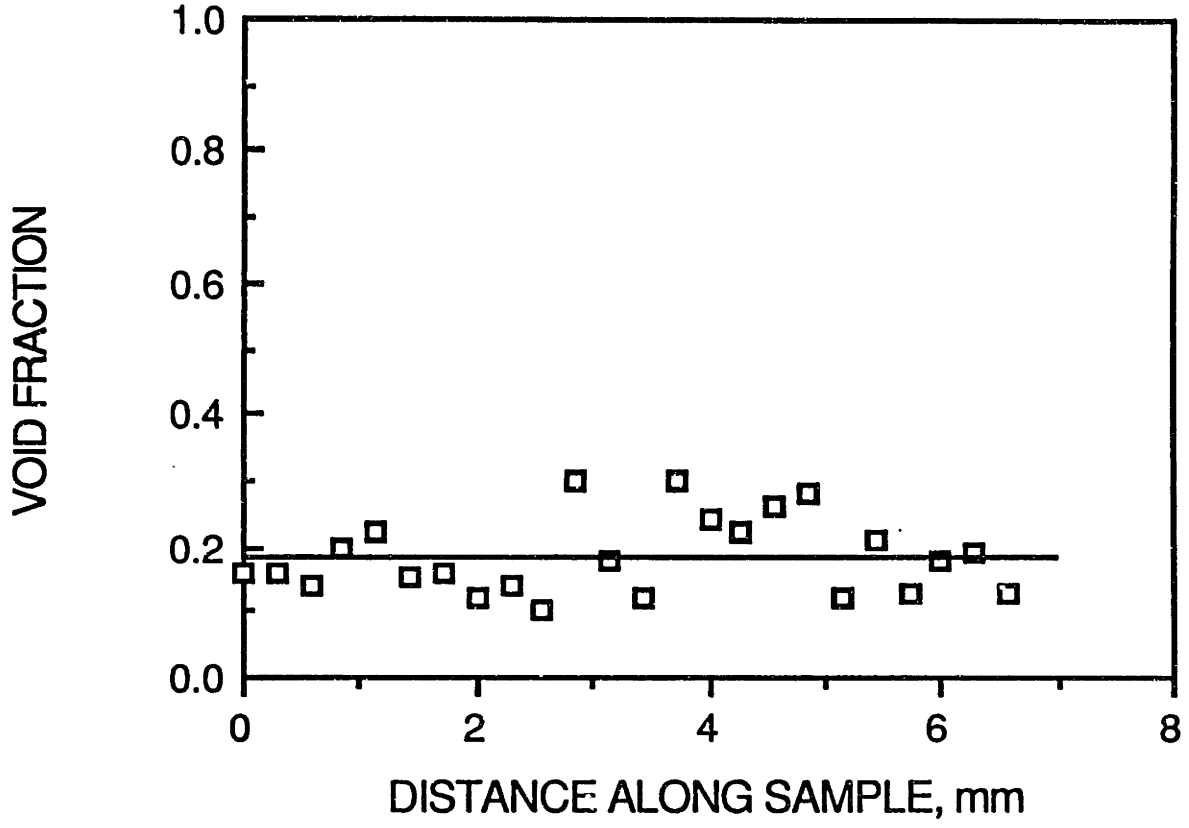

Figure 5.1-4. Void fraction along the sample

5.1.2. Cell structure through thickness

In order to investigate cell structure across the sample thickness, a polystyrene disk of thickness 1.55 mm was saturated at 2000 psi and foamed at 115°C for twenty seconds. The thickness of the foamed disk was approximately 2.1 mm. The structure was studied under a scanning electron microscope, and overlapping micrographs across sample thickness were obtained at about 200μm intervals. Micrographs showing structure across the thickness are shown in Fig. 5.1-5. Cell size and cell density was determined from each micrograph. As the structure was generally symmetric about the center, a reference was established at the center of the sample and cell size and density data equidistant from the center was averaged. This data was then plotted as a function of distance from the center in Fig. 5.1-6.

We can see three distinct zones in Fig. 5.1-5. Region I at the (left and right) edge of the specimen has no bubbles at all. This is the skin of the foam and is made up of original, unfoamed polymer. The skin comprises approximately 10% of the total thickness. Adjacent to the skin is region II, a transitional region, where the cell density increases from zero to a maximum value. The maximum cell density corresponds to the equilibrium nitrogen concentration reached at the saturation pressure. Finally there is region III, the "core", where the cell density is uniform. We note that in Fig. 5.1-6, the deviations in cell density from the average cell density are comparable to the local variations shown in Fig. 5.1-1. This core region comprises approximately 50 to 60% of the sample thickness.

The relative extent of these regions depends on the original sample thickness, as well as on the rate of nitrogen diffusion from the sample and the time over which such nitrogen loss is allowed to occur.

The average cell size in region III is approximately 12 μm and is seen tc be uniform over the entire core region. In region II , the cell size rises to a maximum of 18 μm. The largest cells are seen adjacent to the skin, which is also the region of lowest nitrogen concentration. As mentioned before, the lower nitrogen concentration leads to a lower cell nucleation density, and the cell size adjusts to allow for the appropriate void fraction. Also, the bubbles near the skin region are nucleated first and have relatively more time to grow, becoming larger compared to the interior bubbles.

MICROCELLULAR STRUCTURE ACROSS THICKNESS

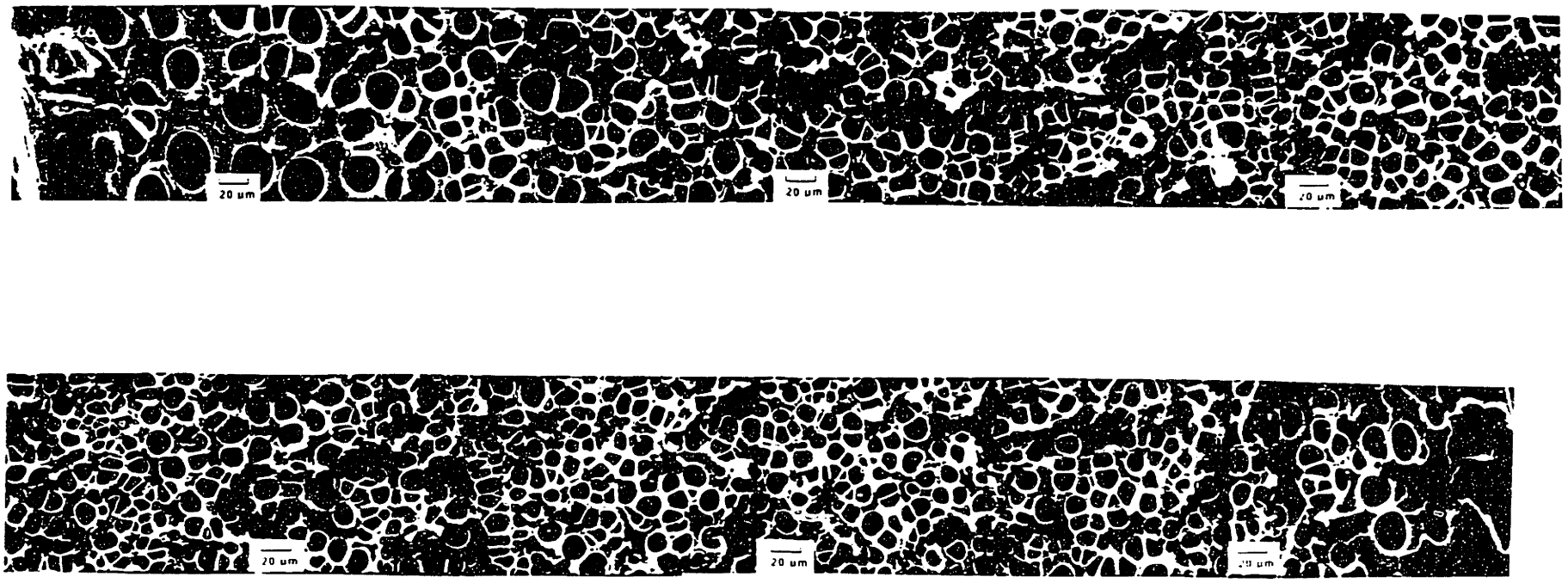

Figure 5.1-5. Scanning electron micrographs showing structure across the thickness of a microcellular foam sample. The picture was assembled from micrographs taken approximately 200 µm apart. The sample thickness after foaming was 2.0 mm.

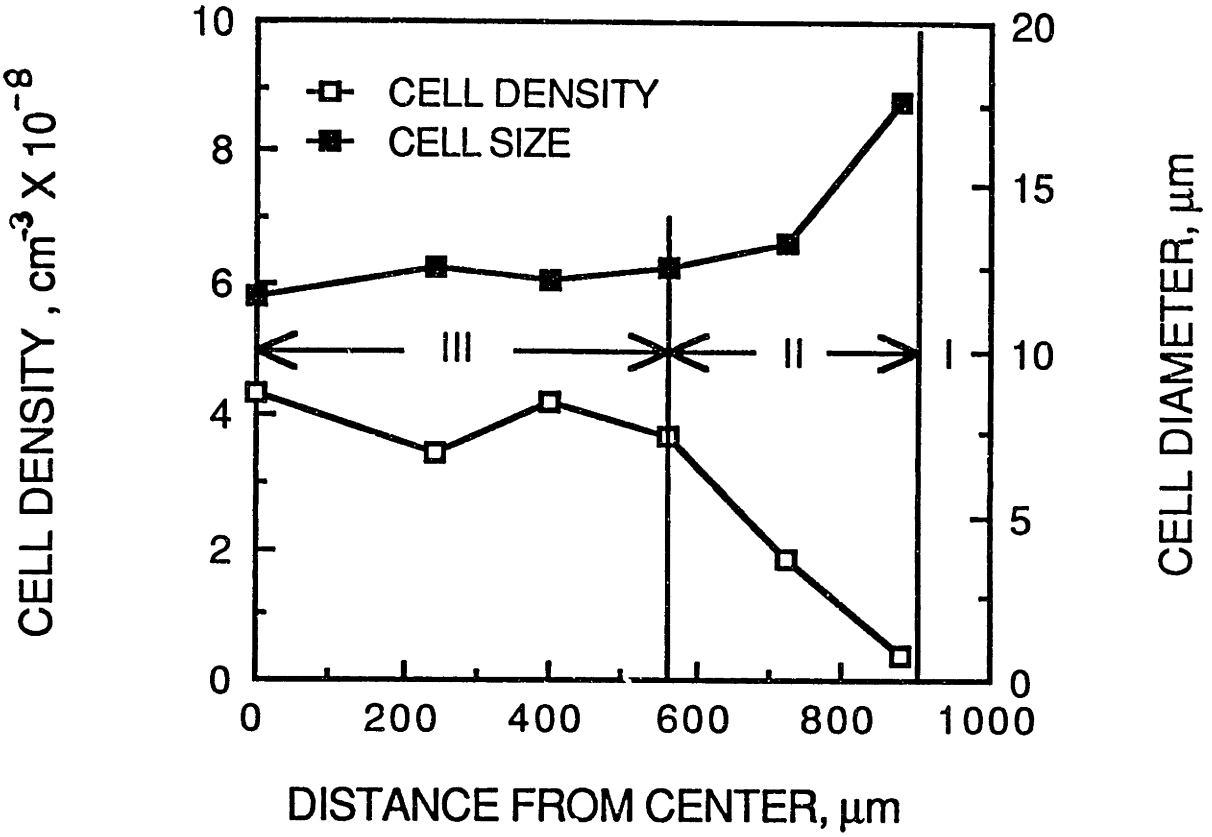

Figure 5.1-6. Variation in microstructure across thickness. The structure is symmetric about the center and has three distinct regions.The data is from one sample.

5.1.3. Skin thickness

The skin, or unfoamed polymer, offers many advantages. It allows for control of texture of the foam surface, as well as adds to the flexural rigidity of the foam. In the procedure for producing microcellular foam, the polystyrene disk is first saturated with nitrogen at the chosen saturation pressure. The disk is then removed from the pressure vessel and heated above the glass transition temperature to create the foam. As soon as we remove the disk from the pressure vessel, creating a supersaturated disk, nitrogen begins to diffuse out of the disk. By controlling the time for which nitrogen is allowed to escape, we can control the thickness of the skin region.

A Model for Skin Thickness

If the region $-l < x < l$ is initially at a uniform concentration C_0 and the surfaces are kept at a concentration C_1 for $t > 0$, then the concentration distribution, symmetric about $x = 0$, is given by (Crank, 1956, p. 45)

$$\frac{C - C_0}{C_1 - C_0} = 1 - \frac{4}{\pi}\sum_{n=0}^{\infty}\frac{(-1)^n}{2n+1}\exp\left(\frac{-D(2n+1)^2\pi^2 t}{4l^2}\right)\cos(2n+1)\frac{\pi x}{2l} \qquad (5.1\text{-}1)$$

Equation (5.1-1) can be written in terms of dimensionless variables, $T = Dt/l^2$ and $X = x/l$, and plotted over the range of T and X. Graphs of $\frac{C - C_0}{C_1 - C_0}$ for various dimensionless times can be found in standard texts (see, for example, Crank, 1956, p46).

For our case the polystyrene disk is saturated at a certain pressure P_S, and then subjected to atmospheric pressure. Assuming that the nitrogen concentration at the surface immediately assumes the equilibrium value corresponding to atmospheric pressure and stays constant thereafter, Eq. (5.1-1) can be used to predict the nitrogen concentration in the disk as a function of time. In our experiments the surface of the disk is subject to atmospheric pressure after obtaining equilibrium concentration C_0, so that $C_1=0$.

If the diffusion coefficient is known, Dt/l^2 can be calculated for different values of desorption time t. We measured the average diffusion coefficient to be 4.2×10^{-8} cm^2/sec (this is in agreement with the value replorted by Colton, 1985). If C^* represents the minimum gas concentration at which nucleation will occur, then the intersection of the horizontal line $(1 - C^*/C_0)$ with the appropriate Dt/l^2 curve establishes the location x/l beyond which there will be no bubble nucleation. Thus (1 - x/l) gives the percentage of the unfoamed thickness that will become the skin of the foam for the particular nitrogen desorption time.

A value of $C^* = 1$ cm^3 (STP)/g was chosen based on the available data (see Martini etal., 1984), and seems to provide satisfactory predictions for skin thickness. For the nitrogen-polystyrene system, $C^* = 1$ cm^3 (STP) per gram of polystyrene corresponds to a saturation pressure of about 25 atmospheres.

In the skin thickness experiments a saturation pressure of 2000 psi was used, corresponding to a gas concentration of 5.44

cm^3 (STP)/g (see section 7.2). For these values the predicted skin thickness values are given in Table 5.1-1.

Table 5.1-1

Calculated Skin Thickness Values

t, hr.	Dt/l^2	x/l	1 - x/l	Skin Thickness (μm)
0.25	0.005	0.98	0.02	17.3
0.5	0.01	0.97	0.03	26.0
1.0	0.02	0.95	0.05	43.2
1.5	0.03	0.94	0.06	51.9
2.0	0.04	0.93	0.07	60.6
3.0	0.06	0.925	0.075	64.9
4.0	0.08	0.91	0.09	77.9
5.0	0.1	0.90	0.10	86.5
6.2	0.125	0.89	0.11	95.2

Experimental results

We investigated the effect of variation in the time allowed for nitrogen to diffuse out on the skin thickness and on the cell size and cell density in the core region. Seven disks were saturated at 2000 psi (13.8 MPa). After saturation, all disks were removed from the pressure vessel. The first disk was foamed 15 minutes after supersaturation (i.e., 15 minutes after removal from the pressure

vessel). The remaining disks were foamed at one-hour intervals. All disks were foamed at 115°C for twenty seconds.

Figure 5.1-7 shows scanning electron micrographs of the skin region in four samples over a range of nitrogen desorption times. We can qualitatively see a growth in skin thickness from these micrographs. The skin thickness has been plotted in Fig. 5.1-8 as a function of nitrogen desorption time.

The skin thickness was determined from the scanning electron micrograph by averaging the distance from edge of the disk to the first bubble for ten or so bubbles. The skin thickness was determined for both left and right edges and averaged to obtain a representative skin thickness for the disk. The skin thickness data has been summarized in Table 5.1-2.

Figure 5.1-8 shows a plot of the calculated and experimental skin thickness values as a function of nitrogen desorption time. There is good agreement between the predicted and observed values except at the small desorption times where the observed thickness is larger than the predicted value. This may be due to a higher diffusion rate in the beginning, as the diffusion rate in polymers is known to be concentration dependent.

Table 5.1-2

Experimental Skin Thickness Data

Desorption Time (hr)	Skin Thickness (μm)
0.25	43
1.25	53
2.25	61
3.25	69
4.25	81
5.25	96
6.25	103

Fig. 5.1-9 shows the effect of loss of nitrogen on the cell size and cell nucleation density in the core of the foamed disks. We find that both cell size and cell density are basically unaffected by the time we wait before foaming the samples. This is not surprising, since nitrogen concentration in the core (region III in Fig. 5.1-6) remains at the equilibrium level reached at the saturation pressure.

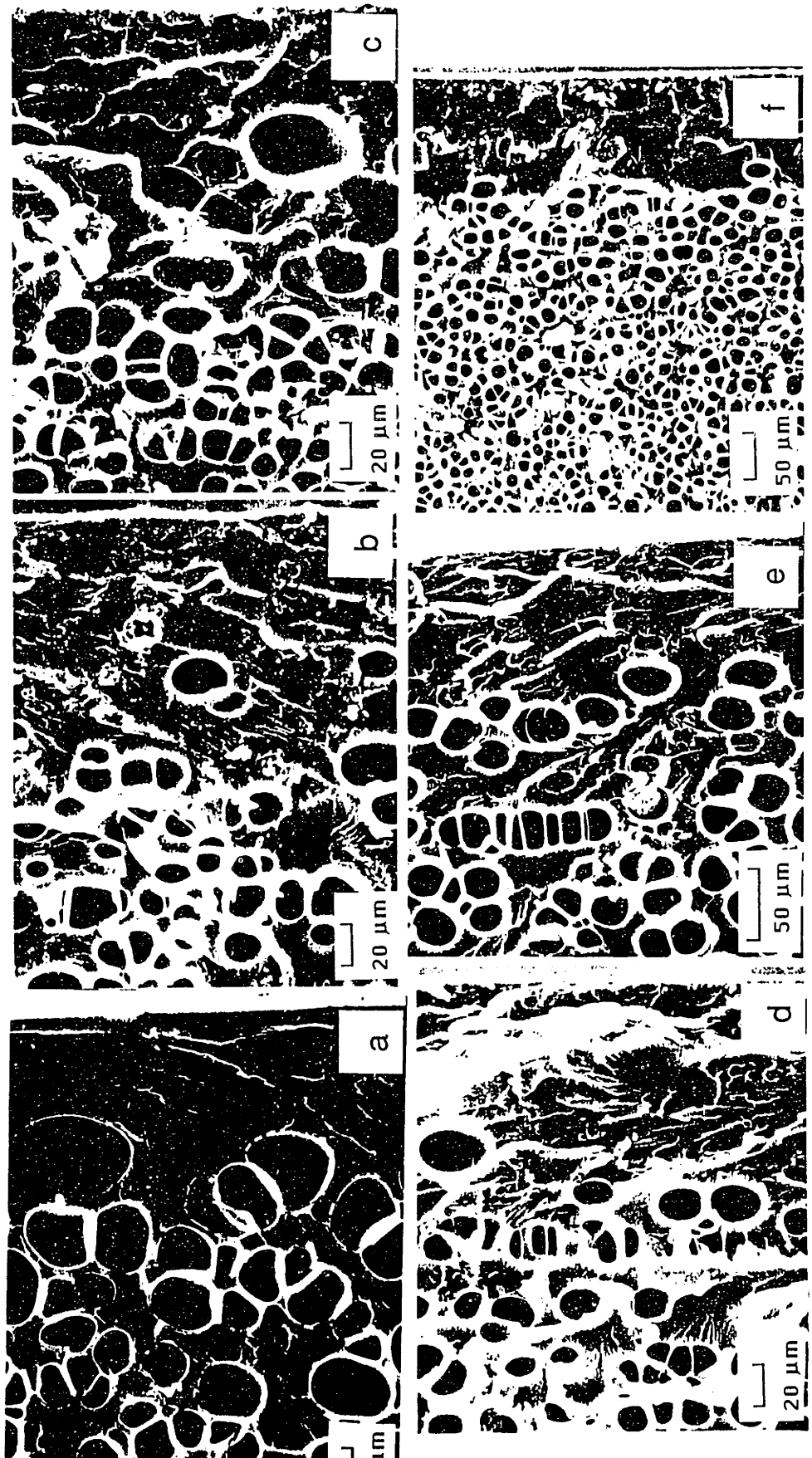

Figure 5.1-7. Scanning electron micrographs showing the skin region in six samples (the micrographs are at different magnifications).The nitrogen desorption times are: (a) 0.25 hours, (b) 1.25 hours, (c) 2.25 hours, (d) 4.25 hours, (e) 5.25 hours, and (f) 6.25 hours.

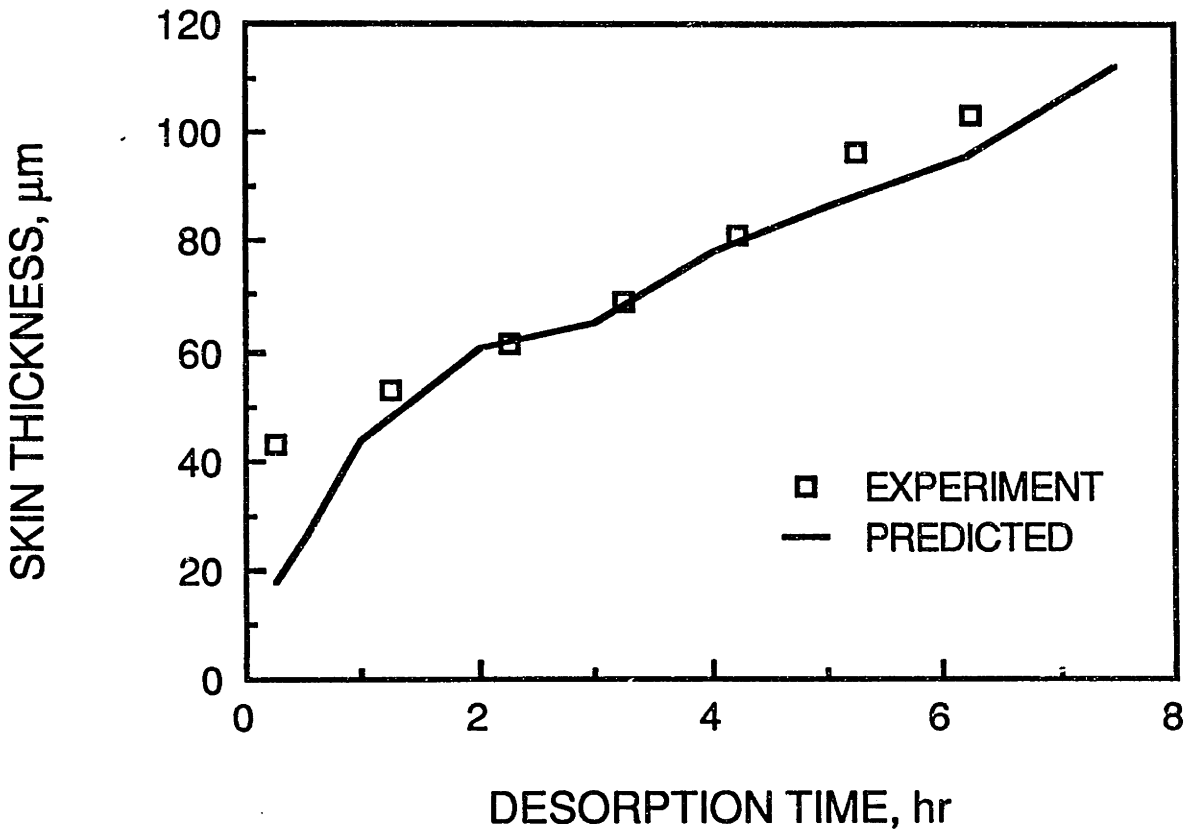

Figure 5.1-8. Skin thickness as a function of nitrogen desorption time- comparison of theory and experiment.

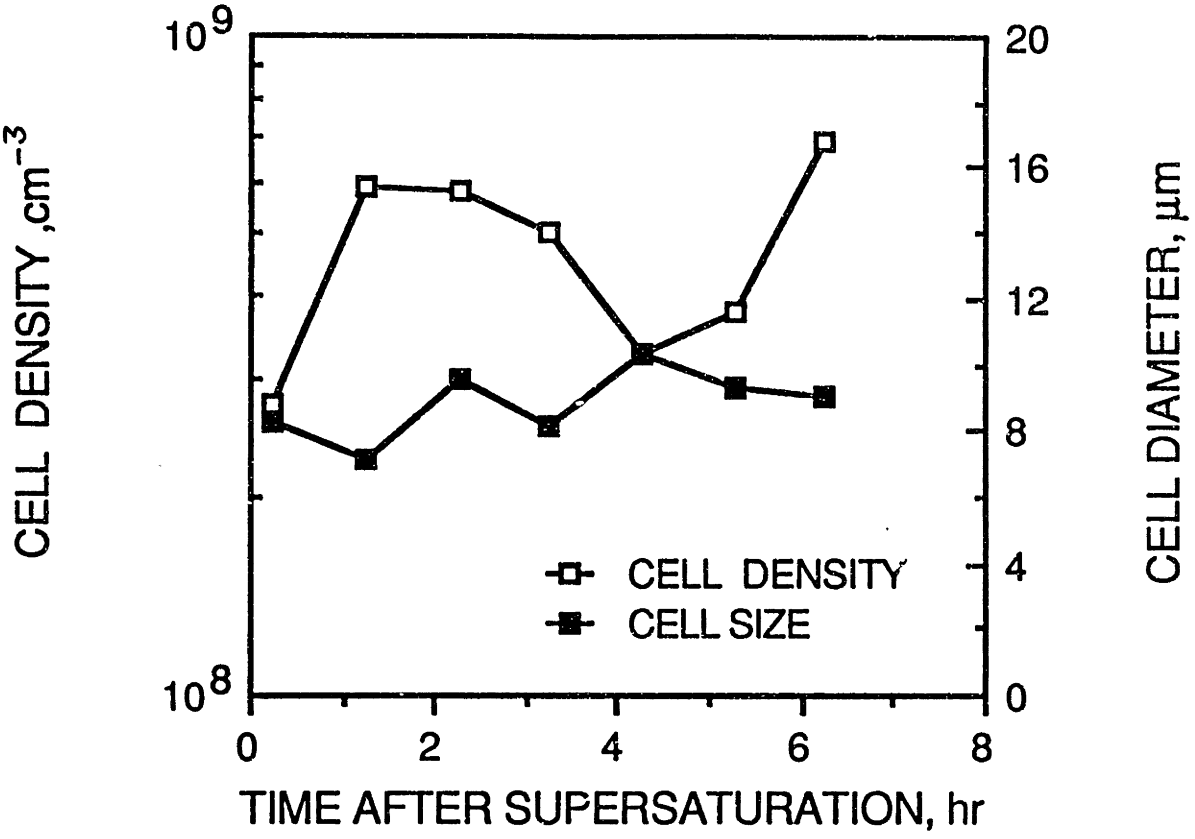

Figure 5.1-9. The effect of nitrogen loss on the cell nucleation density and the cell size.

5.1.4. Reproducibility of microstructure

Reproducibility of microstructure was found to be quite good. Figures 5.1-10 and 11 shows cell density and cell size measured in five samples foamed under identical conditions. All samples were saturated with nitrogen at 2000 psi (13.8 MPa) and foamed at 115°C for twenty seconds. The cell density ranged from 300 million to 600 million bubbles per cm^3 with an average of 440 million The cell size ranged from 6 to 12 microns with an average of 10 microns. These results provide an idea of variability in the cell size and cell density measurements.

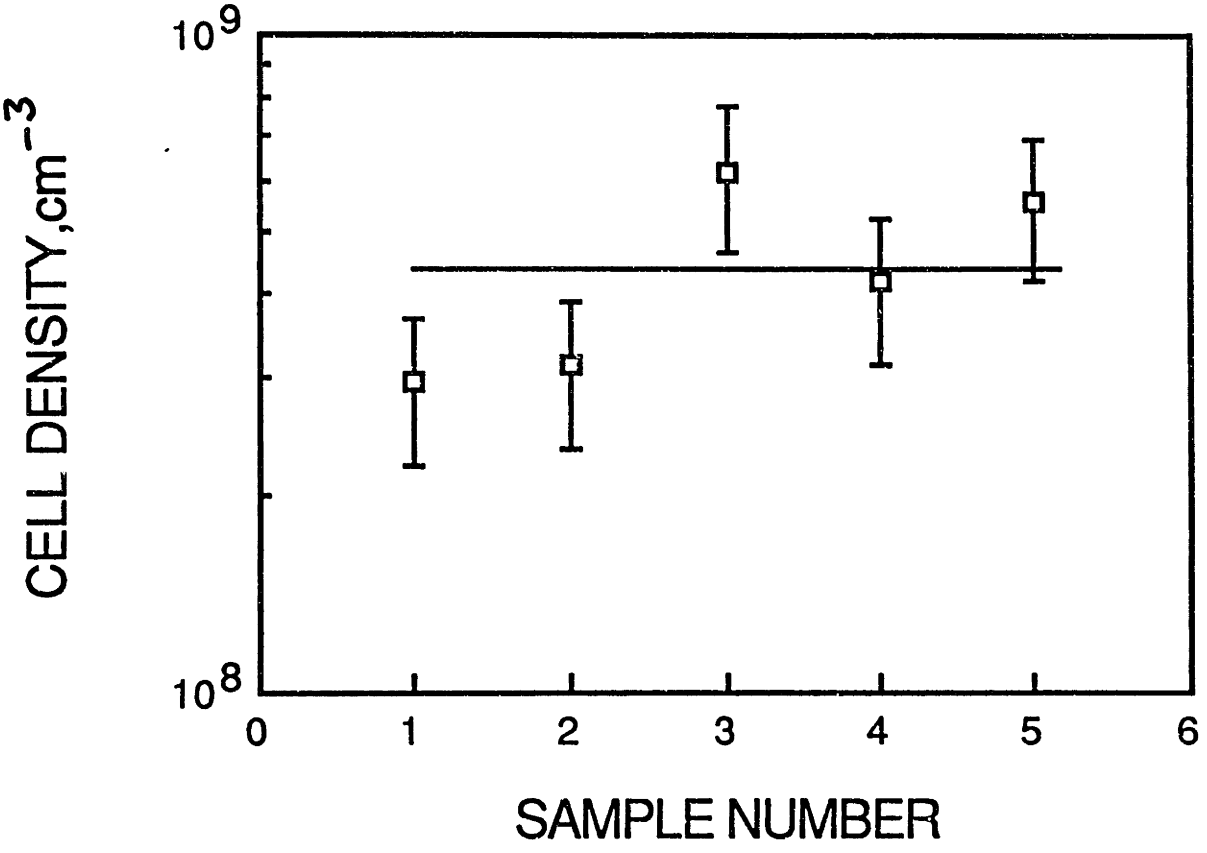

Figure 5.1-10. Cell nucleation density in five identical polystyrene samples.

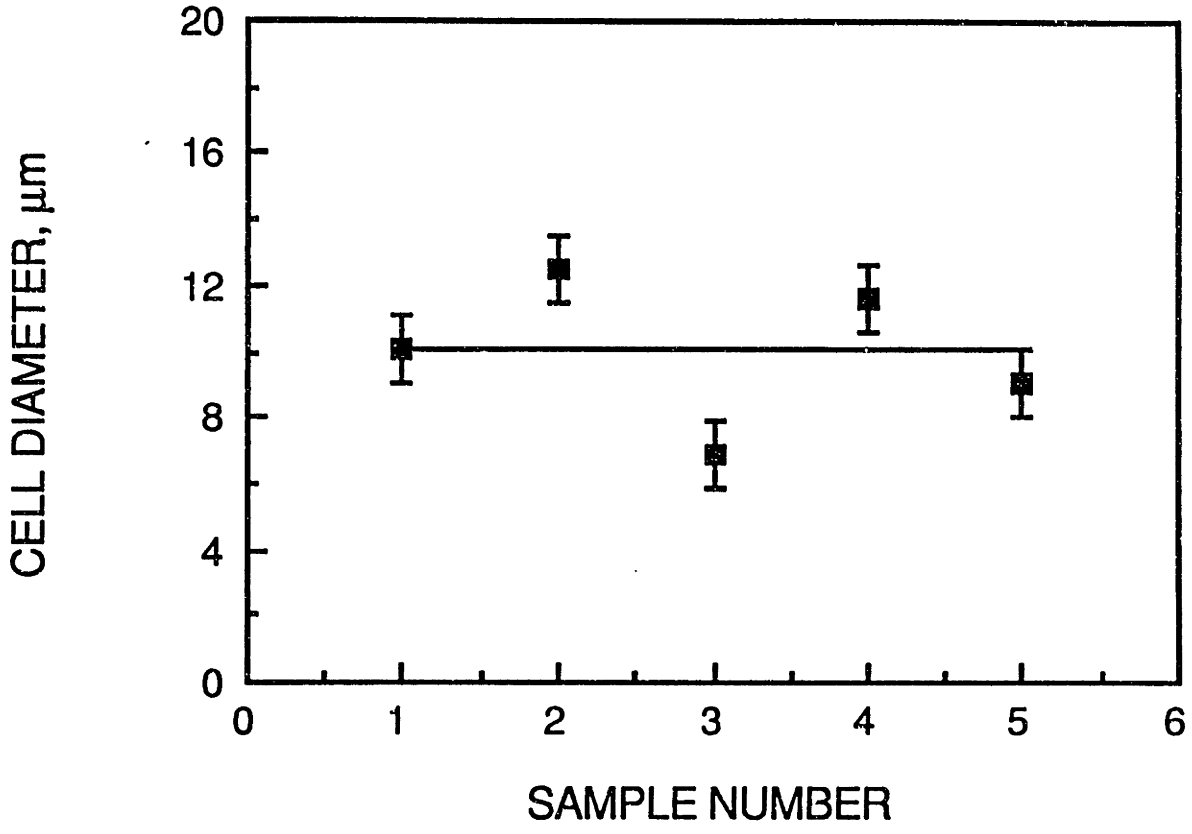

Figure 5.1-11. Average cell size in five identical polystyrene samples.

5.2. Control of cell nucleation density

In section 3.3 we discussed the homogeneous nucleation theory and its application to nucleation in polymers. We concluded that the gas saturation pressure should have a profound effect on the cell nucleation rate. Therefore, the saturation pressure was chosen as the process variable to control the cell nucleation density. In this section, we will experimentally determine the relationship between saturation pressure and the cell nucleation density.

Experimental

To investigate the effect of gas saturation pressure on cell nucleation, polystyrene disks were saturated with nitrogen at pressures of 600, 1000, 1500, and 2000 psi, respectively, and foamed in a glycerin bath at 115°C. The foaming time was approximately 30 seconds for each sample, with the exception of samples saturated at 600 psi which were foamed for 60 seconds to get an appreciable amount of foaming.

Results

Figure 5.2-1 shows micrographs of samples foamed at different gas saturation pressures. The foaming time was kept low in order to prevent cell growth to a point where coalescence can occur, affecting our cell density measurements. An increase in the number of cells with higher saturation pressure can be seen from these micrographs. Cell density data from these and other samples is plotted in Fig. 5.2-2 as a function of nitrogen saturation pressure.

Note that the cell density has been plotted on a log scale. We see that the number of cells nucleated increases exponentially with saturation pressure, at least for the range of saturation pressures in our experiments.

The relationship between the cell nucleation density and the saturation pressure can be described by

$$N_0 = A\, e^{\alpha P_s} \qquad (5.2\text{-}1)$$

where N_0 = number of cells per cm^3, and

P_s = saturation pressure in atm.

In equation 5.2-1, A and α are empirical constants. The solid line in Fig. 5.2-2 is described by

$$N_0 = (1.46 \times 10^6)\ e^{0.0454\, P_s} \qquad (5.2\text{-}2)$$

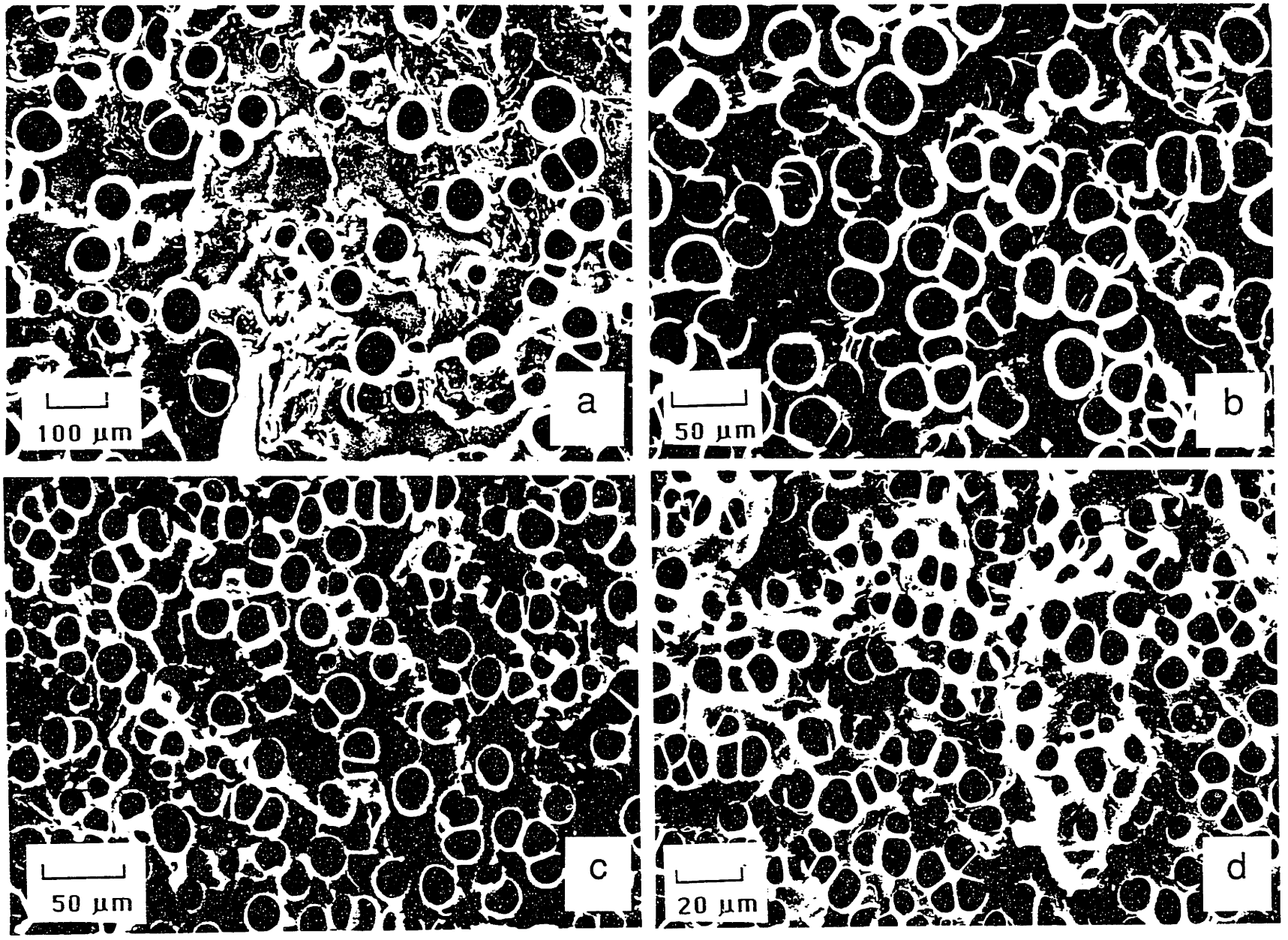

Figure 5.2-1. Scanning electron micrographs of polystyrene samples nucleated at different nitrogen saturation pressures (the micrographs are at different magnifications). (a) 600 psi; (b) 1000 psi; (c) 1500 psi; and (d) 2000 psi. (1000 psi = 6.895 MN/m^2)

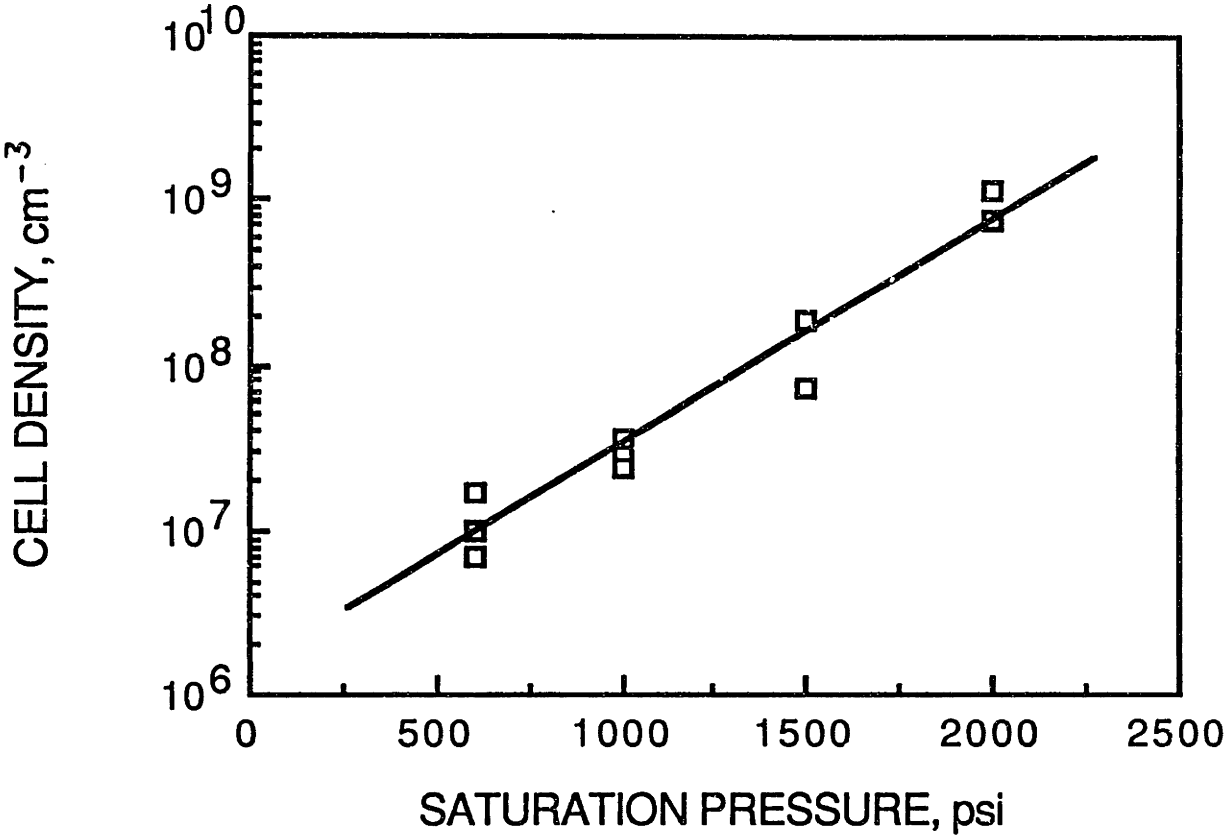

Figure 5.2-2. Plot of cell nucleation density as a function of nitrogen saturation pressure (1000 psi = 6.895 MN/m^2)

Discussion

These experiments were done with pure polystyrene (with no additives.) As there is no second phase of another material present, homogeneous nucleation is believed to be the mechanism responsible for cell nucleation. Colton (1986) has calculated homogeneous nucleation rate in polystyrene at different gas saturation pressures. (see Fig. 5.2-3). If we assume that cell nucleation is 'spontaneous' and that all nucleation occurs in the first second, then the nucleation rate in Fig. 5.2-3 also gives the total number of cells per cm^3. Colton (1985) has implicitly made this assumption (confirmed in a personal communication, Feb. 1988) in comparing his calculated nucleation rates to the experimental cell densities (see Fig. 5.2-4).

In Fig. 5.2-5 we have plotted the predicted cell density for homogeneous nucleation (i.e. the curve for zero zinc stearate in Fig. 5.2-3 together with the spontaneous nucleation assumption) and the average of the data at different saturation pressures in Fig. 5.2-2. Colton's data corresponds to 0% zinc stearate data in Fig. 5.2-3, and is seen to be in good agreement with our measurements. Note that our foaming temperature was 115°C while Colton's calculations and experiments were conducted at 110°C. The small temperature difference can, however, be neglected for all practical purposes.
It is clear from Fig. 5.2-5 that there is a gross disagreement between the experimental data and the cell density prediction by homogeneous nucleation theory. For an increase in saturation pressure from 100 psi to 2000 psi, the homogeneous nucleation theory predicts the cell density to increase from 10^2 cells per cm^3

to 10^{10} cells per cm^3-- an increase of eight orders of magnitude. The measured cell density increases from 5 x 10^7 at 1000 psi to 9 x 10^8 at 2000 psi-- a significant, twenty-fold increase, but some six orders of magnitude less than the predicted value. The cell nucleation phenomenon is much less sensitive to saturation pressure than is suggested by the homogeneous nucleation theory. In terms of predictions at a given saturation pressure, the theory is not consistent. For example, at 1000 psi saturation pressure, the measured cell density is about five orders of magnitude higher than the predicted value of 10^2 cells per cm^3. At 2000 psi saturation pressure, the measured cell density is about two orders of magnitude lower than the theoretical prediction. Clearly, the cell nucleation phenomenon in polystyrene is not well described by the classical homogeneous nucleation theory.

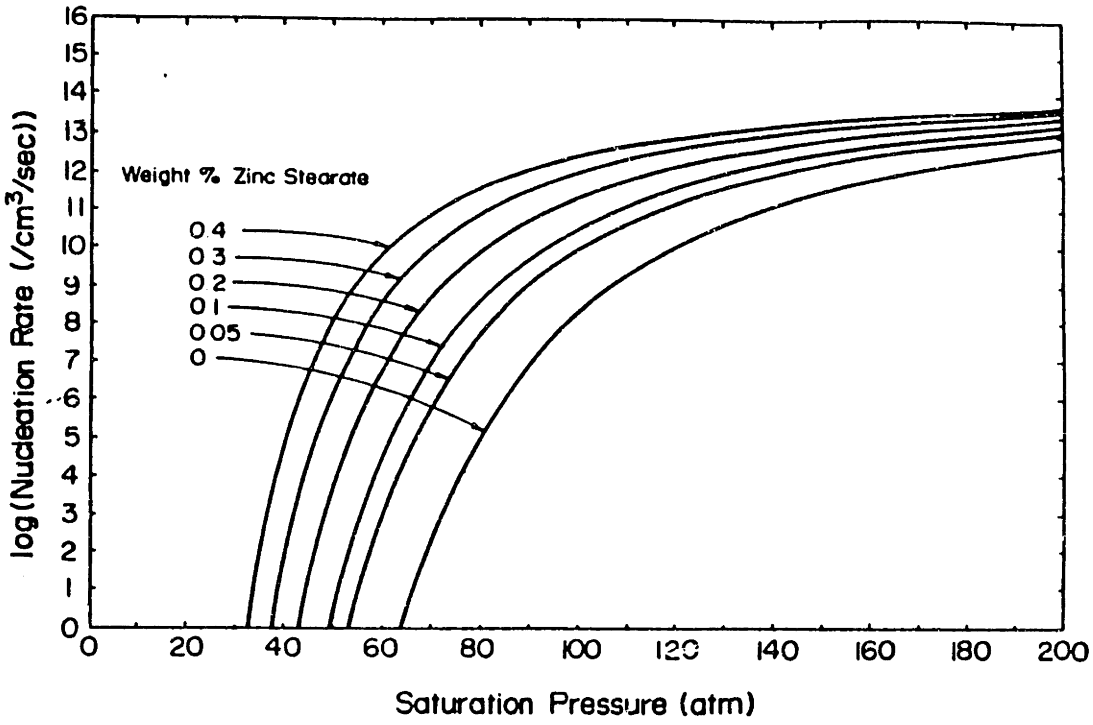

Figure 5.2-3. Homogeneous nucleation rate as a function of saturation pressure. (from Colton, 1985)

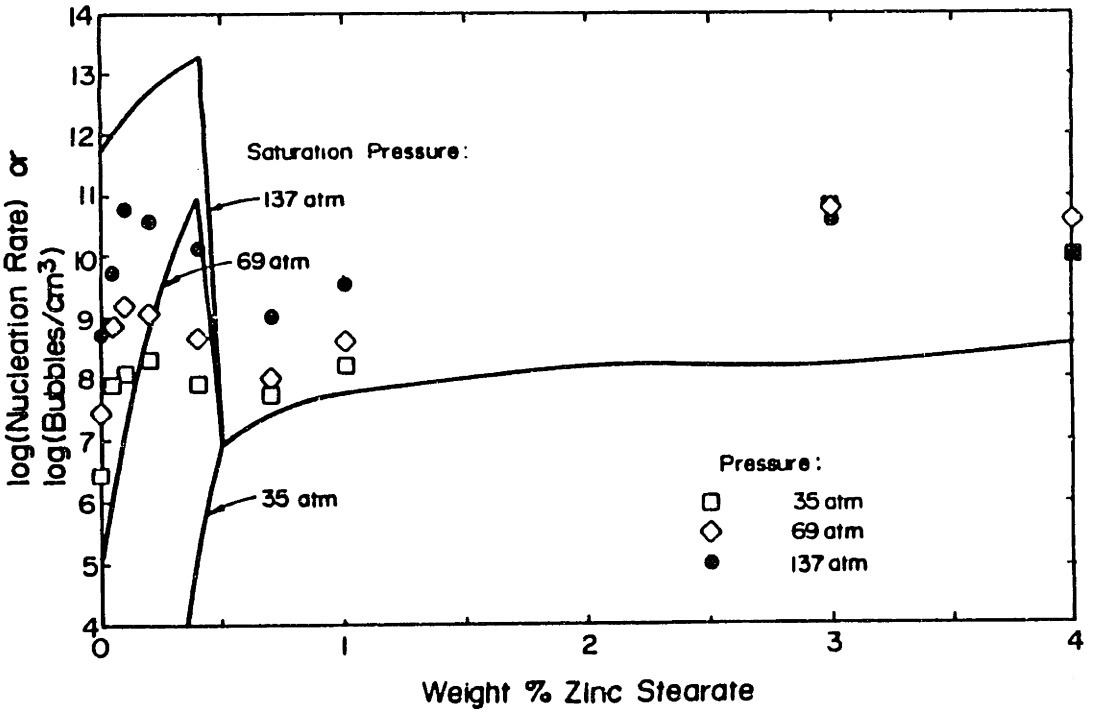

Figure 5.2-4. Comparison of calculated nucleation rate to the experimentally determined cell densities at different saturation pressures. (from Colton, 1985)

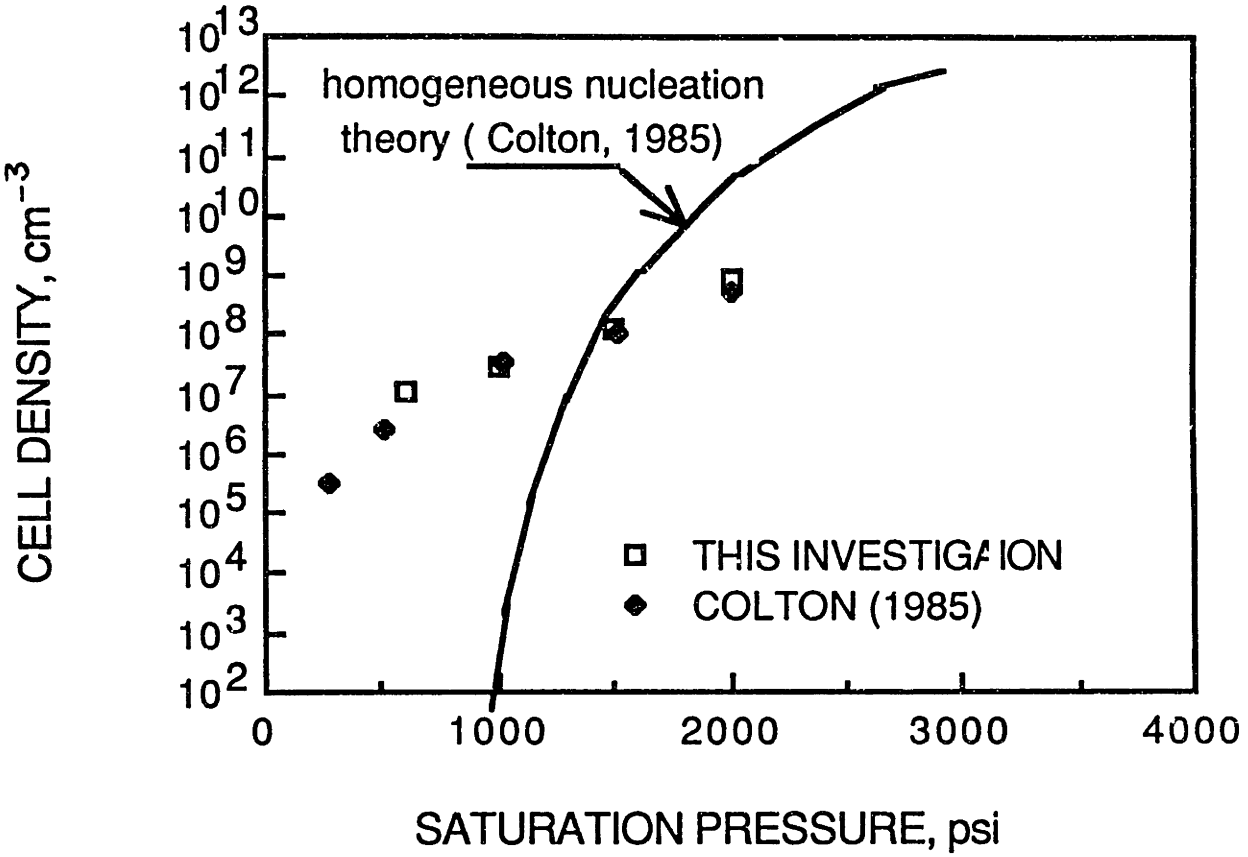

Figure 5.2-5. Comparison of homogeneous nucleation theory and experimental results. (1000 psi = 6.895 MN/m^2)

5.3. Control of cell structure

Background

The microstructure has two basic components, namely the cell nucleation density and the cell size distribution. In section 5.2 we saw how the cell nucleation density can be controlled. In this section we will investigate how to control the cell size distribution.

Once a cell nucleates, it can grow by diffusion of gas to it, or by pushing its boundaries out against the matrix. This is possible if the matrix modulus has sufficiently reduced at the temperature at which the cell growth is occurring. Also, since the plastic matrix is viscoelastic, a longer time will result in a larger cell size at a given temperature. Thus, the simplest way to control the cell size is by controlling the time and the temperature at which the growth is allowed to occur.

Another way to control the cell size could be, for example, by maintaining a suitable external pressure to prevent the cell growth. This pressure will have to be maintained till the plastic is cooled to a temperature below the glass transition temperature. An example of foam produced in this manner is shown in Fig. 5.3-1. A saturated polystyrene sample was placed in a press and pressurized to 350 psi. The sample was heated above Tg and then cooled to room temperature while still under pressure. This procedure produced the morphology shown in Fig 5.3-1(a). In a subsequent experiment, the external pressure was suddenly released while the plastic was still

above Tg. Spontaneous growth was observed in this sample, producing the structure shown in Fig 5.3-1(b).

An interesting feature of Fig. 5.3-1 is the difference in the general morphology in the two micrographs. In Fig. 5.3-1(a) the bubbles are basically apart and spherical. In Fig. 5.3-1(b), the cells have reached the maximum growth under the prevailing thermodynamic conditions, and attained a honeycomb-like structure. The cell geometry (i.e., spherical vs. polyhedral) may have important effect on certain foam properties, e.g. the impact strength. These structure-property issues, however, will not be further addressed in this study.

The above experiment has shown the possibility of using external pressure to control cell growth. However, time-temperature exposure is the more natural parameter to control the cell growth, and will be used in this study as a primary process variable.

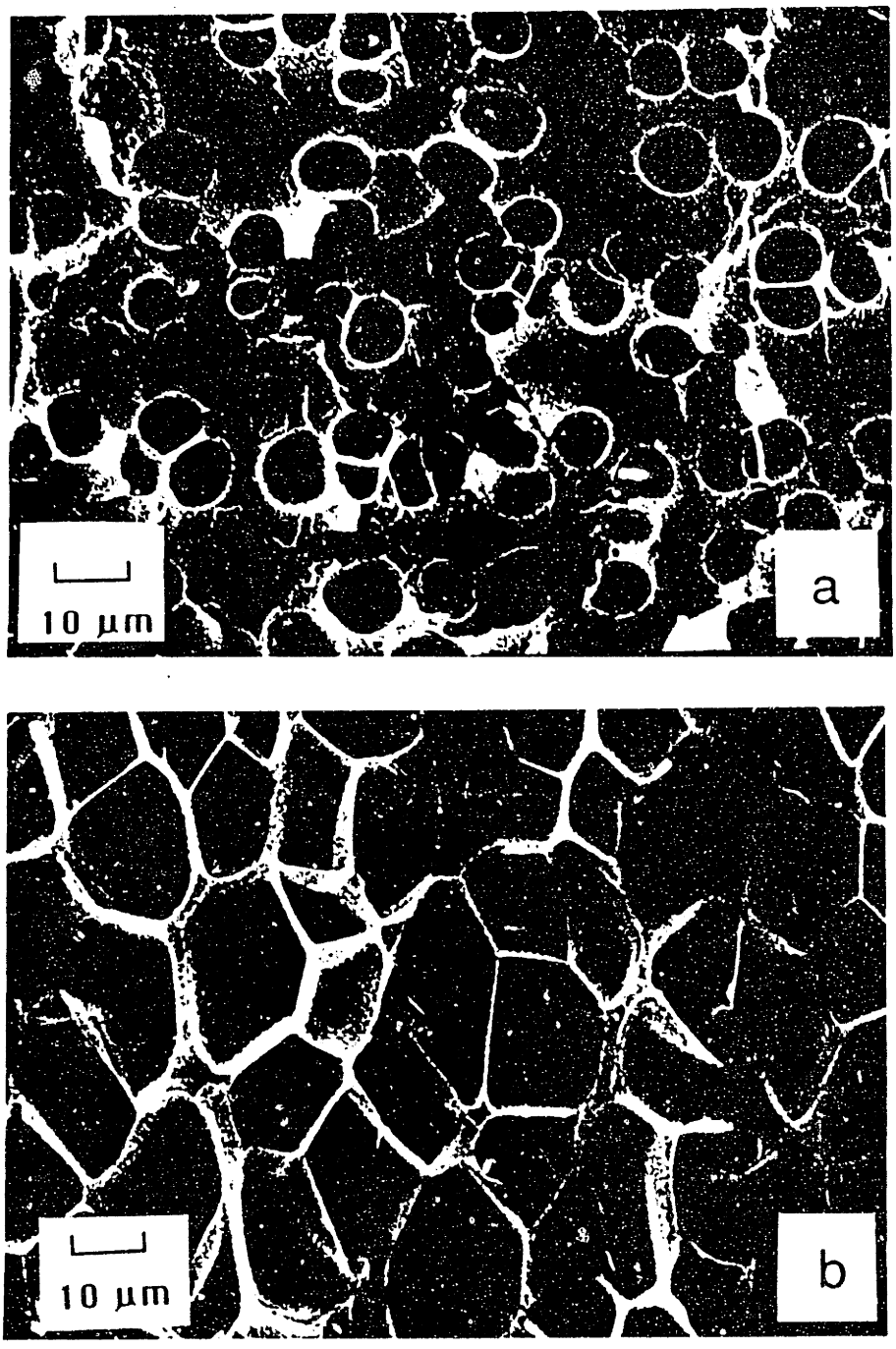

Figure 5.3-1. Scanning electron micrographs of polystyrene samples nucleated under external pressure. In (a), the pressure was maintained during the cooling cycle, while in (b), the pressure was suddenly released before cooing.

Experimental

To study the cell growth behaviour as a function of time, a number of disks were saturated at 2000 psi and foamed for different lengths of time in a glycerin bath maintained at 115 °C. After foaming, the sample was quenched in cold water. The foaming times varied from four seconds to four minutes. The samples were viewed under a scanning electron microscope (SEM) and cell size and cell density were determined. In addition, the density of each sample was measured in order to determine the change in void fraction as a function of time.

Results on cell growth

Fig. 5.3-2 shows a photograph of the samples. The time for which the sample was immersed in the glycerin bath is indicated under each sample. We see that up to about six seconds the samples are essentially clear. At ten seconds the sample has turned fully white indicating complete nucleation of bubbles. However, at ten seconds of foaming there is no significant change in the size of the disks. As we foam for longer periods of time, the thickness and size of the disk increases. We seem to reach the limiting (maximum) cell growth after about two minutes of foaming as there is no significant difference in the size of the disks foamed for two minutes and four minutes respectively.

In Fig. 5.3-3 we have reproduced micrographs from each of the foamed samples. Note that all micrographs were taken at the same magnification (1000 X)in order to enable a visual comparison of cell structure at different foaming times. We see that initially (till

a foaming time of 20 sec.) the cells are spherical and apart from each other. As growth proceeds, the cells begin to touch each other and loose the spherical shape. With further growth, a honeycomb-like structure develops, and a certain amount of coalescence of cells takes place as lower energy configurations are sought by the foam.The cell structure appears to stabilize after, say, 60 seconds of foaming as there is little difference in the structure after this time (see micrographs (h) through (k) in Fig. 5.3-3).

The average cell diameter has been plotted in Fig. 5.3-4 as a function of foaming time. The 10 μm size is reached in about 20 seconds . We see that the cells grow to a size of about 14 μm after two minutes of foaming. and further foaming from two to four minutes does not produce an appreciable increase in the cell size.

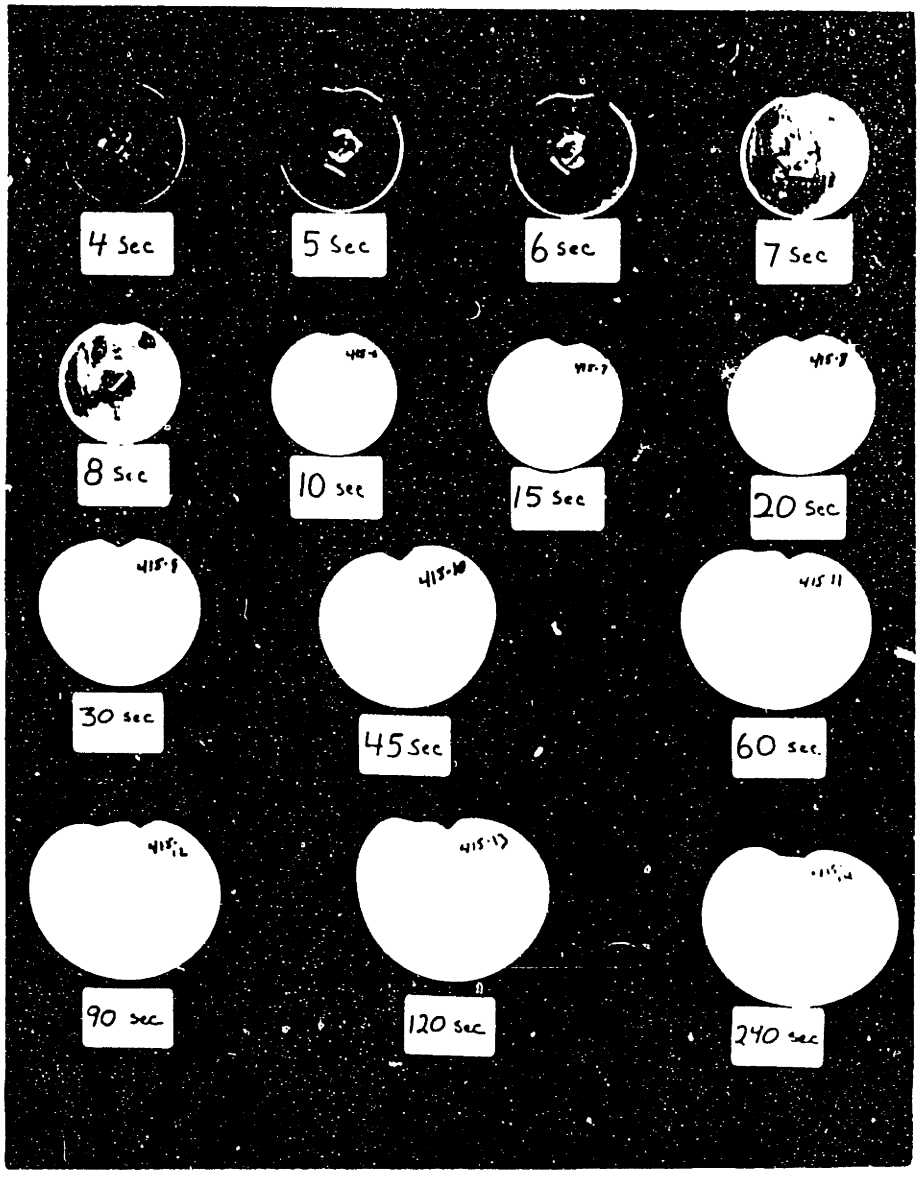

Figure 5.3-2. Photograph of polystyrene samples foamed for different lengths of time. at 115 C.

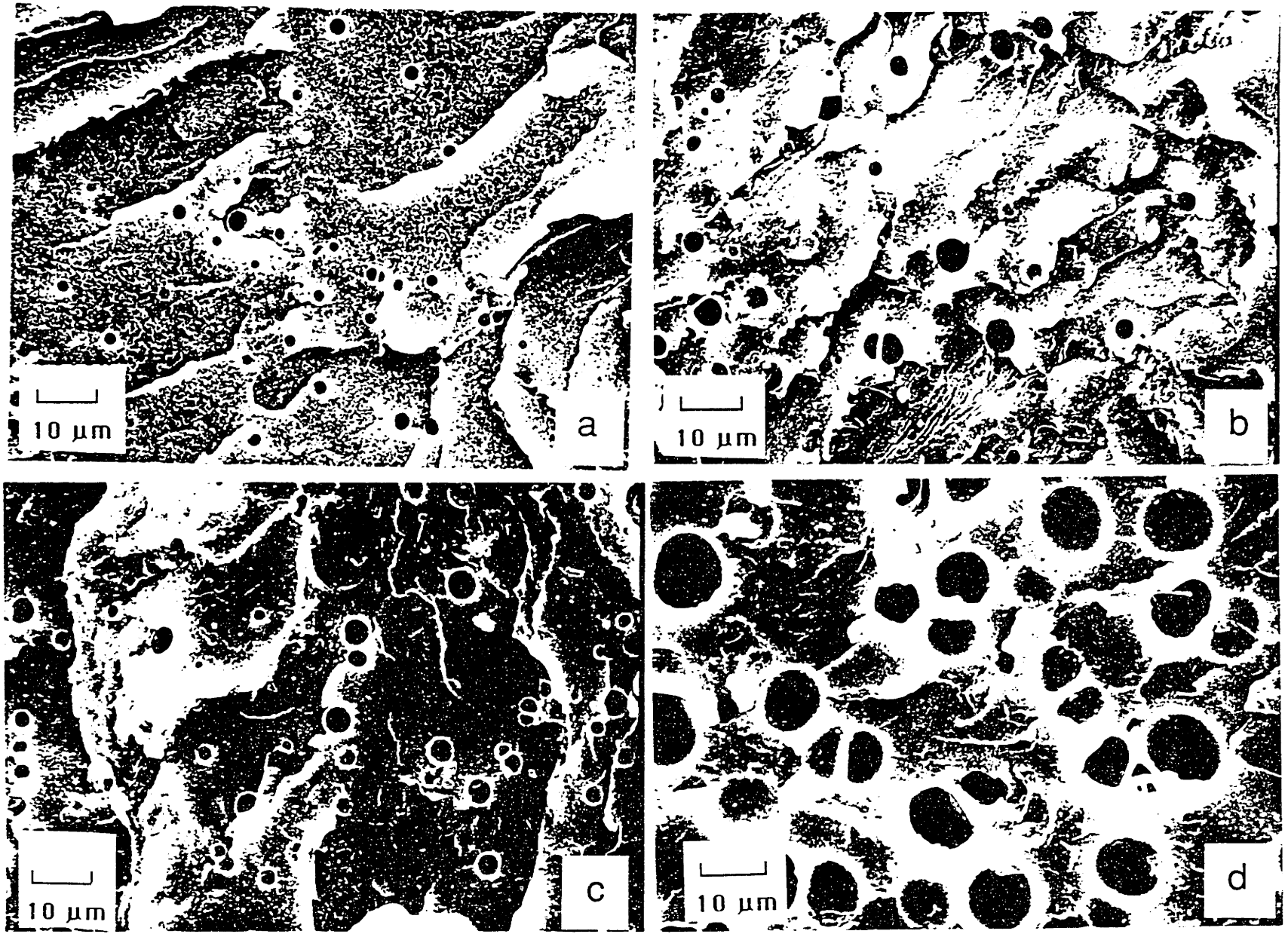

Figure 5.3-3. Scanning electron micrographs showing cell structure at increasing foaming times. (a) 7 sec; (b) 8 sec; (c) 10 sec; and (d) 15 sec.

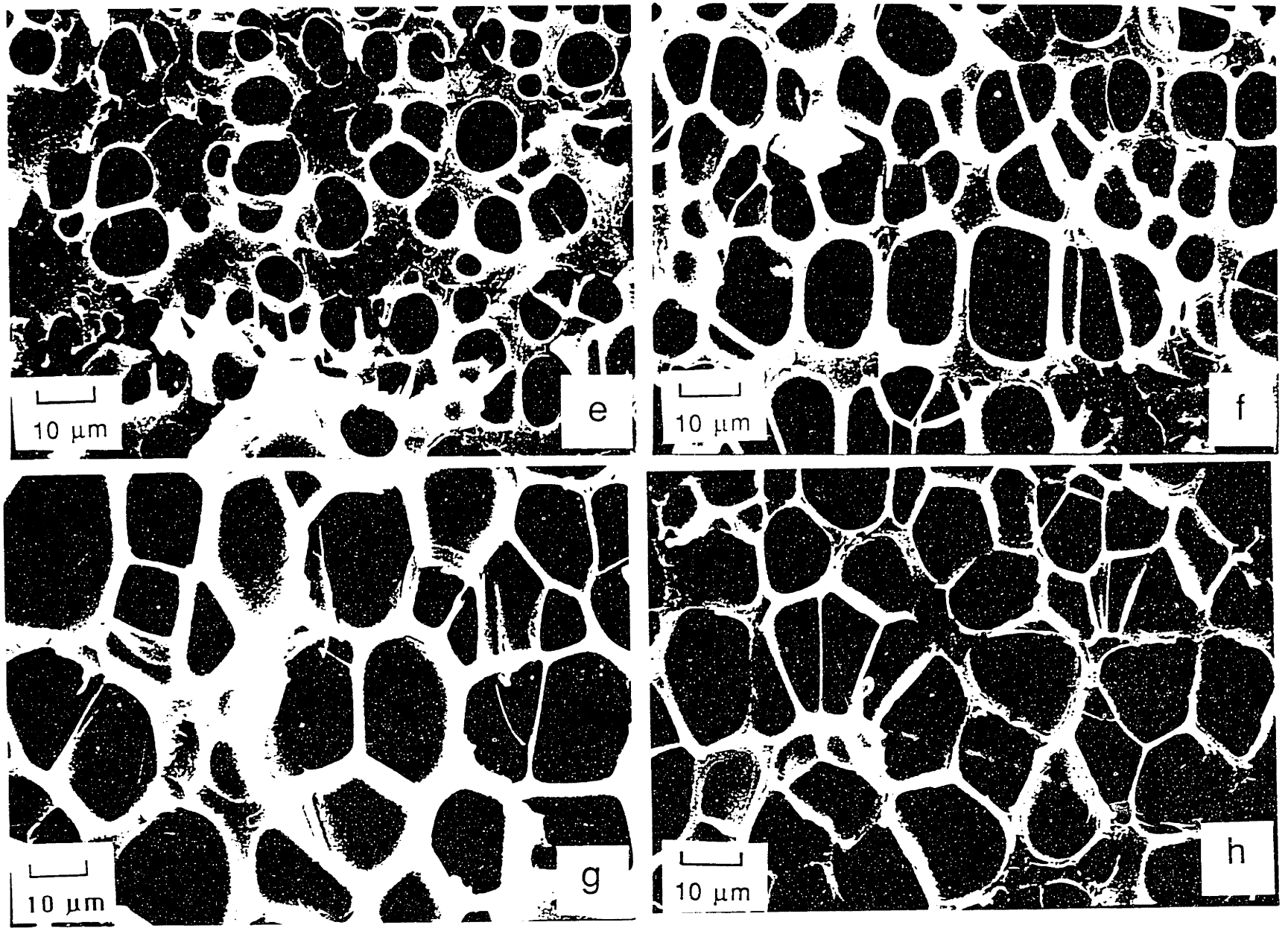

Figure 5.3-3 (continued). Scanning electron micrographs showing cell structure at increasing foaming times. (e) 20 sec; (f) 30 sec; (g) 45 sec; and (h) 60 sec.

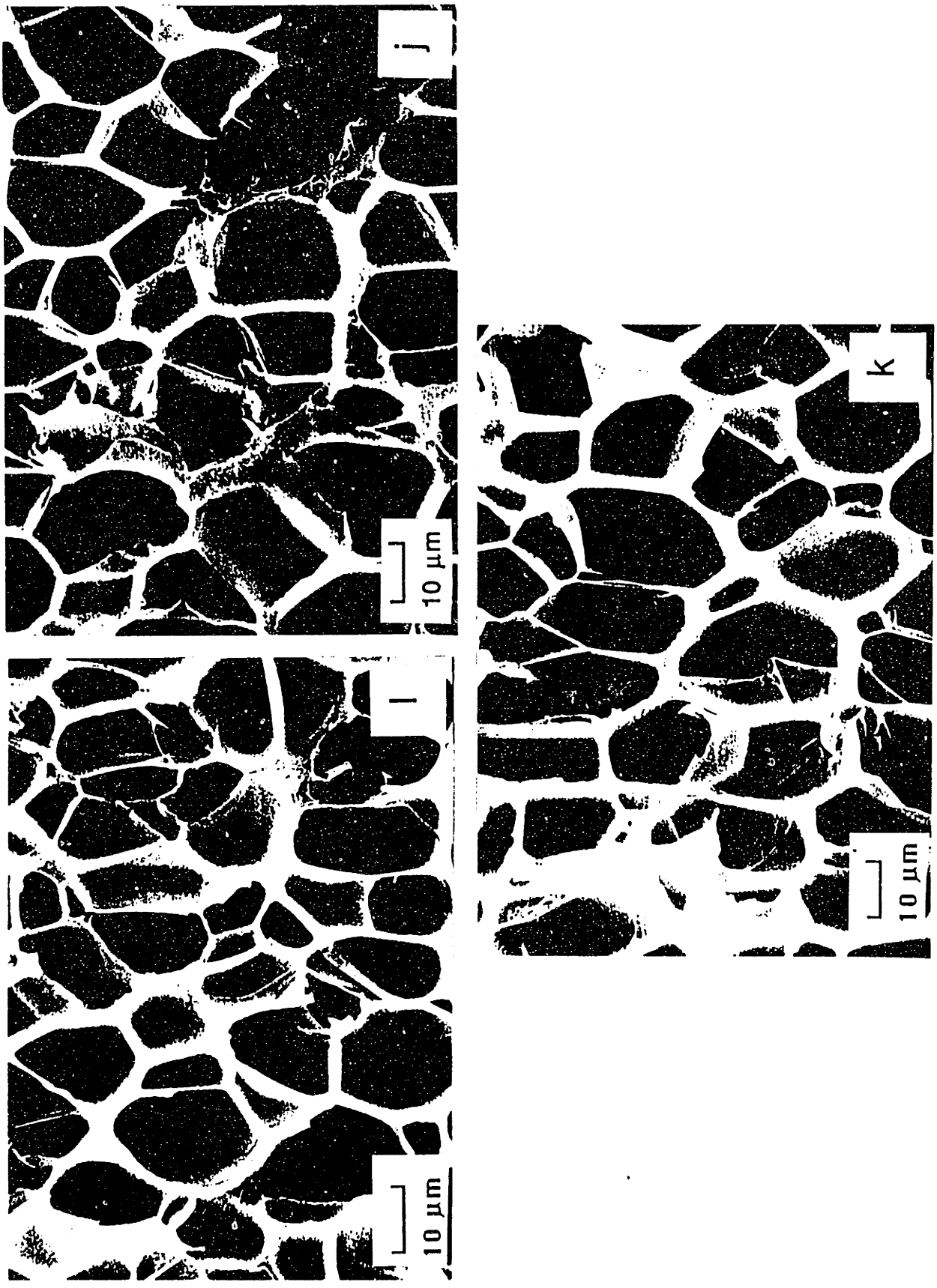

Figure 5.3-3 (continued). Scanning electron micrographs showing cell structure at increasing foaming times. (i) 90 sec; (j) 120 sec; and (k) 240 sec.

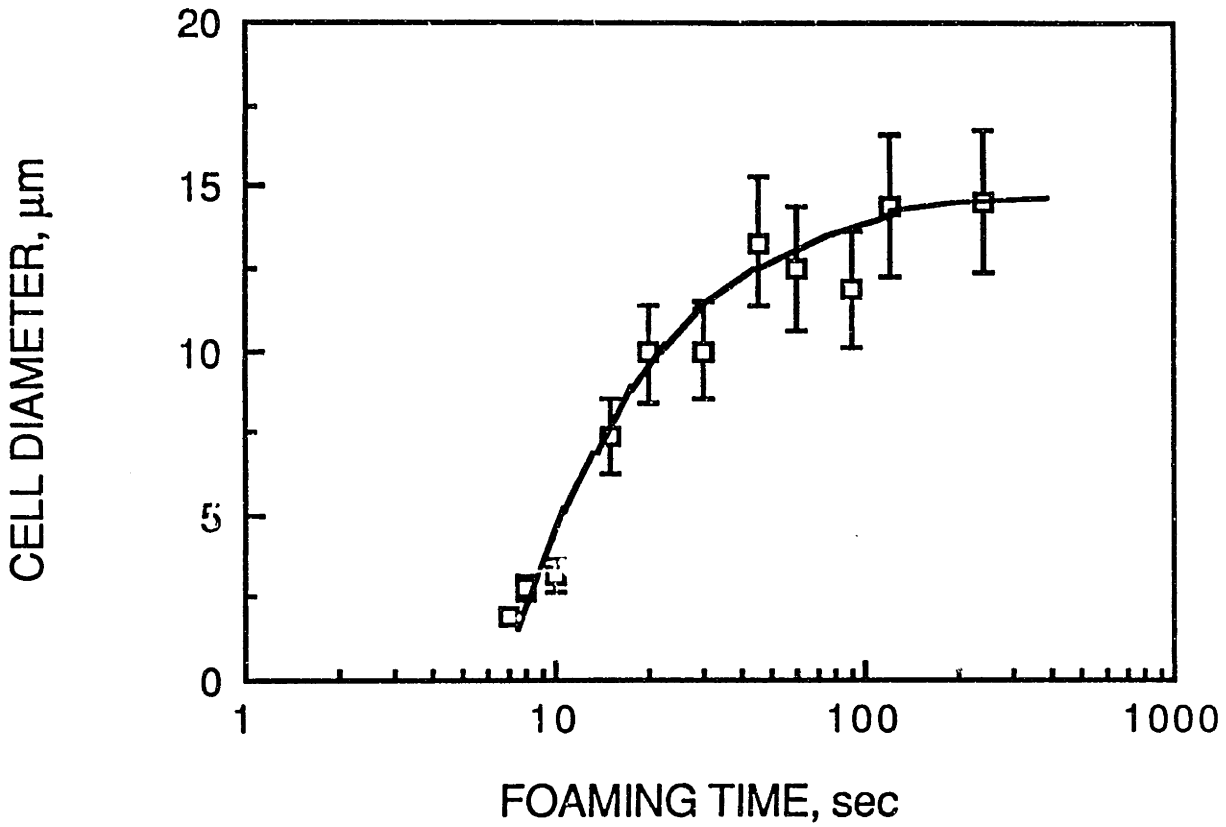

Figure 5.3-4. Growth in average cell size as a function of time.

Results on void fraction

The foam density and void fraction (computed from foam density measurements) have been plotted in Fig. 5.3-5. We see that the density has reduced from 1.05 g/cm^3 for unfoamed polystyrene to 0.2 g/cm^3 for the fully foamed samples. The corresponding void fraction of 0.82 was reached after four minutes of foaming. The maximum void fraction obtainable based on nitrogen absorbed at 2000 psi (13.8 MPa) and a foaming temperature of 115°C is 0.84. Thus we have experimentally obtained a void fraction very close to the maximum theoretical void fraction, showing that there is no significant loss of nitrogen in the process.

In Fig. 5.3-6 we have cross-plotted void fraction as a function of average cell diameter. At small cell sizes, say below 5 μm, the void fraction is negligible. If we impose a target cell size of 10 μm on the process, then a void fraction in the 0.5 to 0.6 range can be achieved.

One of the most significant results from this experiment is that a very high void fraction of 0.82 was achieved with average cell size still under 15 microns. Previously the highest void fraction was reported to be in the 0.25 to 0.30 range (Martini, et al., 1984). This experiment shows that much larger void fractions are possible while still maintaining a microcellular structure. This, of course, is made possible by nucleating a very large number of cells.

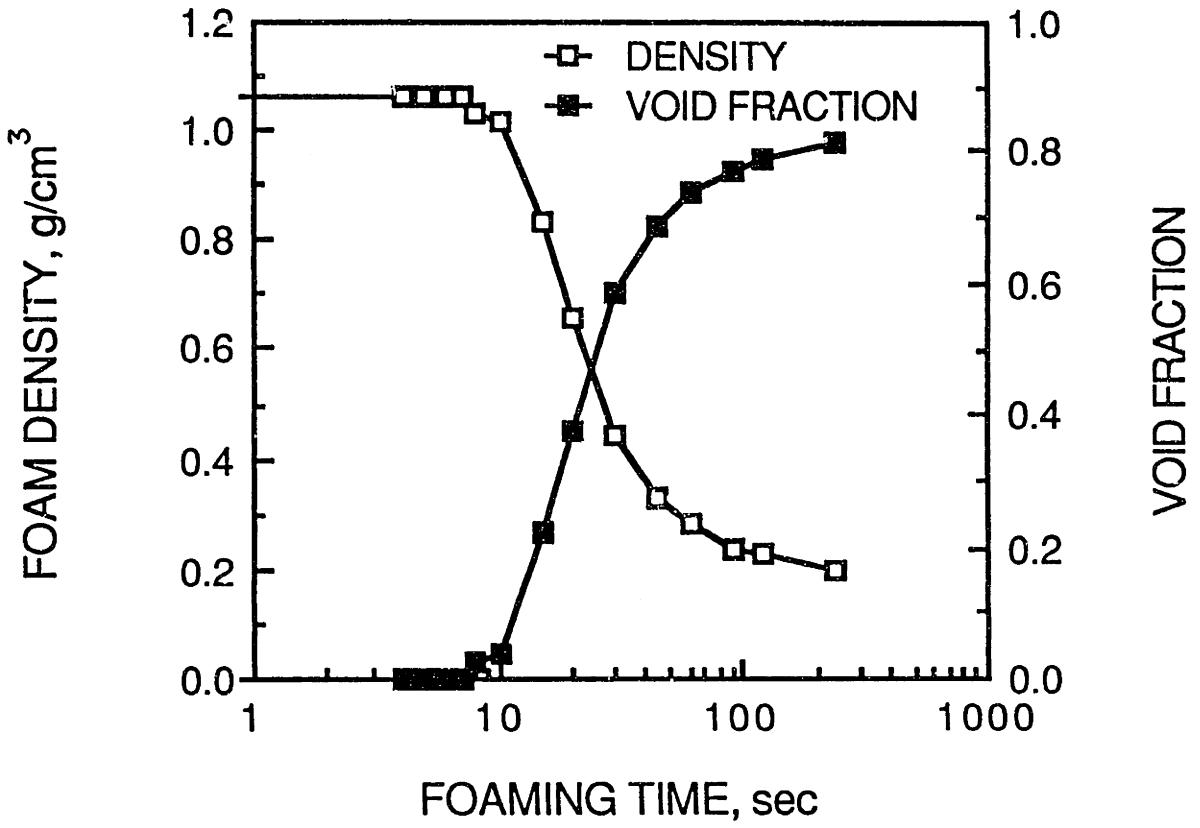

Figure 5.3-5. Foam density and void fraction as a function of time

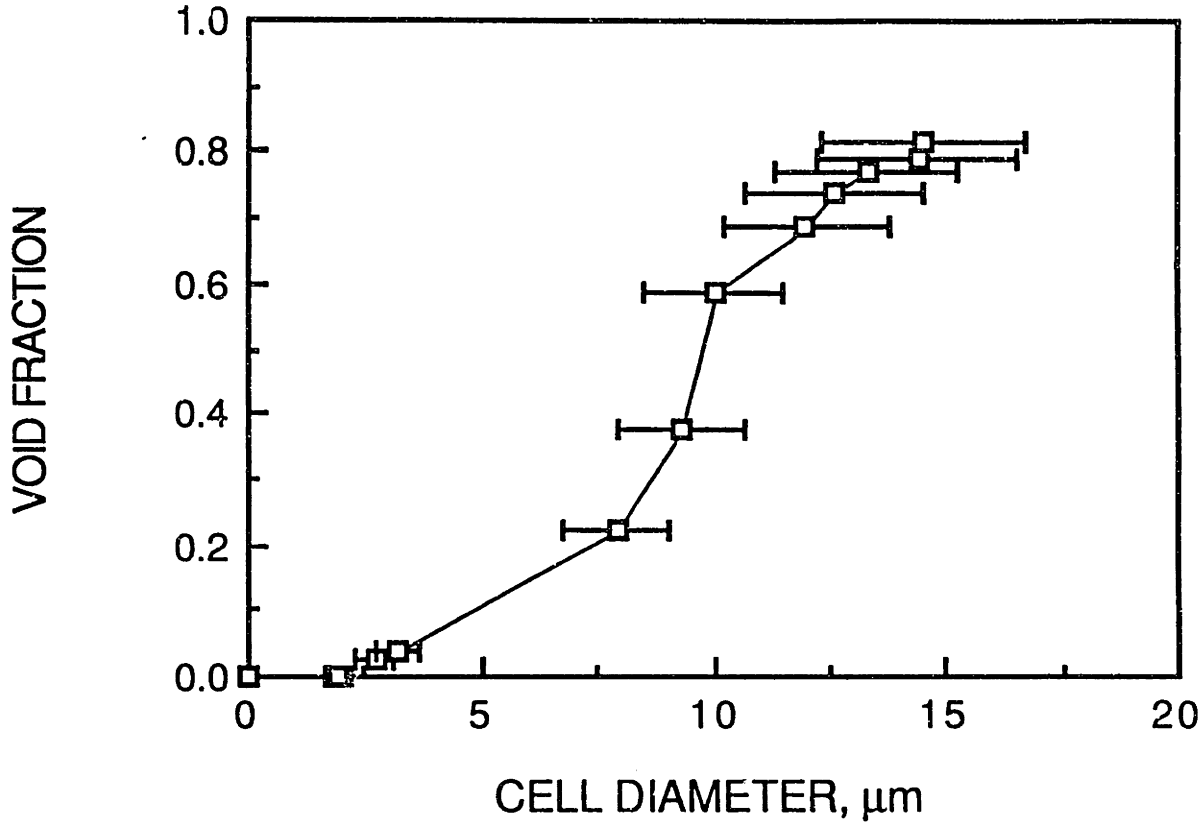

Figure 5.3-6. Void fraction as a function of average cell size.

6.0 DETERMINATION OF FUNCTIONAL COUPLING IN THE PROCESS

A number of experiments were carried out in order to study the extent of coupling between the different functional requirements. Such coupling can come about, for example, if one of the process variables affects more than one functional requirements. In general, in a design problem with many functional requirements, one has to make a judgement on whether the extent of coupling can be neglected for the purpose at hand. In order to make a rational judgement on the significance of coupling that may exist, an acceptable tolerance has to be stated for each functional requirement. If for a given FR the system response (system here refers to the particular design being evaluated) is within the acceptable limits when the design parameters vary over their intended range, then any coupling can be neglected for constructing the design matrix and the off diagonal terms corresponding to that FR can be taken to be zero.

In this chapter a number of experimental results are reported. The purpose these experiments is to determine the extent of coupling that exists between the process variables and the functional requirements. An attempt has been made to understand the physics involved, and where possible, a physical model has been proposed to explain the experimental results.

6.1 Effect of saturation pressure on cell size

The gas saturation pressure is a primary process variable. Its main function is to control the cell nucleation density. However we are concerned with any coupling that saturation pressure might cause between the functional requirements of high cell density and small cell size. As we have seen in section 5.2, high saturation pressures are needed to get high cell nucleation rates. For a given concentration of gas, the bubble size will be smaller when the number of cells nucleated is large. On the other hand, high saturation pressures will also tend to create large bubbles since the dissolved gas volume increases at higher saturation pressure Thus there is a possibility of coupling between the functional requirements of high cell density and small cell size. We will address this issue in this section.

6.1.1. A semiempirical model for cell size prediction

Consider one gram of polymer that is saturated with a gas at temperature T_S and a pressure P_S . The amount of gas dissolved in the polymer is given by Henry's Law (Durrill and Griskey, 1969):

$$C = H P_s \qquad (6.1\text{-}1)$$

where C = gas concentration at saturation, cm^3 (STP)/g of polymer,

H = Henry's Law Constant for the gas-polymer system, cm^3(STP)/g atm,

P_S = gas saturation pressure, atm.

The volume that the dissolved gas would occupy at saturation condition is:

$$V_s = C \left(\frac{P_0}{P_s}\right) \left(\frac{T_s}{T_0}\right) \qquad (6.1\text{-}2)$$

where T_0 and P_0 refer to the standard conditions. Upon substituting for C from Eq. 6.1-1, we get,

$$V_s = H \left(\frac{T_s}{T_0}\right) \qquad (6.1\text{-}3)$$

where we have used the fact that p_0 = 1.0 atm. Note that if saturation occurs at T_0 (i.e., 20 °C), then the volume occupied by the dissolved gas at saturation per gram of polymer is simply equal to the Henry's Law constant expressed in cm^3.

Now assume that the saturated plastic is foamed at a constant temperature T_2 at atmospheric pressure. Assuming ideal gas behavior, the volume occupied by the dissolved gas at foaming temperature is:

$$V_2 = H P_s \left(\frac{T_2}{T_0}\right) \qquad (6.1\text{-}4)$$

Equation 6.1-4 shows that the dissolved gas volume at foaming temperature goes up linearly with the gas saturation pressure. The bubble size, however, depends on the number of bubbles present.

Let N_0 be the number of bubbles nucleated per cm^3 of unfoamed plastic. If d_0 is the density of the unfoamed plastic, then the number of bubbles nucleated is one gram of plastic, N_0', is

$$N_o' = \frac{N_0}{d_0} \qquad (6.1\text{-}5)$$

Let us assume that all bubbles have the same diameter d. Then equating the volume occupied by bubbles to RHS of Eq. 6.1-4 gives:

$$d^3 = \left(\frac{6 H d_0}{\pi N_0}\right) \left(\frac{T_2}{T_0}\right) P_s \qquad (6.1\text{-}6)$$

The data in Fig. 5.2-2 shows that the cell density N_0 increases exponentially with saturation pressure, i.e.

$$N_0 = A e^{\alpha P_s} \qquad (5.2\text{-}1)$$

where A and α are empirical constants. Substituting for N_0 in Eq. 6.1-6 gives

$$d^3 = \left(\frac{6 H d_0}{\pi A}\right) \left(\frac{T_2}{T_0}\right) P_s e^{-\alpha P_s}$$

or

$$d = \left(\frac{6 H d_0 T_2}{\pi A T_0}\right)^{\frac{1}{3}} P_s^{\frac{1}{3}} e^{-\frac{\alpha P_s}{3}} \qquad (6.1\text{-}7,\ 8)$$

Equation 6.1-8 shows the effect of saturation pressure, P_s on average cell size D. Due to the exponential increase in the number of

cells nucleated, the cell size is expected to decrease as the saturation pressure is raised.

Experimental

To investigate the effect of gas saturation on cell size, polystyrene disks were saturated at different nitrogen pressures, and allowed to foam in the glycerin bath at 115 °C for a sufficiently long time in order to develop the limiting (maximum) void fraction. The average cell size was obtained from the scanning electron micrographs of the samples.

Results and discussion

The average cell size in the fully foamed samples (i.e., having achieved the maximum cell growth) of this experiment has been plotted in Fig. 6.1-5 as a function of nitrogen saturation pressure. The theoretical line is a plot of Eq. 6.1-8. There is good qualitative agreement between the model and the experimental results. The model seems to consistently predict a higher cell size for a given saturation pressure. This is due to two main reasons. First, the model assumed that all cells were of equal size. In reality we have a distribution of sizes. The cells that are larger than the average size in fact contribute much more to the volume occupied by the cells since the cell volume is proportional to the cube of the cell diameter. Second, we assumed that there is no loss of nitrogen in the process and all the dissolved gas is converted into bubbles. Certain amount of gas, however, does diffuse out of the sample before it is foamed.

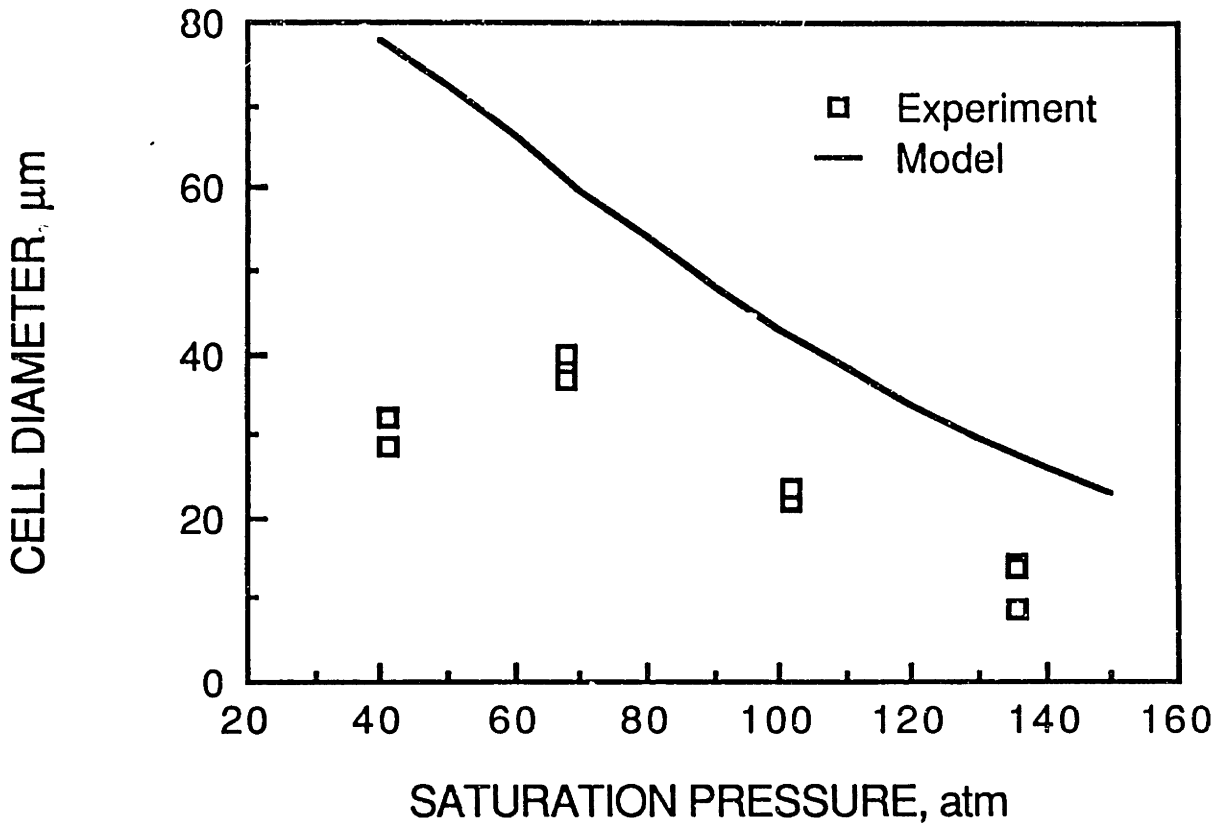

Figure 6.1-1. The effect of nitrogen saturation pressure on the average cell size-- comparison of the theoretical model with experiment.

The average cell size is seen to decrease with increase in saturation pressure. The average bubble volume is equal to the available gas volume divided by the number of bubbles nucleated. As saturation pressure is raised, the total volume occupied by voids increases in proportion to the saturation pressure. However, due to the exponential increase in the number of cells, the average volume occupied by an individual cell in fact decreases as the saturation pressure is raised. Therefore, the saturation pressure does not cause an undesirable coupling between cell density and cell size, and consequently coefficient a_{21} in Eq. 2.2-3 can be taken to be zero.

Corrections Applied To The Model

1. Correction for Lost Gas

The model represented by Eq. (6.1-8) assumes that all the nitrogen dissolved comes out during foaming and shows up in bubbles. In the experiments reported in Fig. 6.1-1, there was typically a fifteen minute time lapse from the time a polystyrene disk was removed from the pressure vessel to the time it was foamed. We can estimate the amount of nitrogen that diffuses out of the polystyrene disk during this time as follows.

Consider a plane sheet of thickness l that is initially at a uniform concentration C_0. If the surfaces are kept at a constant concentration C_1 (corresponding, in our case, to the gas concentration at atmospheric pressure), the solution to the diffusion equation may be approximated by

$$\frac{M_t}{M_\infty} = 1 - \frac{4}{\pi}\left(\frac{Dt}{l^2}\right)^{\frac{1}{2}} \qquad (6.1\text{-}9)$$

for early stages of desorption (Crank, 1956, § 11.6).

Here M_t is the amount of gas left in the disk at time t, and M_∞ is the equilibrium sorption of gas that existed before desorption started. It is assumed that the diffusion process is characterized by a constant diffusion coefficient D.

For l = 0.173 cm, D = 4 x 10^{-8} cm^2/sec, and t = 900 sec, we get M_t/M_∞ = 0.92. Thus approximately 8% of nitrogen that dissolved in the pressure vessel is lost prior to foaming in our experiments.

2. Correction for Distribution of Cell Sizes

In our simple model leading to Eq. 6.1-8 we had assumed that all bubbles had a diameter d. The predicted average diameter d (based on a uniform cell size assumption) was compared to the experimentally obtained average diameter in Fig. 6.1-1. In reality we have a distribution of bubble sizes. Since the bubble volume is proportional to the cube of the diameter, the bubbles larger than the average d contribute significantly more to the occupied void volume than is accounted for by the term (πD^3/ 6) in Eq. 6.1-6.

Let $d^* = \beta\ d$ represent an effective average cell diameter such that (πd^{*3}/6) represents the average volume occupied by a cell. Then if there are N_f bubbles per cm^3 of foam, the volume occupied by the bubbles per cm^3 of foam is:

$$v_f = \left(\frac{\pi \bar{d}^{*3}}{6} \right) (N_f) \qquad (6.1\text{-}10)$$

Here, V_f is the void fraction for the foam.

To determine the correction factor β we may assume, say, a Gaussian distribution for the cell size distribution with a certain variance of s^2. The volume-average diameter d^* can then be related to average cell diameter d as a function of s^2. However, we will need to establish the variance in cell size distribution experimentally.

We used the following alternative procedure. d^* and d were measured experimentally, and the ratio d^*/d established β. Polystyrene sample was foamed for a sufficiently long time until the maximum cell growth was realized. The void fraction in the sample was determined by measuring the foam density. The average cell size d and cell density in the foam N_f was determined from the scanning electron micrographs of the sample.

The average cell volume was now determined from

$$\left(\frac{\pi \bar{d}^{*3}}{6} \right) = \frac{v_f}{N_f} \qquad (6.1\text{-}11)$$

using the experimental values for V_f and N_f, from which the volume-average diameter d^* was calculated. The ratio of d^* thus obtained

and the previously determined d (from micrographs) gave the factor β.

This procedure was used for the two polystyrene samples showing matured growth in the cell growth experiment, foamed for two minutes and four minutes respectively (refer to section 5.3 and Figure 5.3-4), giving β = 1.419 and 1.416 respectively (See Table 6.1-1). A value of 1.42 was chosen to represent the effect of distribution of cell sizes.

When the above two corrections are applied to the model, the net result is a multiplication of the RHS of Eq. 6.1-8 by 0.68. A much closer agreement is now seen between the predicted and observed average cell diameters as a function of saturation pressure. This comparison is shown in Figure 6.1-2. The significant conclusion is that the average cell diameter goes down as the saturation pressure increases, showing that there is no coupling between cell size and cell density on account of the saturation pressure.

Table 6.1-1

Summary of Calculations for β

Sample	d (μm)	N_f (cm^{-3})	v_f (measured)	d^* (μm)	β
1	14.4	1.96×10^8	0.788	20.44	1.419
2	14.5	1.94×10^8	0.816	20.53	1.416

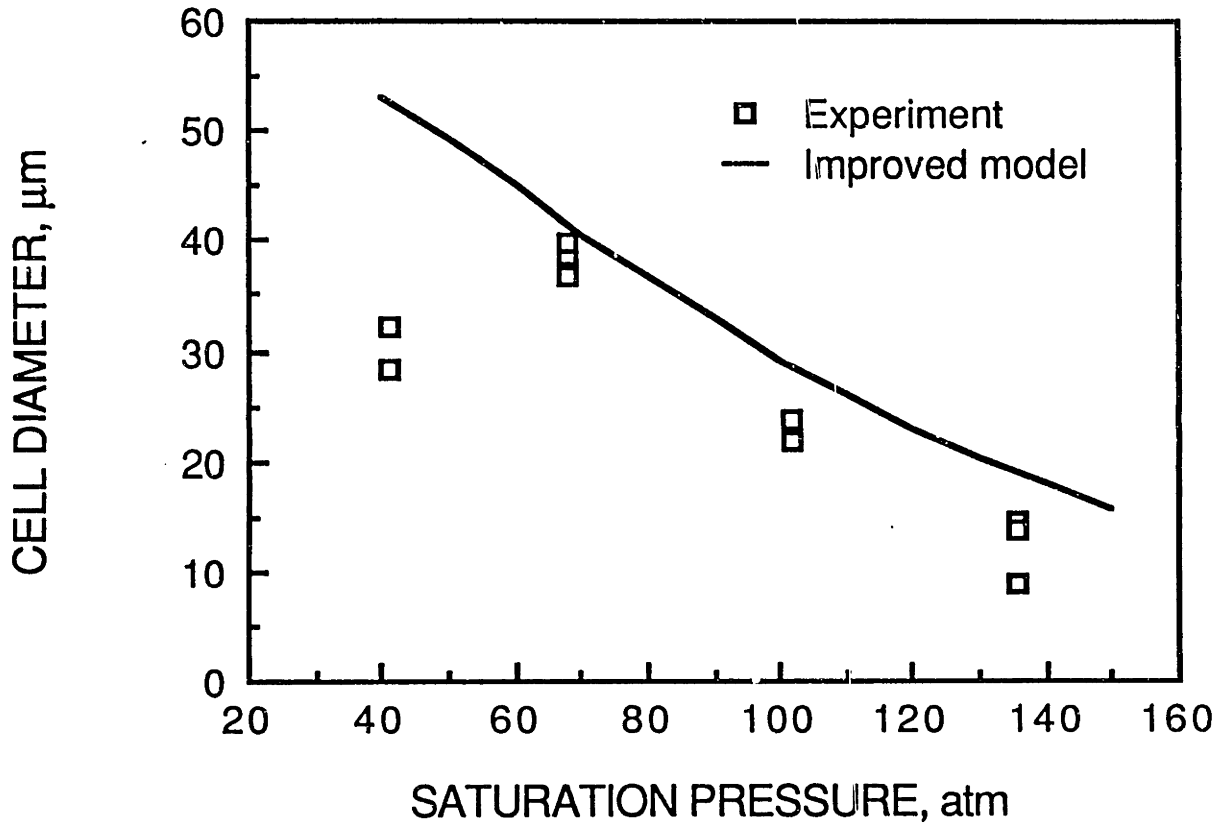

Figure 6.1-2. The effect of nitrogen saturation pressure on the average cell size-- comparison of the improved model with experiment.

6.2 Effect of time-temperature exposure on cell nucleation

6.2.1 Effect of temperature

Background

The homogeneous nucleation rate is given by:

$$N_{HOM} = f_0 C_0 \exp\left[\frac{-\Delta G^*}{kT}\right] \qquad (3.3\text{-}1)$$

From Eq. 3.3-1 we expect Arrhenius type dependence of cell density on temperature. From a process standpoint we are interested in knowing at what temperature does the polystyrene disk begin to nucleate as it is heated from below T_g (typically starting at room temperature where the disk is saturated with nitrogen) to a temperature above Tg. Previous researchers (Martini ,1981, Waldman, 1982, and Colton , 1985) used an oven pre-heated to a temperature above Tg (typically 10 °C above Tg) in which the saturated disk was foamed, and did not address the question "at what temperature does nucleation begin".

Experimental

In order to determine the effect of temperature on cell nucleation density and the temperature at which nucleation began, the following experiment was conducted. A number of disks were saturated at 2000 psi. The glycerin bath was heated to 80 °C. A sample was immersed in the bath for one minute and observed. The

temperature of the bath was then raised by one or two degrees.C and allowed to equilibrate. Then another saturated disk was immersed for 60 sec. and its foaming behavior was observed. This procedure was continued till the bath temperature reached 120 °C The foamed samples were studied under a scanning electron microscope and the cell density was determined for each sample.

Results and discussion

Figure 6.2-1 shows a photograph of various samples in the experiment. The temperature at which the sample was foamed is indicated under the sample. All samples were held in the bath for 60 sec. with the exception of samples 6A and 7A which were foamed for 20 sec.in order to get an accurate cell density count at the higher temperatures. The samples below 90 °C are not included in the photograph as they were all "clear", showing no signs of nucleation. The most interesting observation in Fig 6.2-1 is the *sudden* appearance of bubbles at 92 °C. Note that at 91 °C the disk is clear showing no nucleation. At 92 °C, it has become somewhat cloudy showing that cells have nucleated and are large enough to scatter light i.e., are one-half micron or larger. At 93 °C,the sample is cloudy and whiter that at 92 °C, implying the cells are somewhat bigger.

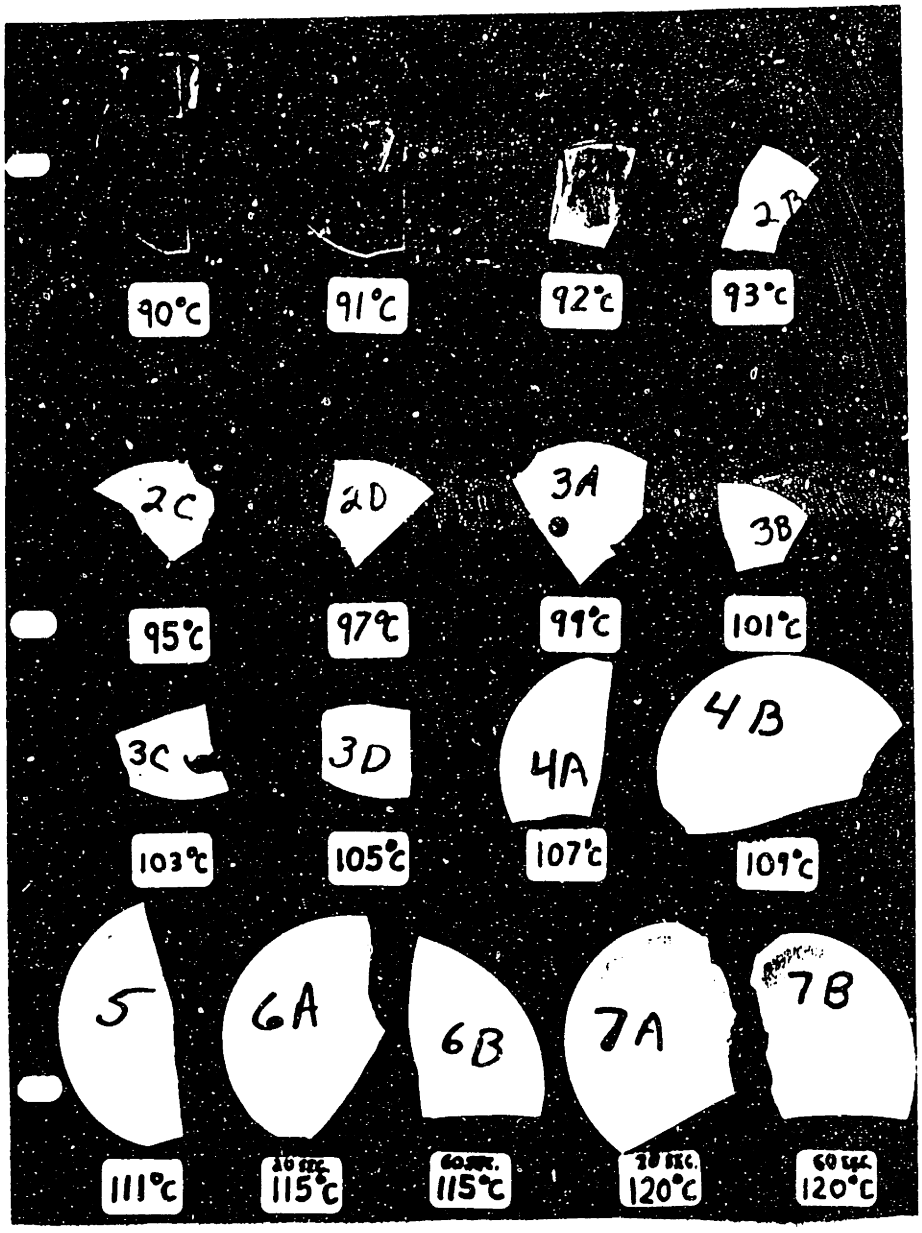

Figure 6.2-1. Photograph of polystyrene samples foamed at different temperatures. Note that samples at 90 C and 91 C are clear, showing no nucleation, while the sample at 92 C has become cloudy-- a visual sign that nucleation has occured.

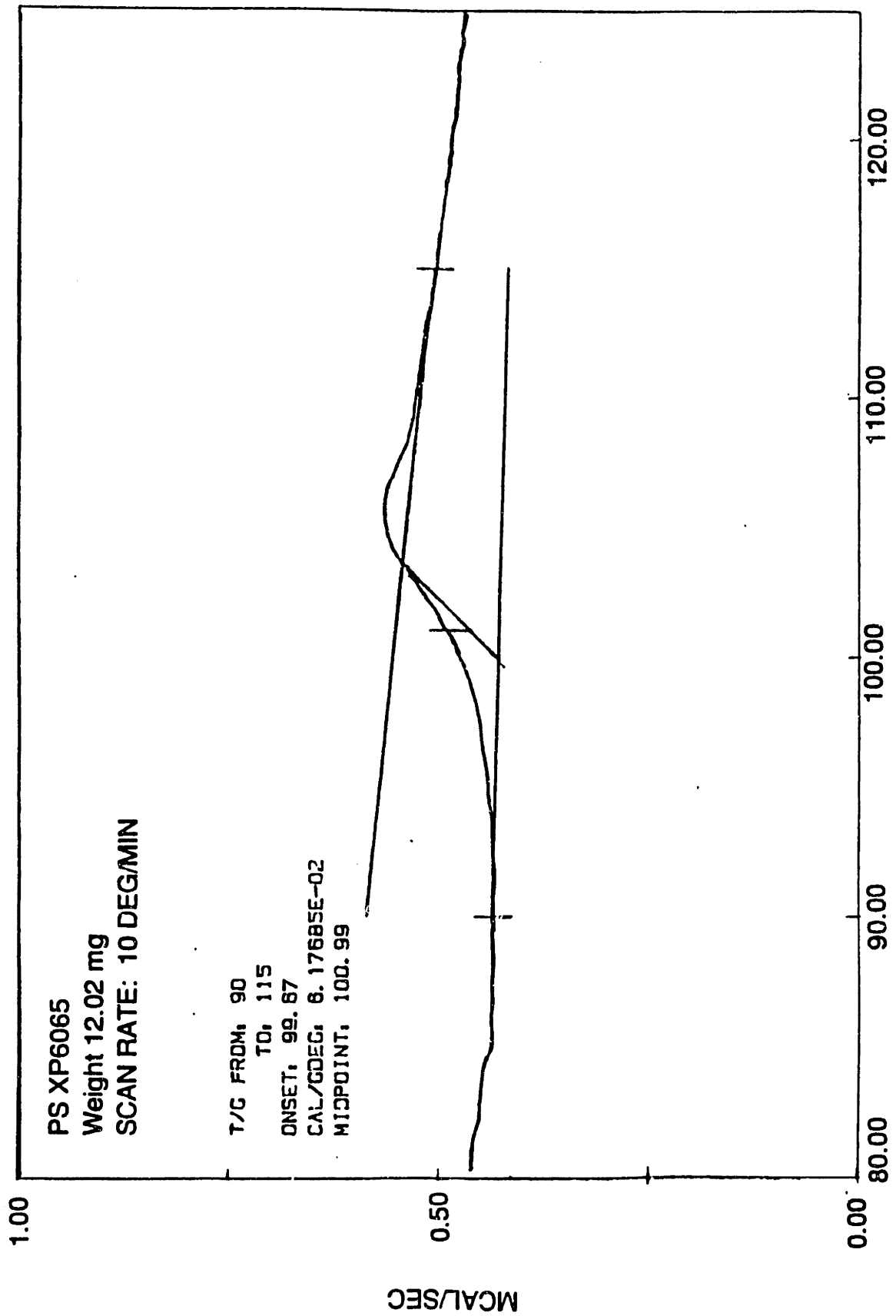

Figure 6.2-2. Differential Scanning Calorimetry results on DOW 6065 polystyrene. Note that the first signs of thermal mobility appear near 92°C, the temperature at which nucleation is first seen to occur in Fig. 6.2-1.

The cell density at 92 °C was determined to be 270 million bubbles per cm^3, while cell density at 102 °C, the glass transition temperature for DOW 6065, (Colton ,1985, page 161) was found to be 340 million bubbles per cm^3. This shows that full nucleation has occurred at 92 °C.

To investigate the phenomena around 92 °C we performed differential scanning calorimetry (DSC) on DOW 6065 at a low scanning rate of 10.°C per minute. The DSC result are shown in Fig. 6.2-2. Note that the first signs of thermal mobility in the polymer occur near 92..°C, although the glass transition temperature defined at the midpoint of the transition range occurs at 101 °C. .This suggests that the cell nucleation occurs as soon as the polymer molecules begin to move in the matrix, allowing the excess gas to precipitate in the free volume pockets.

The cell density has been plotted in Fig. 6.2-3 as a function of temperature. The effect of temperature is more clearly seen in Fig 6.2-4 where cell density (on a log scale) has been plotted against reciprocal temperature. The solid line in Fig 6.2-4 is represented by the equation:

$$N_o = (5.075 \times 10^{16}) \times 10^{-3056.7\,(1/T)} \qquad (6.2\text{-}1)$$

From Eq. 6.2-1, activation energy $\Delta G^* = 9.72 \times 10^{-20}$ J was determined for nucleation in polystyrene. Thus the Arrhenius type dependence of cell density on temperature is confirmed by experiment.

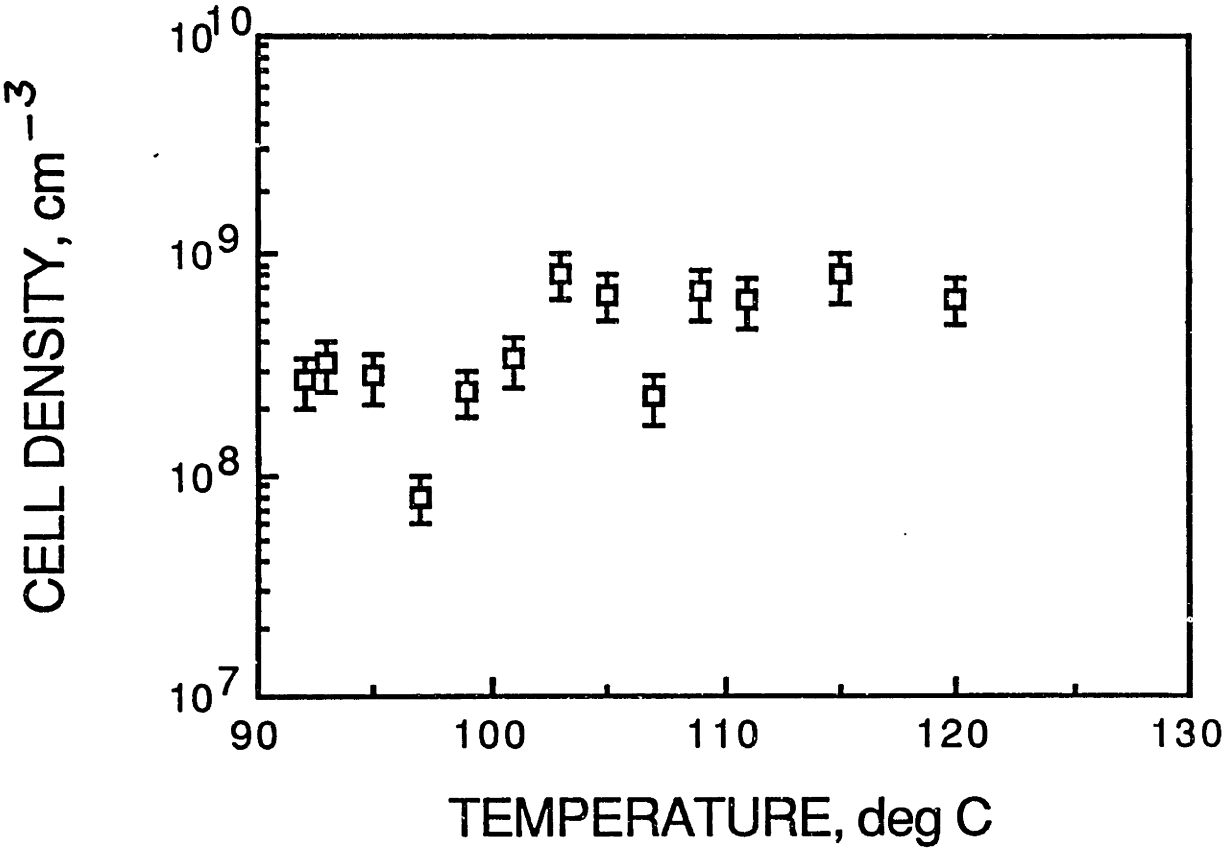

Figure 6.2-3. Cell nucleation density as a function of temperature.

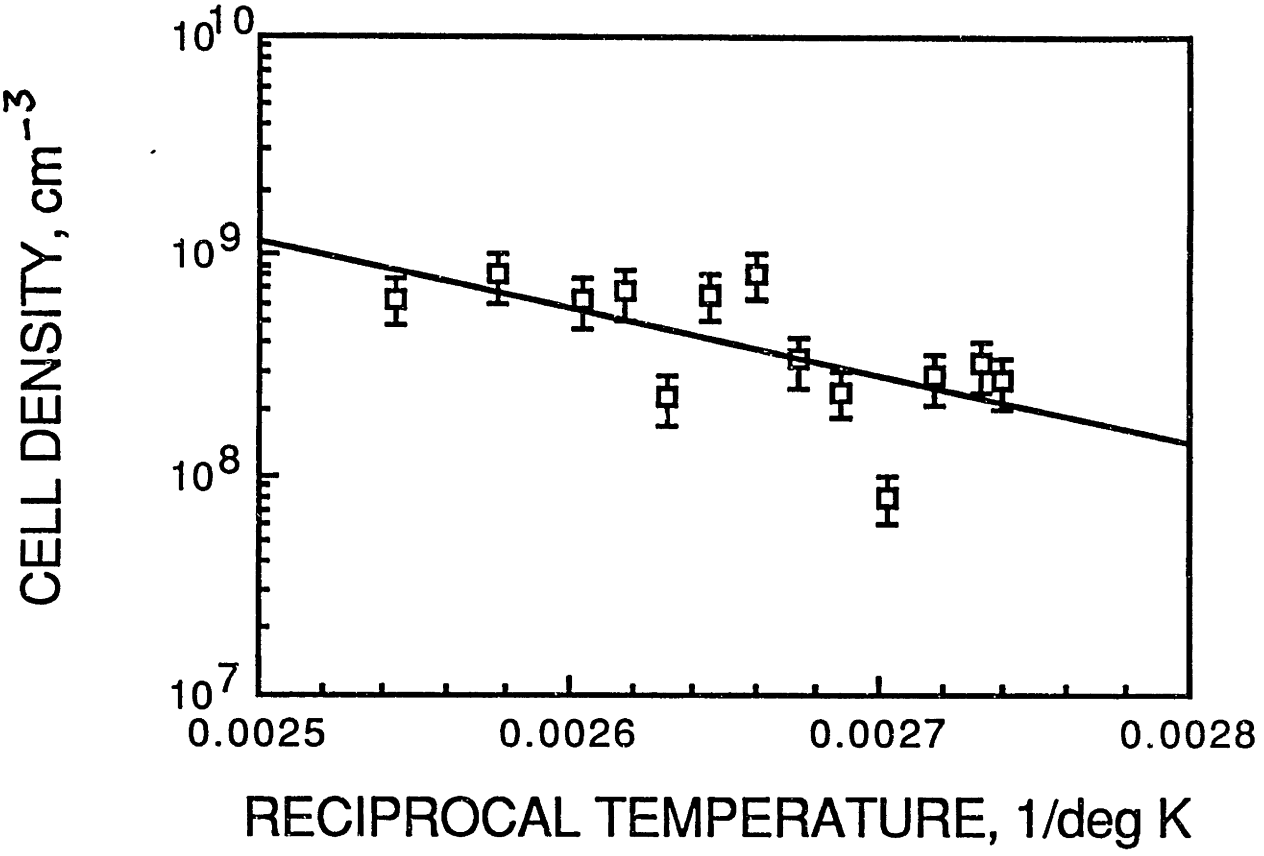

Figure 6.2-4. Plot of cell density vs. reciprocal temerature. Note that the cell density has been plotted on a log scale.

6.2.2 Effect of foaming time on nucleation density

Background

The effect of foaming time on cell nucleation is not of primary concern in our process design. Our objective in obtaining the data reported here was to see if there is significant additional nucleation after the initial 'spontaneous' nucleation.

Experimental

In this experiment a number of disks were saturated at 2000 psi and foamed for different lengths of time. The foaming was done in the glycerin bath at 115 °C. The foaming times varied from four seconds to four minutes as shown in Fig. 6.2.1. The samples were viewed under a scanning electron microscope (SEM) and cell size and cell density were determined. In addition, the density of each sample was measured in order to determine the change in void fraction as a function of time.

Results and discussion

From micrographs of samples in Fig. 5.3-3, the cell density was determined at different foaming times. In addition, the size of each bubble in the micrographs from samples (a) through (f) was determined to get an idea of cell size distribution at different foaming times. Fig 6.2-5 shows the number of cells in different size ranges at foaming times of 10, 15, 20, and 30 seconds, respectively. Note that up to a foaming time of 10 sec , all cells are 6 μm or less. However, at a later time , say 20 sec., 18 bubbles out of 57 in the

micrograph, or about 30%, are 6μm or less, suggesting that these smaller bubbles were nucleated later. At 30 sec, only about 10% of bubbles are less than 6μm suggesting that the rate of nucleation has slowed down due to the depletion of gas supersaturation.

Cell density as function of foaming time is shown in Fig. 6.2.6. We see that the cell density rises till about thirty seconds foaming time and then starts to decrease reaching a limiting cell density of about two hundred million cells per cm^3 after ninety seconds of foaming. The early cell density rise has been plotted in Fig. 6.2-7. Up to about thirty seconds of foaming, the cell density can be considered to increase approximately linearly with time, corresponding to a steady-state rate of nucleation. Beyond this time, the rate of nucleation decreases, as the driving force for nucleation gets depleted. These data show that the nucleation of cells takes place over a finite time (on the order of 30 sec) and is not 'instantaneous' as assumed by previous investigators (Colton,1985).

The cell density starts to decrease after the cells get large enough to hit each other. This happens at a cell size of approximately twelve microns in this experiment. As the cells grow further they coalesce, reducing the cell density. This phenomenon is evident in Fig. 6.2.8, where cell density has been cross-plotted as a function of cell size.

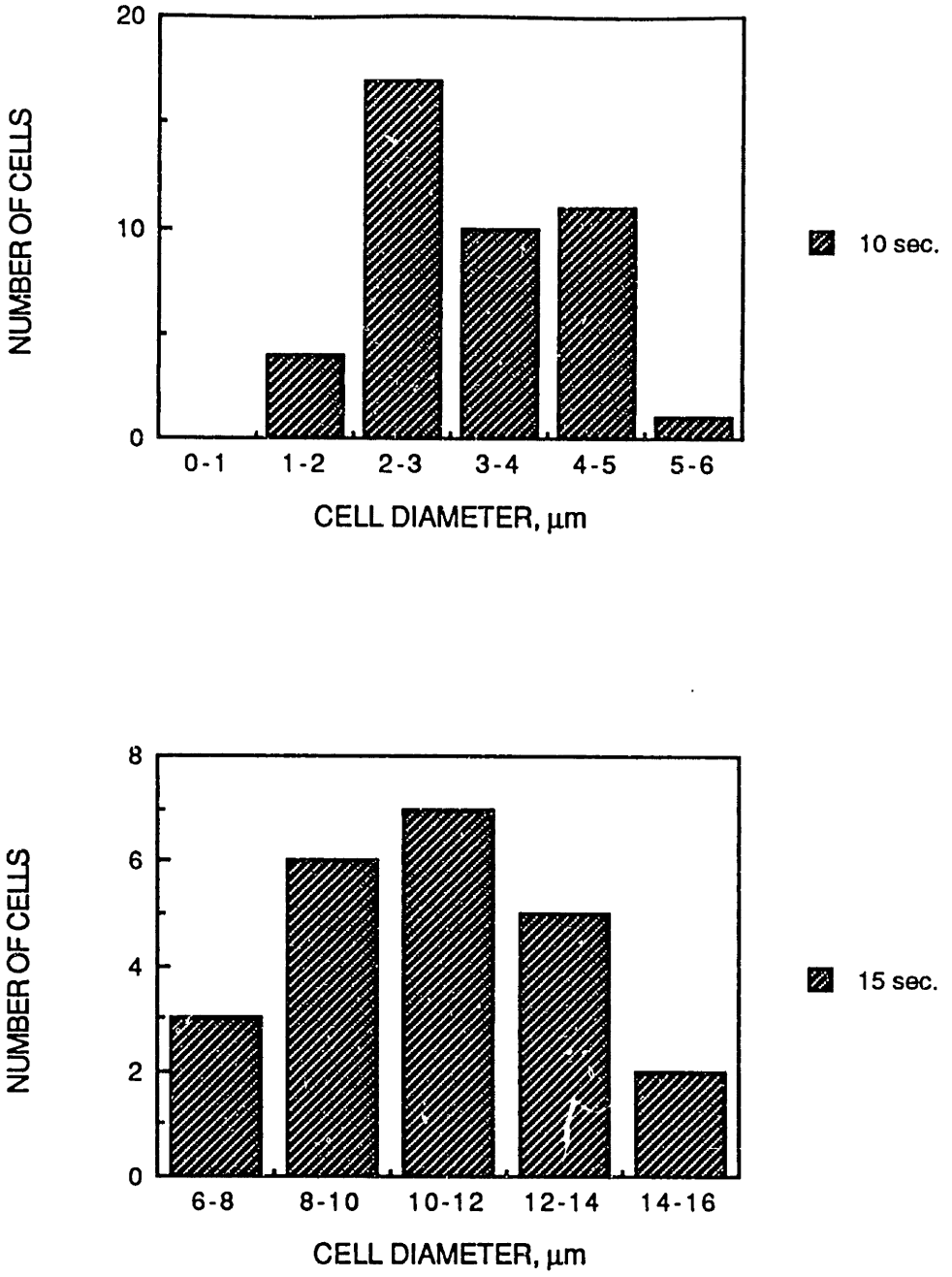

Figure 6.2-5. Histogram of cell size distribution in the early stages of foaming.

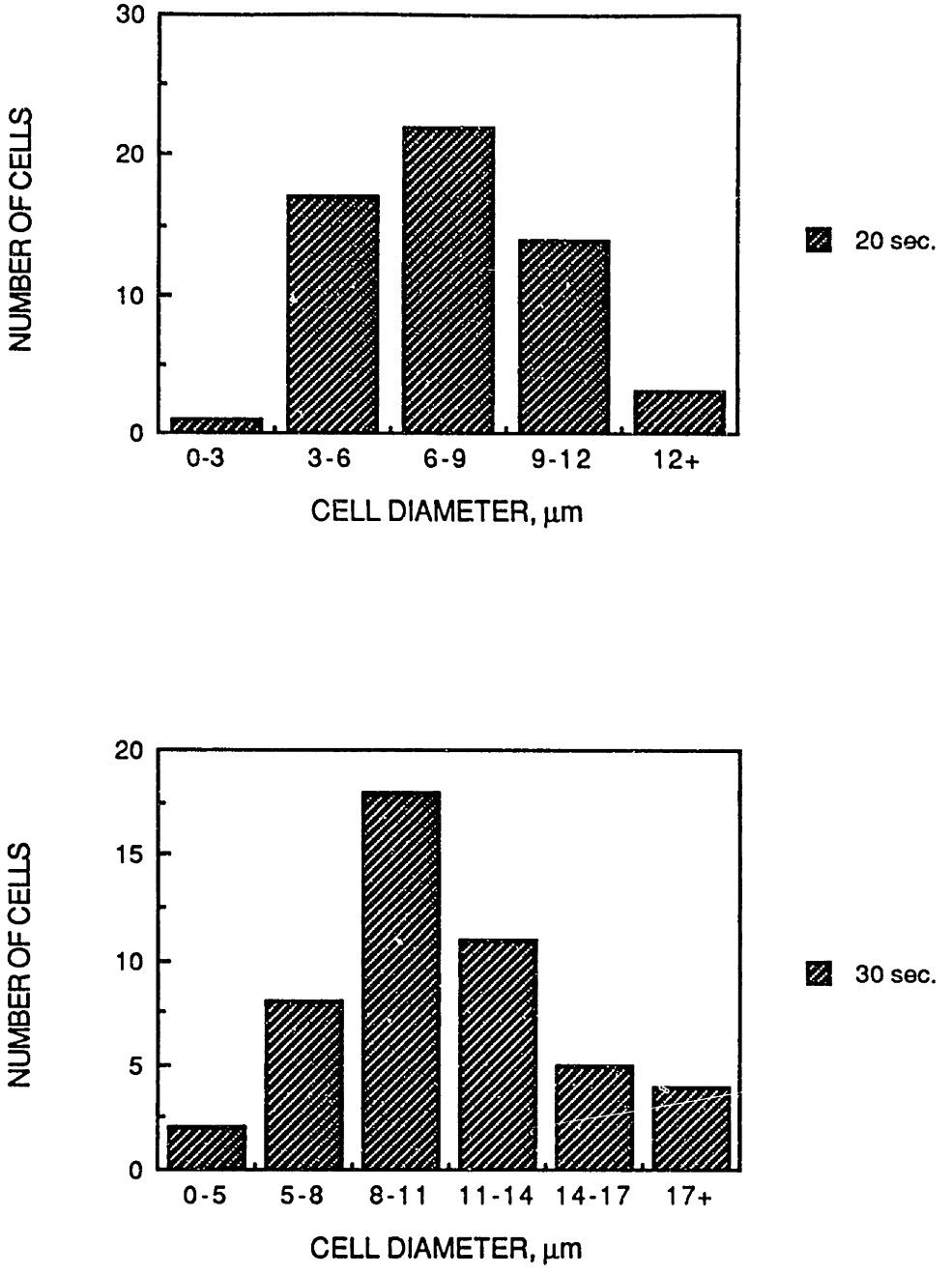

Figure 6.2-5. (continued) Histogram of cell size distribution in the early stages of foaming

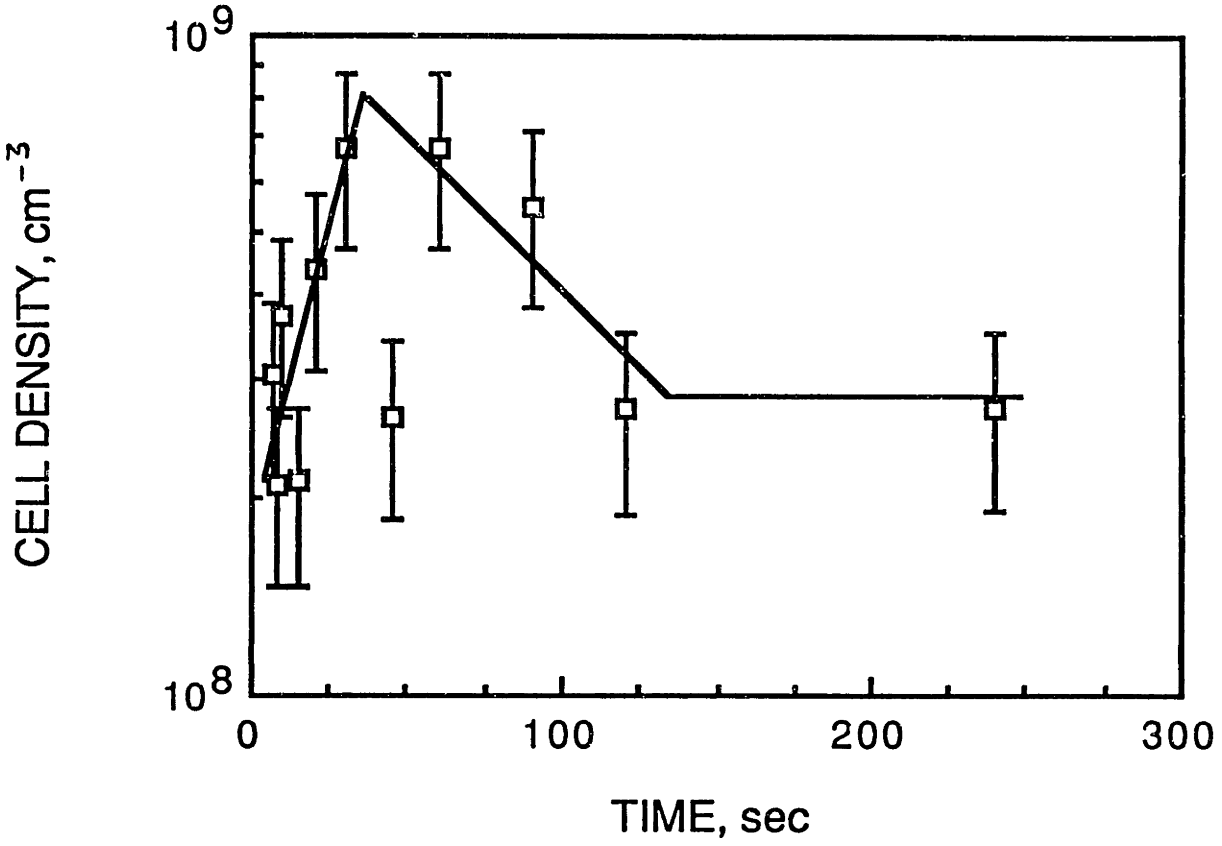

Figure 6.2-6. Plot of cell density as a function of foaming time.

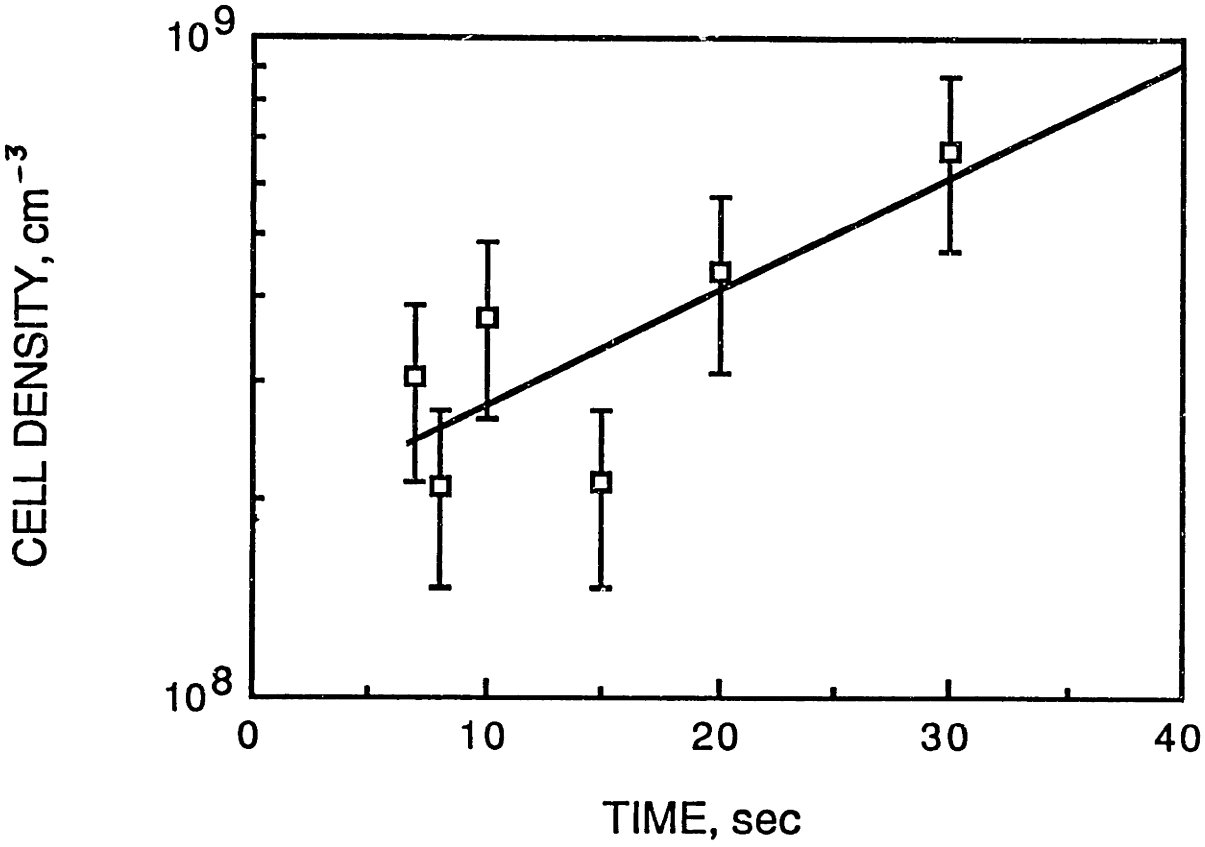

Figure 6.2-7. Cell density as a function of foaming time in the early stages of foaming.

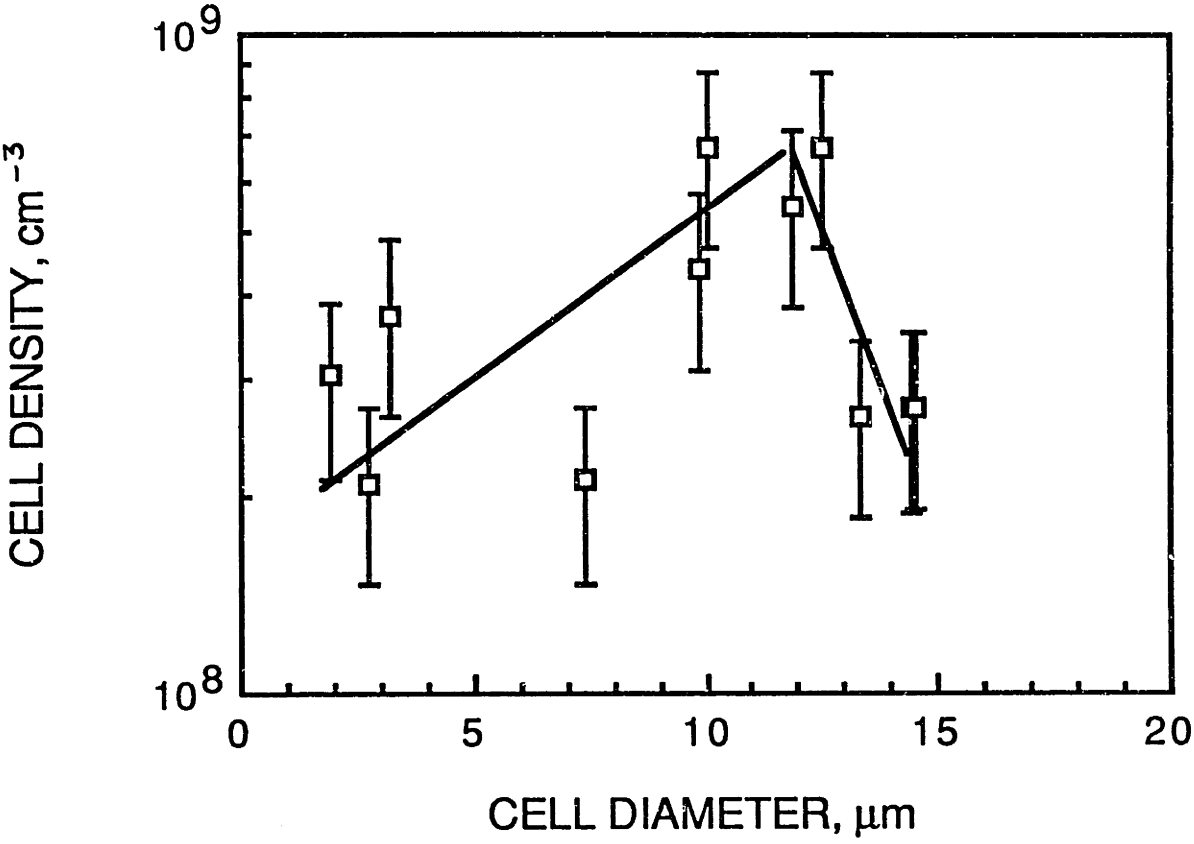

Figure 6.2-8 Cell nucleation density as a function of cell size.

6.3 Effect of external pressure on cell nucleation

Background

The homogeneous nucleation rate is given by:

$$N_{HOM} = f_0 C_0 \exp\left[\frac{-\Delta G^*}{kT}\right] \qquad (3.3\text{-}1)$$

where the activation energy is obtained from:

$$\Delta G^* = \frac{16\pi \gamma^3}{3(P_s - P_0)^2} \qquad (3.3\text{-}2)$$

where γ = surface energy of the polymer,
P_S = gas saturation pressure,
and P_0 = ambient pressure.

In Eq. 3.3-2, P_s is the saturation pressure used and P_0 is the pressure at which nucleation occurs which normally is the atmospheric pressure. Thus $(P_s - P_0)$ represents the degree of supersaturation, the main driving force for nucleation. When nucleation occurs under an external pressure, P_0 can be replaced by P_{ext} in Eq 3.3-2 and $(P_s - P_{ext})$ now represents the degree of supersaturation. Thus higher the external pressure, higher the activation energy and lower will be the number of cells nucleated. In the limit, when the external pressure equals the saturation pressure, there can be no nucleation, since all the gas will stay

dissolved under this condition. In terms of Eq. 3.3-2, the condition $P_{ext} = P_s$ represents an infinite activation energy , predicting a zero nucleation rate.

In order to uncouple cell nucleation from deformation, it was proposed to get the part geometry first and then obtain the microstructure. Since we needed to heat the supersaturated polystyrene sheet above the glass transition temperature before we could deform it, we had to somehow suppress cell nucleation during the deformation step. If sufficient external pressure is maintained during deformation-- either mechanical or hydrostatic pressure-- then cell nucleation can be effectively suppressed, since the external pressure will reduce the driving force for cell nucleation. After the deformation is completed, the external pressure will be reduced, allowing cells to nucleate.

Under this scheme, the cells will not nucleate under external pressure. We need to make sure that a sufficient number of cells will nucleate when pressure is released, for otherwise deformation and cell nucleation would remain coupled, defeating the original purpose.

Experimental

To study the effect of external pressure on cell nucleation, the setup shown in Fig.6.3-1 was used. A polystyrene disk saturated at 2000 psi was placed between the platens of the hydraulic press. The control program on the IBM PC was instructed to maintain the desired external pressure on the disk. The platens were then heated

to 115.°C for a few minutes and cooled to room temperature. A constant external pressure was maintained during the entire thermal cycle. Finally the polystyrene disk was removed and a sample near the center of the disk (away from the edges) was examined under the scanning electron microscope to determine the nucleation density. This procedure was repeated at different external pressures.

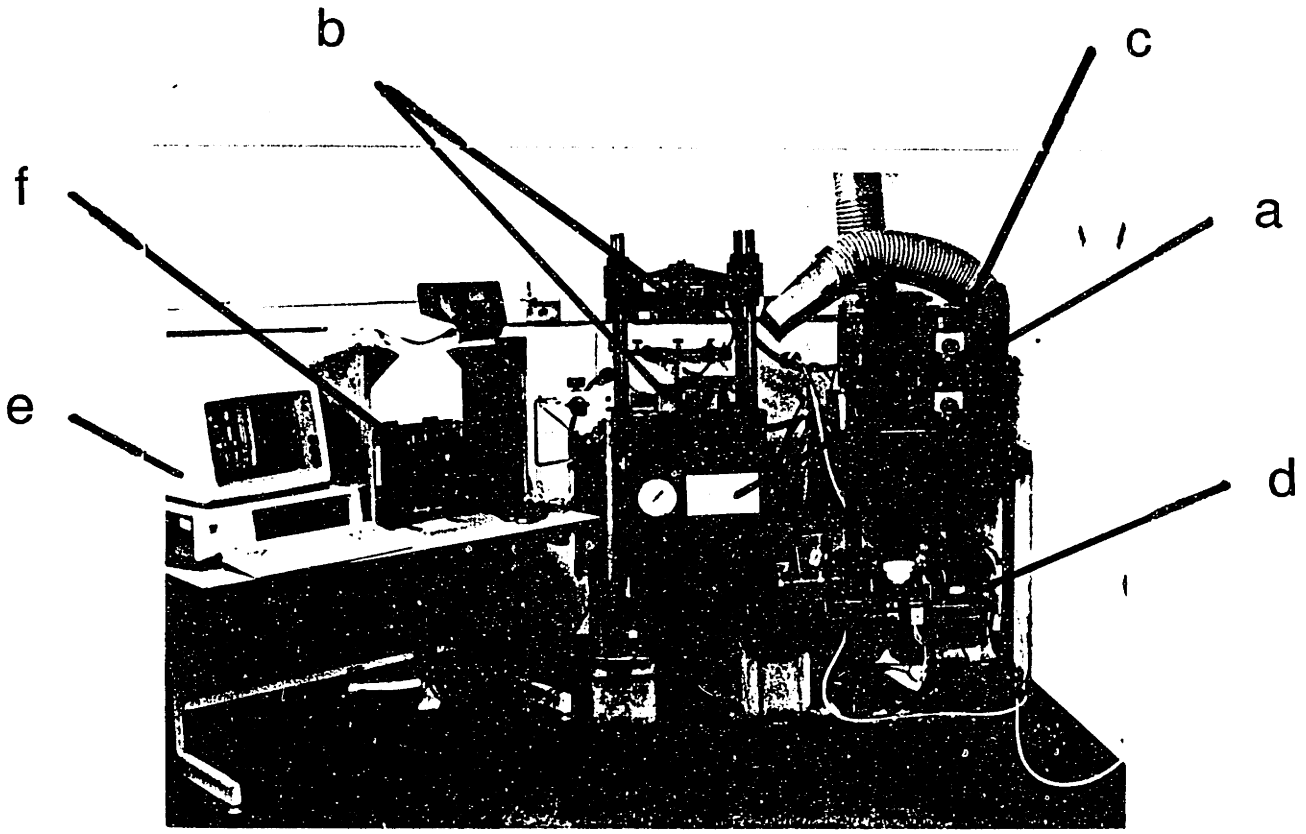

Figure 6.3-1. Photograph of the setup for study of nucleation under external pressure.

a. Hydraulic press.
b. Plattens of the press with heating elements.
c. Platten temperature controller.
d. Gear pump for maintaining oil reservoir pressure.
e. IBM PC with control and data acquisition software.
f. Controller

Results and discussion

The cell density data from the squeeze pressure experiment has been plotted in Fig. 6.3-2. The prediction from homogeneous nucleation theory has also been plotted for comparison. In this calculation the effect of external pressure is accounted for as given in Eq. 6.3-3. According to this model, the cell nucleation density should drop by some eight orders of magnitude as the external pressure increases from atmospheric to 1000 psi. (Zero external pressure in Fig 6.3-2 corresponds to nucleation at atmospheric pressure.) The data, however, shows no effect of external pressure on the number of cells nucleated! Clearly there is no agreement between the theory and the experiment and we need to find an explanation.

The implication of the experimental data in Fig. 6.3-2 is that the cell nucleation can not be suppressed by maintaining an external pressure. this result has serious consequences on our process strategy, since we were counting on external pressure to suppress nucleation in order to decouple nucleation from deformation. We must, however, regard this conclusion as tentative in view of the discrepancy between the theory and experiment shown in Fig. 6.3-2.

In the squeeze pressure experiments the edges of the polystyrene disk were exposed to atmospheric pressure. It was decided to repeat the experiments so that the sample is subject to a hydrostatic external pressure. The experimental setup was modified as shown in Fig. 6.3-3. The polystyrene sample was now placed in a high pressure mold and was subject to a desired external pressure

by a compressed nitrogen cylinder. Nucleation experiments were conducted using the same thermal cycle as in the squeeze pressure experiments at cavity pressure of 500,1000 and 1500 psi,respectively.The experiment with nucleation at atmospheric pressure was also repeated for comparison.

Figure 6.3-4 shows scanning electron micrographs of samples foamed under different hydrostatic pressures, showing significant cell nucleation in each experiment. Note that in Fig.6.3-4(a),the cells are larger than in the other micrographs as the nucleation was carried out at atmospheric pressure in this case. In the micrographs (b), (c), and (d), the presence of external pressure prevented cell growth.

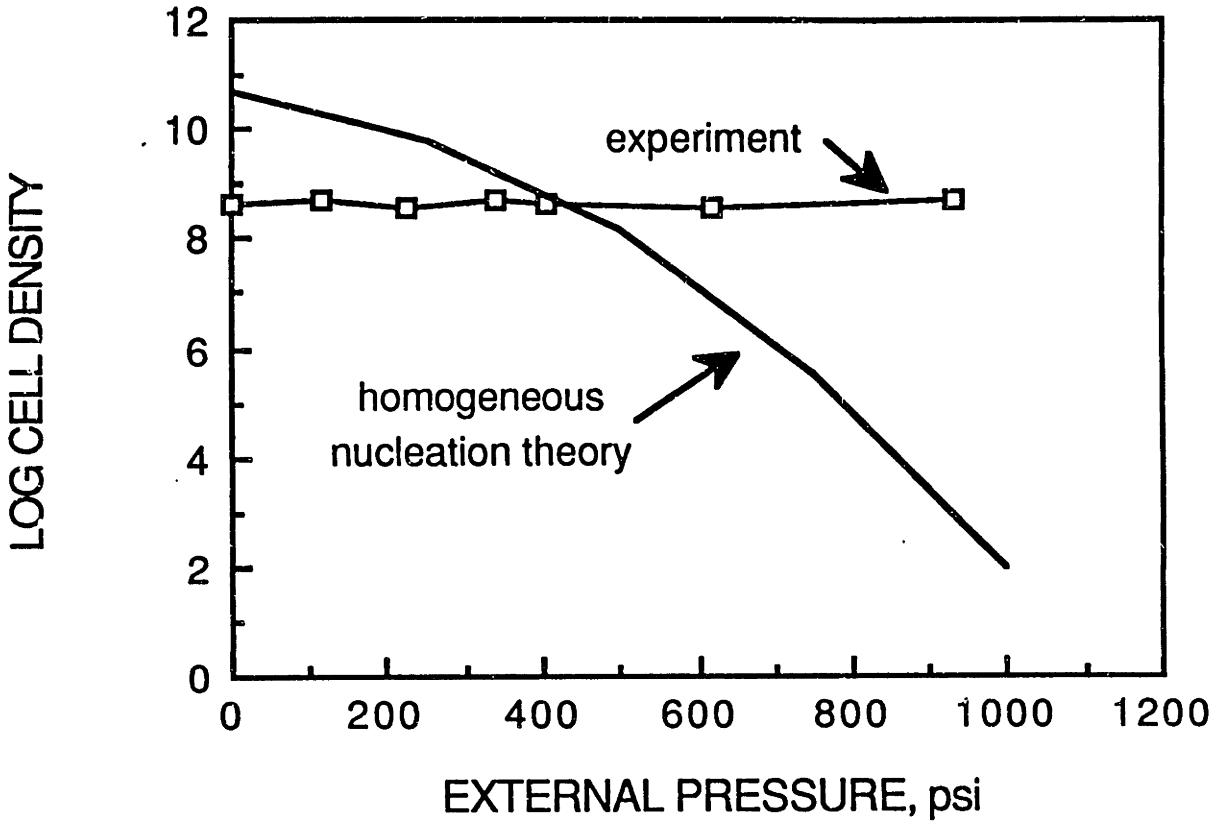

Figure 6.3-2 Plot of logrithm of cell nucleation density as a function of the external pressure. The experimental data is from the squeeze pressure experiment

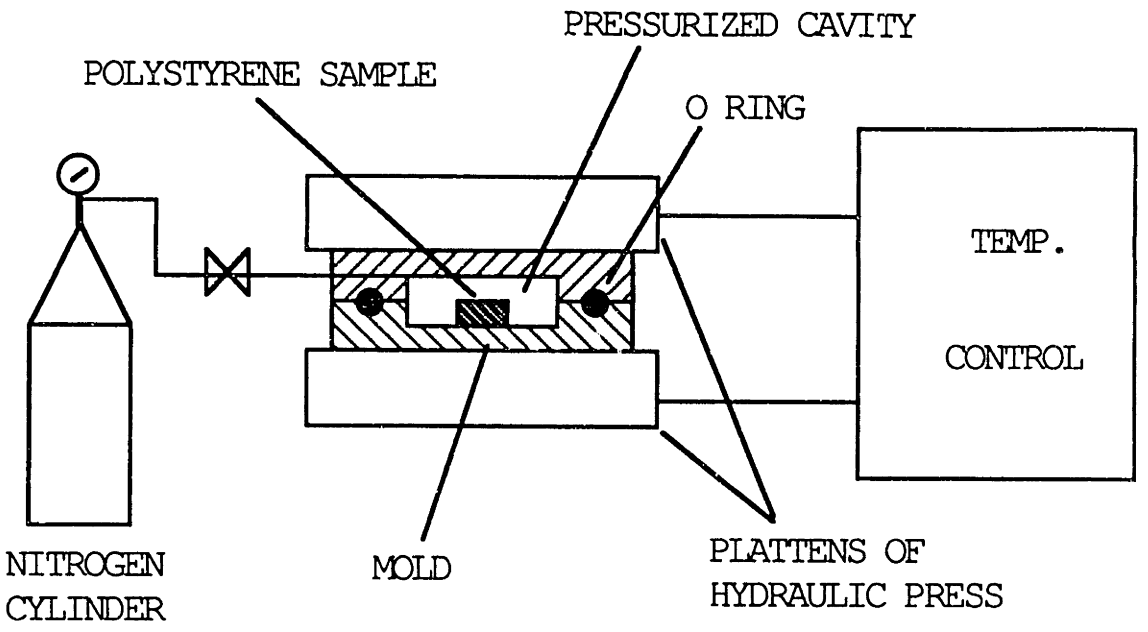

Figure 6.3-3. Schematic of the experimental setup for nucleation under controlled hydrostatic pressure.

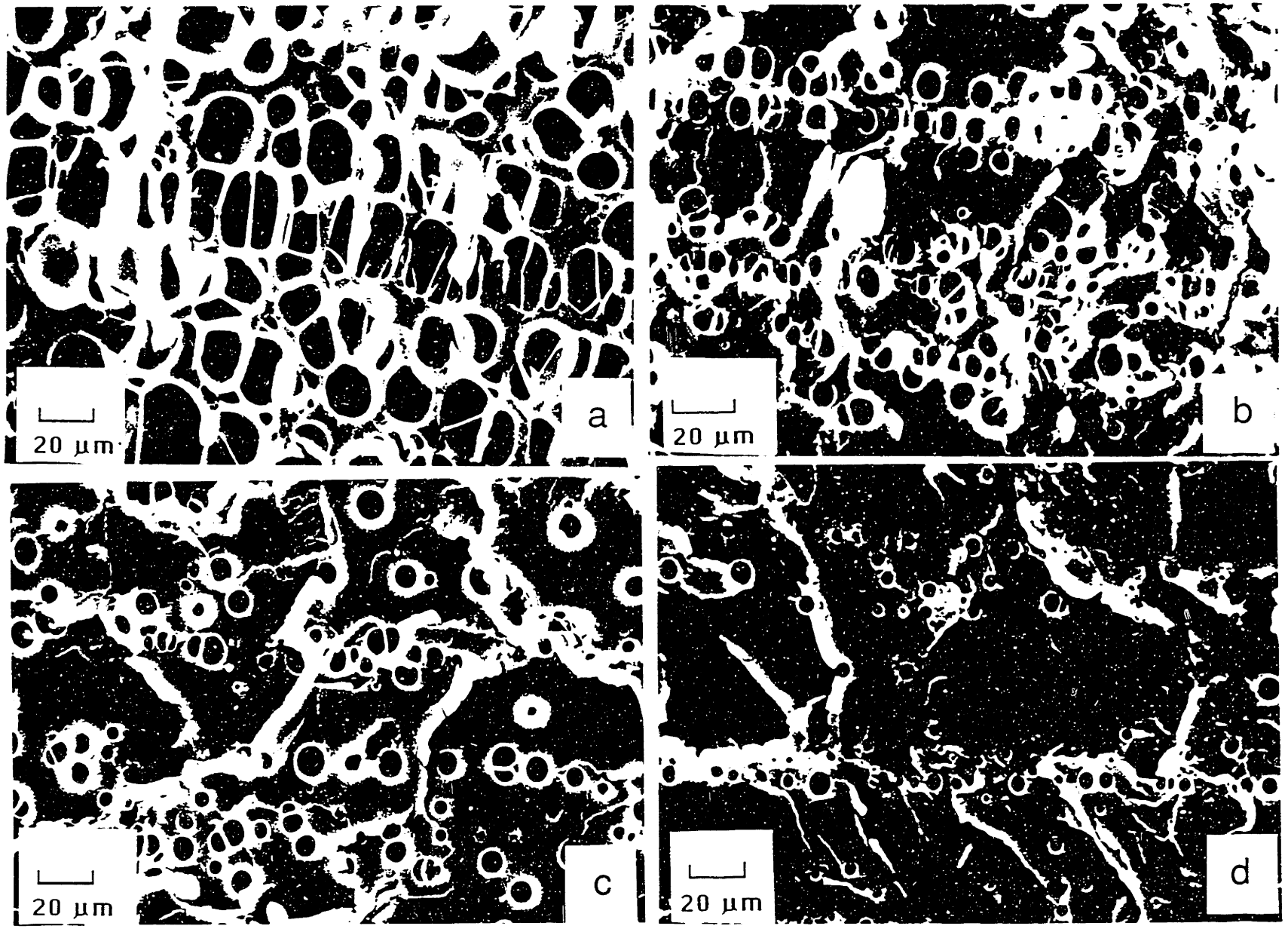

Figure 6.3-4. Scanning electron micrographs of samples nucleated under different hydrostatic pressures: (a) atmospheric pressure; (b) 500 psi; (c) 1000 psi; (d) 1500 psi.

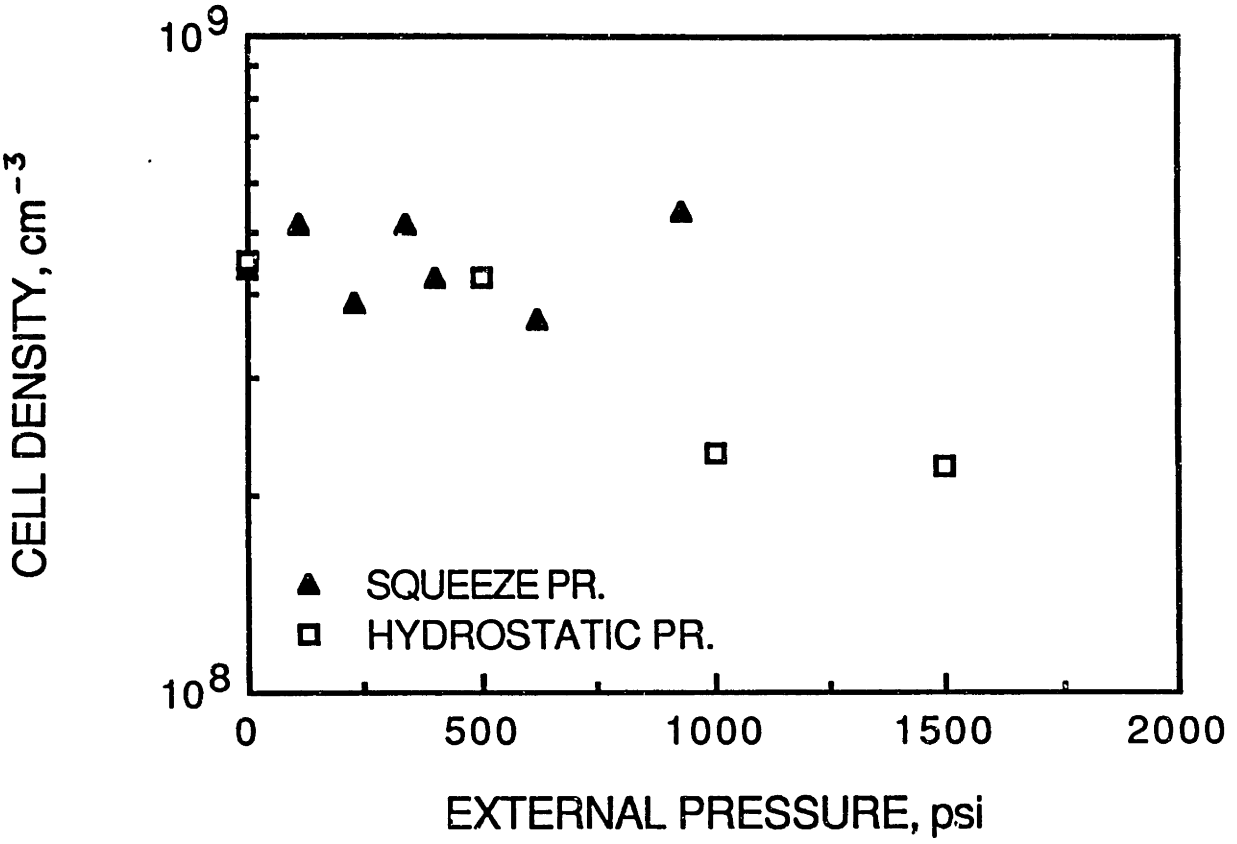

Figure 6.3-5. Experimental data for cell nucleation density as a function of external pressure. All samples were saturated at 2000 psi and foamed at 115 C.

The results from hydrostatic external pressure experiments are shown in Fig. 6.3-5. The data plotted is average of three measurements. For the entire range external pressures tested the cell density lies between 200 million and 500 million bubbles per cm^3. The cell densities in the squeeze pressure experiment lies between 300 million to 500 million bubbles per cm^3. In view of the possible scatter in cell density measurements (see Fig. 5.1-10, where cell densities in identical samples were found to vary by a factor of two) we can say that there is no significant difference in the cell density data from the two experiments.

We can therefore conclude that external pressure has no significant effect on cell nucleation density. In other words, the *cell nucleation cannot be suppressed by maintaining an external pressure.* Thus it is physically impossible to deform the plastic before the bubbles have nucleated in it. We are therefore forced to abandon our process strategy of decoupling microstructure from deformation by deforming first, and nucleating cells afterwards. We will have to find another way to accomplish this decoupling. (Discussion of the unexpected experimental result is continued in section 7.1.)

7.0. THE FINAL PROCESS

7.1. A critical experiment in cell nucleation

Background

The external pressure experiments described in section 6.3 provided a most surprising result, namely that the cell nucleation density is unaffected by the external pressure under which the nucleation is occurring. Till now we have assumed that nucleation in polystyrene is homogeneous, since we are working with pure polystyrene (no additives). however, as pointed out with reference to Fig. 6.3-2, the homogeneous nucleation theory predicts a drop of some eight orders of magnitude as the external pressure is raised from zero to 1000 psi. Even if this theory is not strictly applicable, we nevertheless expected a drop of several orders of magnitude in cell density over the range of external pressures used in the experiments. But we did not see a drop of even one order of magnitude in our experiments.

One possible explanation of data in Fig. 6.3-2 is that nucleation in polystyrene is heterogeneous, not homogeneous. Colton (1985,1987) has shown that if a sufficient number of heterogeneous nucleation sites is available, then the cell nucleation is essentially independent of the degree of supersaturation. This could be the case if, for example, there were a large number of dust particles embedded in the matrix during the manufacturing of the polymer resin, offering heterogeneous nucleation sites. But, if this were the

case, we could not explain the exponential rise in cell nucleation density with saturation pressure (Fig 5.2-2). Clearly heterogeneous nucleation is not a complete explanation.

The total insensitivity of cell density to the substantial external pressure at nucleation (see Fig 6.3-2) is rather intriguing. What will happen if we increased the external pressure to the value at which the plastic was saturated with gas? Will there still be cell nucleation? We decided to perform this experiment, basically out of curiosity, but expected no nucleation since at a pressure equal to saturation pressure all nitrogen in the polymer should stay dissolved.

Experimental

A polystyrene disk was saturated at 2000 psi and placed in the mold (see Fig.6.3-3). The cavity was pressurized to 2000 psi (13.8 MPa) and then heated to 115 °C for a few minutes. The mold was then cooled to room temperature. The cavity pressure was maintained at 2000 psi through the entire thermal cycle.After cooling, the cavity pressure was brought to atmospheric,and the sample was removed and examined.

Results and discussion

Since in this experiment an external pressure equal to the saturation pressure was maintained, we expected no bubbles at all since there is no supersaturation of nitrogen to cause cell nucleation. Much to our surprise, the disk had turned white, showing that bubbles had nucleated!

Figure 7.1-1 shows a SEM micrograph from this sample. The cells are small, in the 3 to 4 μm range. A cell density of 44 million per cm^3 was determined for this sample, showing substantial nucleation. This data has been plotted in Fig 7.1-2, where previous data from external pressure experiments has been included for comparison. we see from Fig 7.1-2 that the cell density in this experiment, in which there was no gas supersaturation to drive nucleation, is only about one order of magnitude less than at zero external pressure (cell density of approximately 400 million per cm^3),where full driving force of supersaturation was available. This experiment was repeated twice with similar results. This shows conclusively that there exists a mechanism for nucleation that is independent of gas supersaturation.It also shows that this mechanism provides a driving force for cell nucleation that is comparable to that provided by the gas supersaturation.

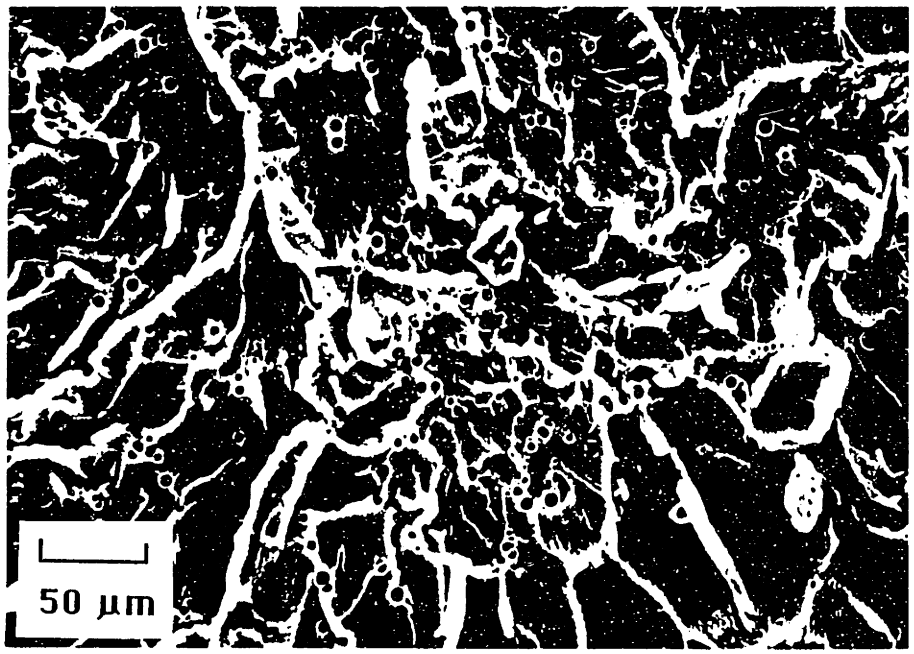

Figure 7.1-1. Scanning electron micrograph showing cell nucleation in the critical experiment.

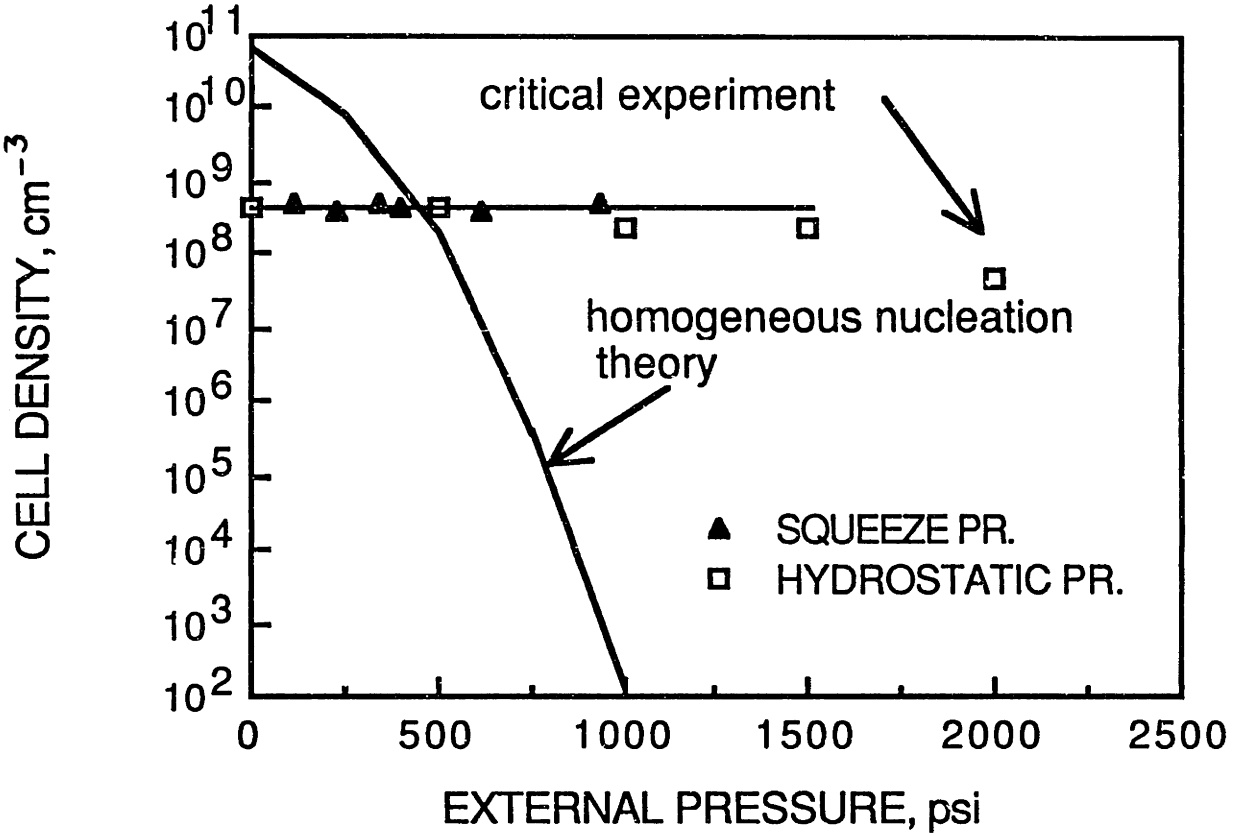

Figure 7.1-2. Cell nucleation density in the critical experiment. Data from earlier experiments on the effect of external pressure on cell density has been included for comparison. (1000 psi = 6.895 MPa)

7.2. Solubility of nitrogen in polystyrene

Background

A decrease in solubility of nitrogen with temperature would explain the cell nucleation in the critical experiment described in section 7.1. Indeed, a review of literature showed that solubility of nitrogen in polystyrene at the melt temperature (Durrill and Griskey, 1969) was lower compared to the room temperature solubility. Unfortunately no data was found on solubility at the glass transition temperature.

Experimental

We measured solubility of nitrogen in polystyrene as a function of temperature. The setup shown in Fig 7.2-1 was used for the solubility measurements. Note that this is the same setup that was used to study the effect of hydrostatic external pressure on cell nucleation. Polystyrene samples were placed in the mold and pressurized with 1500 psi (10.3 M Pa) nitrogen. The mold was heated to the desired temperature. At regular intervals, the samples were withdrawn from the mold and weighed on a Mettler (Model H51AR) balance capable of detecting changes in weight up to 10 micrograms.

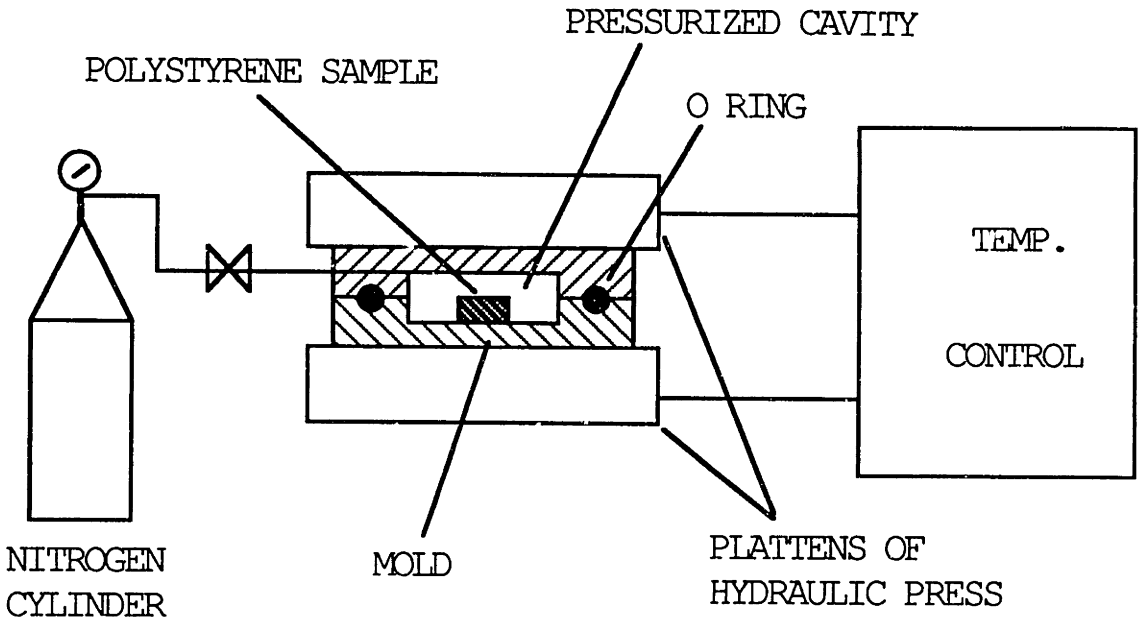

Figure 7.2-1. Schematic of the experimental setup for measurement of nitrogen solubility.

After each reading, the mold pressure was restored to 1500 psi and the mold was re-heated to the temperature at which the solubility is being determined. This procedure was repeated until two consecutive weight readings showed that the samples had saturated with nitrogen. Solubility in mg of nitrogen per gram of polystyrene was obtained from the weight measurements, and converted to the units of cm^3 (STP) per gram of polystyrene per atmosphere, in which the Henry's Law constant is customarily reported. This experiment was performed at a number of temperatures between room temperature and 115 °C. The mold pressure was maintained at 1500 psi for all experiments.

Results and discussion

The solubility data are shown in Fig. 7.2-2 which shows the Henry's Law constant as a function of temperature. We see that solubility drops by nearly 40% as the temperature increases from room temperature to the glass transition temperature.

In Fig. 7.2-3 we have plotted negative log of Henry's law constant as a function of 1/T. this plot shows that the Henry's law constant follows a relation of the form

$$H = H_0 \exp(-E_s/RT) \qquad (7.2\text{-}1)$$

where H = Henry's law constant,

H_0 = Henry's law constant at a reference temperature,

E_s = Heat of solution, and

RT = Gas constant times the absolute temperature.

From Fig. 7.2-3 we determined the heat of solution of nitrogen in polystyrene to be -1.2 Kcal/mole. The drop in solubility of nitrogen in polystyrene explains the cell nucleation the critical experiment described in section 7.1.

As the temperature is raised from room temperature (when the polystyrene disk was saturated at a certain pressure) to just below Tg, we have a thermodynamic instability due to the drop in solubility. This is analogous to the thermodynamic instability due to supersaturation that was believed to be the sole cause of nucleation in the past.

The experimental results are consistent with the thermodynamic state of matter, which is typically a function of two thermodynamic properties. In this case, the solubility varies as a function of pressure and temperature. The effects of both pressure and temperature on solubility are significant.

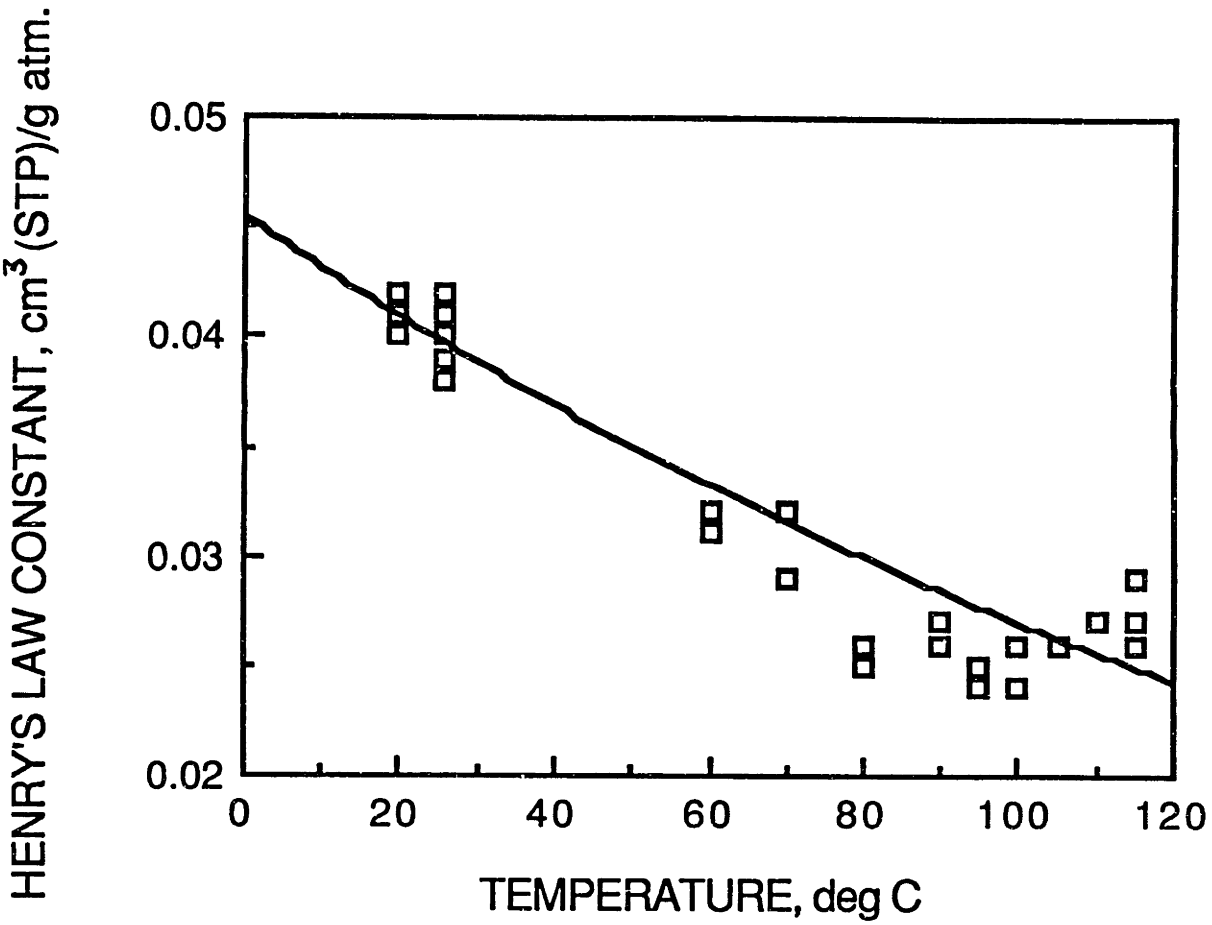

Figure 7.2-2 Solubility of nitrogen in polystyrene as a function of temperature.

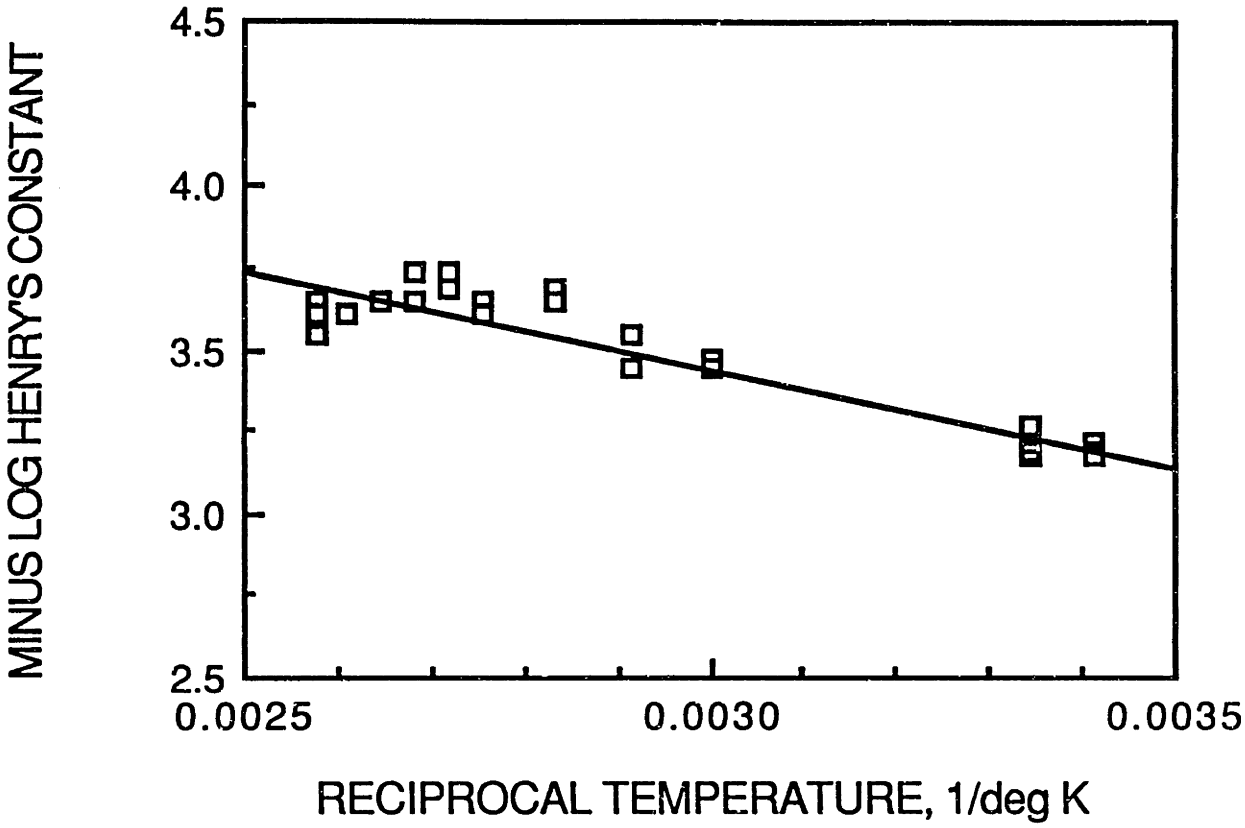

Figure 7.2-3 Minus natural log of Henry's law constant as a function of reciprocal temperature, 1/T.

7.3. Proposed process

This new understanding of the role of temperature in cell nucleation in polystyrene led us to re-evaluate the process strategy. It became clear that cell nucleation cannot be suppressed by employing external pressure only. Therefore, we physically cannot deform the plastic before cell nucleation. On the other hand, the cells will nucleate as soon as we reach the glass transition temperature due to the drop in nitrogen solubility, regardless of any external pressure, as already seen in section 6.3. Thus we have a mechanism for cell nucleation in which the cell density is not affected by the external pressure distribution that may be present during the deformation process. This realization leads to a rather simple process described below.

Our basic goal was to realize a given part geometry without harming the microstructure. We considered the idea of deforming soon after cell nucleation when the cells are still small.The majority of cell growth will take place after deformation in a heated mold at a suitable temperature. This process is schematically shown in Fig. 7.3-1. The idea to first nucleate the bubbles, then apply deformation and finally grow the bubbles in a heated mold appeared feasible since deformation can be accomplished in a short period of time relative to the time needed to get significant cell growth.

In section 5.3, we studied cell growth as a function of foaming time. Refer again to Fig. 5.3-4 showing average cell size as a function of time. At the foaming temperature of 115 °C, it takes

some 25 seconds to reach an average cell size of 10μm, and some 100 seconds to approach the limiting final cell size. By contrast, the deformation can be imposed in one to two seconds. It is therefore possible to attain the part geometry while the cells are still small.

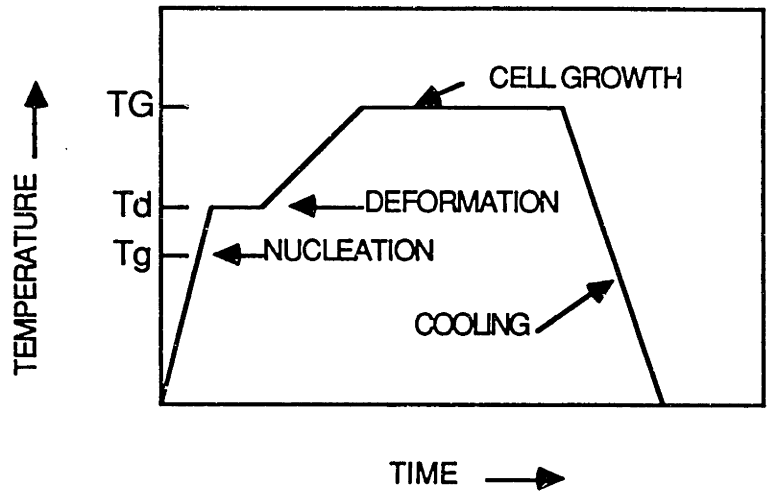

Tg = The glass transition temperature
Td = The deformation temperature
TG = The cell growth temperature

Figure 7.3-1. Schematic of the proposed process.

Note that in the process proposed in Fig. 7.3-1 there is the possibility that the just-nucleated cells may become non-spherical under deformation. Subsequent cell growth, however, will tend to restore the spherical shape. If cells are allowed to grow to form a honeycomb like structure then the initial shape will not be of any consequence.

7.4. Process demonstration

The set up shown Fig 7.4-1 was used to show the feasibility of the proposed process. A conventional thermoforming machine was equipped with a mold to produce a plastic container. The bottom half of the mold was connected to a thermolator and could be heated to a desired temperature. A commercial grade high impact polystyrene sheet was saturated with nitrogen at 2000 psi (13.8 M Pa) and placed in the thermoformer. The sheet was heated in an infrared oven and foamed into a container using a heated mold in a plug-assist vacuum forming process.

A sample from the bottom of the container and one from the wall of the container was studied under the Scanning Electron microscope. Fig. 7.4-2 shows a picture of the container and the micrographs from these samples. We see that microcellular structure has successfully been produced in the container. In Fig. 7.4-3, a closeup of the microstructure shows that an average cell size of approximately 7 μm was obtained.

This demonstrates the feasibility of the process concept.

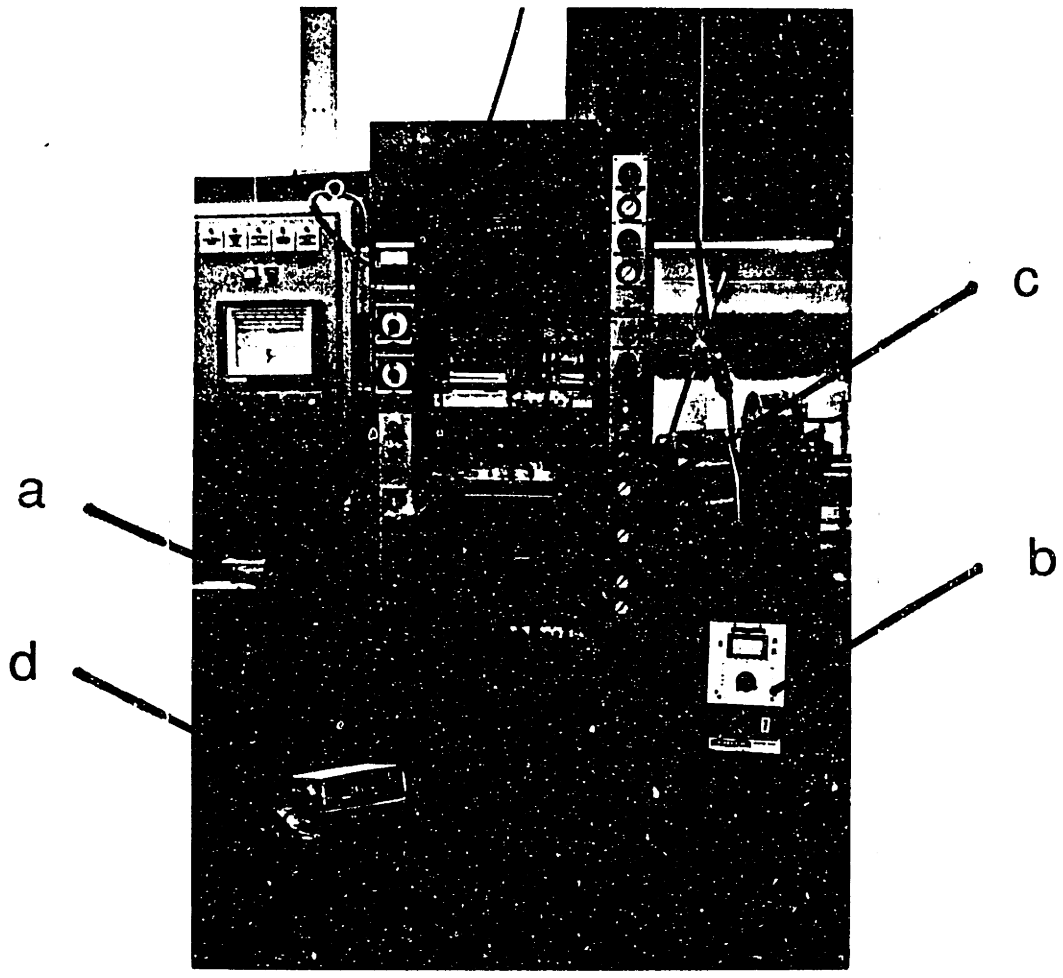

Figure 7.4-1. Photograph showing experimental setup for process demonstration.

a. Thermoforming machine.
b. Thermolator.
c. Mold.
d. Digital thermocouple reader.

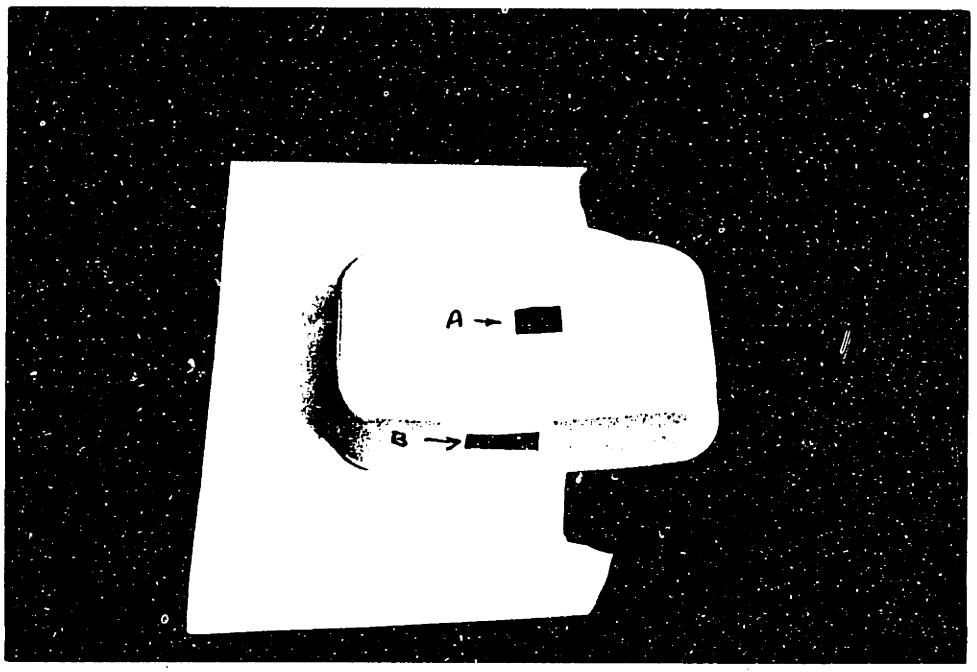

Figure 7.4-2. Photograph of a microcellular container made by the process outlined in Fig. 7.3-1.

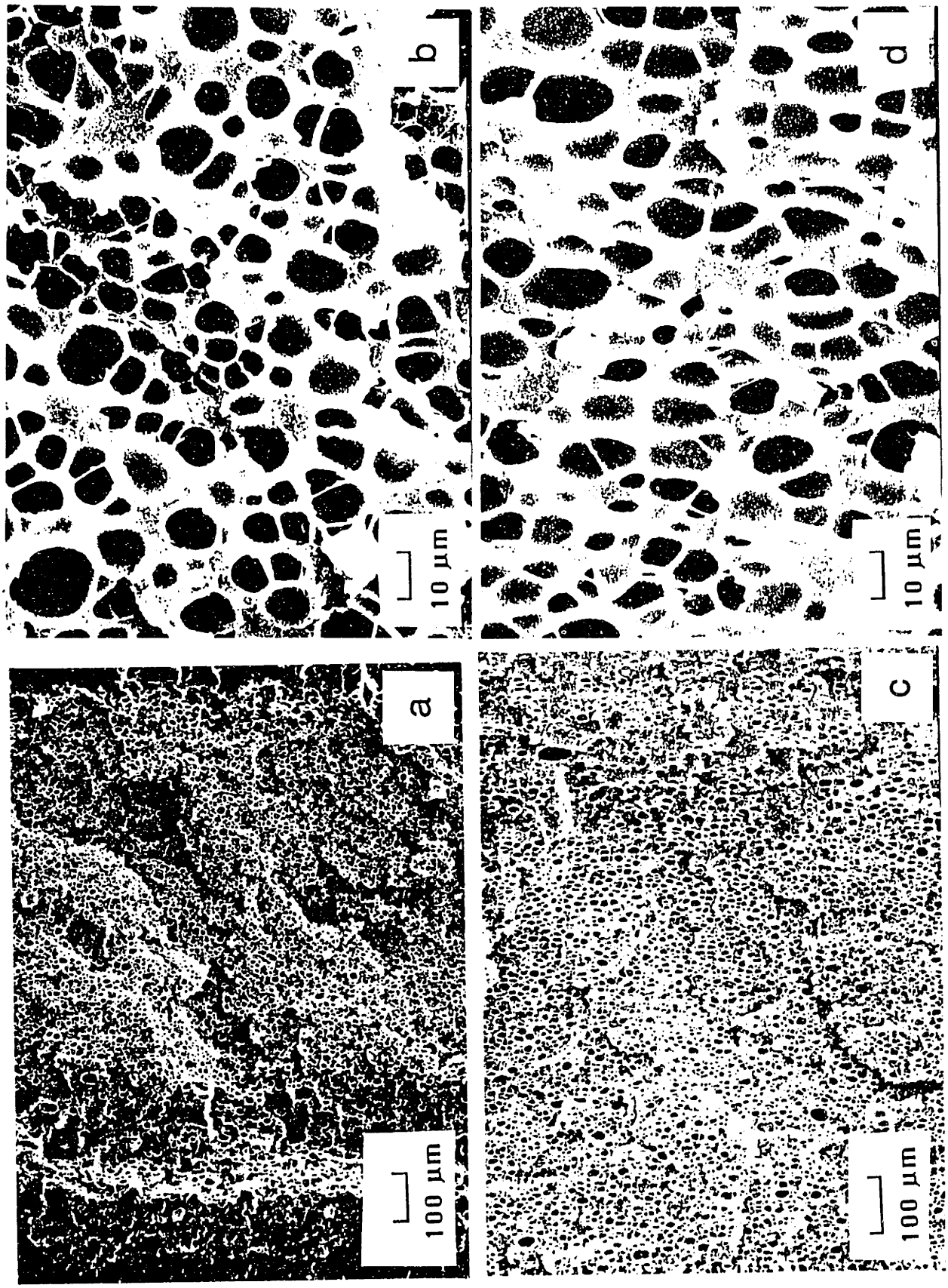

Figure 7.4-3. Scanning electron micrographs of samples from the microcellular container: (a) sample from container bottom; (b) close-up of bottom; (c) sample from container wall; and (d) close-up of wall.

7.5. Process design-matrix

Let us examine the non-diagonal elements of the design matrix for this process. Coefficient a_{12} represents the effect of time-temperature exposure on cell nucleation density. In our process cell nucleation occurs before deformation as the sheet is heated to the glass transition temperature while the cell growth occurs later at temperature T_G. Therefore, the time-temperature cycle does not couple cell density and cell size, and we can set $a_{12} = 0$.

Coefficient a_{13}, the effect of deformation on cell density, is clearly zero since cell nucleation precedes deformation (see Fig. 7.3-1).

Coefficient a_{21} represents the effect of saturation pressure on cell size. We have shown in Section 4.1 that saturation pressure does not cause any coupling between cell density and cell size; thus $a_{21} = 0$.

In our process cell growth predominantly occurs after deformation. Therefore we may set $a_{23} = 0$, signifying that deformation (PV_3) has no significant effect on final cell size distribution. It should be noted, however, that the possibility for deformation to affect the shape of cells still exists, and process conditions will have to be adjusted to keep the shape within acceptable limits.

Saturation pressure (PV_1) and time-temperature exposure for cell growth have no bearing on part geometry; therefore, $a_{31}=a_{32}= 0$.

With all the off diagonal terms equal to zero for this process, we have obtained a diagonal design matrix, which was the objective of axiomatic design.

8.0 CONCLUSIONS AND RECOMMENDATIONS

8.1 Conclusions

1. We were able to synthesize a process in which deformation and microstructure are uncoupled. The process has a diagonal design matrix, showing that the functional requirements can be independently controlled in this process. Finally, the process concept was demonstrated on a conventional thermoforming machine. The development of a process to produce parts has brought us significantly closer to realizing the potential of microcellular plastics.

2. This process is based on the recognition that the amount of gas dissolved in the polymer is a function of both temperature and pressure (as expected from thermodynamics). More importantly, we found that the reduction of nitrogen solubility in polystyrene with temperature provides a driving force for nucleation that is comparable to that provided by gas supersaturation. A combined evaluation of the process in terms of the thermodynamics and kinetics of bubble nucleation and growth and the design axioms yielded an uncoupled process.

3. A number of insights into the nature of microcellular foam were gained from the experimental work performed in this thesis. The main conclusions are summarized below.

(a) The microcellular structure is reproducible. The structure in the core region across thickness and in the plane of the foam is very homogeneous.

(b) Cells coalesce if allowed to grow beyond the point where they start to touch each other, resulting in a drop in cell density. For maximum cell density, therefore, the growth should be stopped before coalescence begins.

(c) The cell density may vary locally (say over 5 mm in the plane of the foam) by a factor of two. We found that the local cell size distribution adjusts to the local cell density variations in a way that the void fraction remains constant. This is to be expected if a uniform gas concentration was achieved prior to foaming.

(d) The skin thickness in microcellular foam can be controlled by varying the nitrogen desorption time prior to foaming. This opens the way to design of composite structures with microcellular foam.

(e) Ultra thin sections can be foamed by the microcellular process. (In our experiments, a 0.016 in (0.4 mm) thick sample of polystyrene was foamed with a 50% increase in thickness and some 50 bubbles across the thickness).

(f) high void fraction foams with microcellular structure can be produced. This conclusion is especially important in view of the concern about ozone layer depletion, and the need to find more benign ways to foam plastics. (We achieved 82% void fraction with 14 μm average cell size in our experiments.)

4. A number of conclusions can be drawn from the experimental data that bear on the physics of the microcellular process:

(a) Substantial cell nucleation is seen to occur at saturation pressures far below the pressures predicted by the homogeneous nucleation theory. There are heterogeneities present in the polymers that reduce the activation energy for homogeneous nucleation near the glass transition temperature by two to three orders of magnitude. The precise nature of these heterogeneities is not yet understood.

(b) The time over which steady-state nucleation occurs in polystyrene is on the order of thirty seconds. Beyond this time the nucleation rate begins to drop because of depletion of the driving force.

(c) The number of cells nucleated increases exponentially with increasing supersaturation pressure. On the other hand, the cell nucleation density was found to be totally insensitive to the presence of a hydrostatic external pressure. In a

liquid, a hydrostatic external pressure will directly reduce the driving force for nucleation, i.e. the degree of supersaturation. However, in an amorphous polymer near its glass transition, the external pressure does not seem to affect the driving force for nucleation. This experimental observation may hold the key to understanding the mechanisms for nucleation in polymers near the glass transition temperature.

8.2 Recommendations for future work

We are very optimistic about the future of microcellular plastics as a new class of engineering materials. These materials will find widespread applications far beyond the packaging industry for which the idea was originally conceived. Many technical challenges remain, however, before the potential of microcellular foam can be fully realized. Some areas that need to be addressed. have been outlined below

1. Polymer saturation time

The time required to saturate the polymer with gas is very high. For example, for the nitrogen-polystyrene system, it takes about 72 hours to saturate 1/16" thick sheet at room temperature. It was thought that this time could be reduced substantially by diffusing the gas at an elevated temperature. However, we have learned in this study that solubility of nitrogen in polystyrene goes down with temperature significantly, and the extra nitrogen absorbed at room temperature is in fact needed to drive nucleation. Therefore, diffusion at an elevated temperature is not a viable option. This may not be a limitation, however, for other gas-polymer systems.

One idea to reduce the diffusion time is to reduce the diffusion distance and start with polystyrene powder[1]. The saturated powder may then be molded directly into a microcellular part. Although the sintering process may lead to lower strength, it may still be sufficient for many applications.

2. Mechanical properties

The mechanical property data available on microcellular foam to date is of a preliminary nature. Although these data show some basic trends, they are not comprehensive. The variation in the cell nucleation density can be a major source of variation in mechanical properties. We found that the cell density and cell size can vary by a factor of two or more under identical conditions. This in turn can introduce significant variation in properties such as impact strength. We need to establish tensile strength, flexture modulous, and impact strength as a function of (a) average cell size, and (b) void fraction.

3. Continuous production

The microcellular process developed to date is a batch process. Ways to produce microcellular foam in a continuous process must be sought to make this process competitive with current mass production processes.

---

[1]This idea originated in a conversation with Dr. Karl Seeler, a former MIT colleague, who is now at the University of Pittsburgh

4. Nucleation mechanisms

Understanding the nucleation mechanisms in production of microcellular foam is of fundamental importance. We have seen that substantial cell nucleation takes place in polystyrene at gas saturation pressures far below the levels predicted by homogeneous nucleation theory. There are heterogeneities in the polymer that act to reduce the activation energy for homogeneous nucleation by two to three orders of magnitude. We need to understand the precise nature of these heterogeneities.

5. Foaming of new materials

Most of the work done on microcellular foams to date has been on polystyrene. Other polymer-gas systems should be evaluated. In particular, semicrystalline polymers in general use such as polypropylene, polyethylene, and polyesters offer great potential as microcellular materials.

Bibliography

Blander, Milton and Katz, Joseph (1975), "Bubble Nucleation in Liquids," *AIChE Journal*, 21 (5), p. 833-848.

Blander, M. (1979), "Bubble Nucleation in Liquids", *Advances in Colloid and Interface Science,* 10, pp. 1-32.

Colton, J.S. (1985), "The Nucleation of Thermoplastic Microcellular Foam," Ph.D. Thesis, Mech. Eng. Dept., MIT (1985).

Colton, J., and Suh, N.P. (1987), *Polymer Eng. Sc.*, 27, p 485.

Durrill, P.L. and Griskey, R.G. (1966), "Diffusion and Solution of Gasses in Thermally Softened or Molten Polymers: Part I," *AIChE Journal*, vol. 12, no. 6, Nov. 1966, p. 1147-1151.

Durrill, P.L. and Griskey, R.G. (1969), "Diffusion and Solution of Gasses in Thermally Softened or Molten Polymers: Part II," *AIChE Journal*, vol. 15, no. 1, Jan. 1969, P.106-110.

Einstein,A. (1910), *Ann. d. Physik,* 38, p 1275.

Frenkel, J. (1955), "Kinetic Theory of Liquid", Dover.

Gent, A.N. and Tompkins, D.A. (1969), "Nucleation and Growth of Gas Bubbles in Elastomers," *J. Appl. Physics.*, 40 (6), p. 2520-2525.

Gibson, L.J., Ashby, M.F., and Schajer, G.S. (1982), "The Mechanics of Two-Dimensional Cellular Materials", *Proc. R. Soc. Lond.*, A382, pp 25-42.

Gibson, L.J., Ashby, M.F., (1982), "The Mechanics of Three-Dimensional Cellular Materials", *Proc. R. Soc. Lond.*, A382, pp 43-59.

Han, C.D., and Villamizar (1978), "Studies on Structural Foam Processing -The Rheology of Foam Extrusion," *Polymer Eng. and Sci.*, July 1978, 18 (9), p. 687-698.

Hansen, Ralph (1962), "Production of Fine Cells in the Extrusion of Foams," *SPE J.*, 18 (1), Jan. 1962, p. 77-82.

Hobbs, S.Y. (1975), "The Application of Structure - Property Studies to Structural Foams," *Polymer Eng. and Sci.*, Dec. 1975, 15 (12), p. 854-862.

Jackson, C.L., Shaw, M.T., and Samulski, E.T. (1986), "Cell Size Distribution of Micropourous foams", *SPE Technical Papers*, Vol. XXXII, pp. 42-44.

Maiti, S.K., Gibson, L.J., and Ashby, M.F. (1984), "Deformation and Energy Absorption Diagrams for Cellular Solids", *Acta. Metall.*, Vol. 32, No. 11, pp. 1963-1975.

Martini-Vvedensky, J.E., Suh, N.P., and Waldman, F.A., (1984) U.S. Patent # 4,473,665.

Martini, J.E. (1981), "The Production and Analysis of Microcellular Foam," S.M. Thesis, Mech Eng. Dept., MIT, May 1981.

Martini, J., Waldman, F.A., and Suh, N.P. (1982), *S.P.E. Tech. Papers, XXVIII*, 674-676

Michaels, A.S., and Parker, R.B. Jr. (1959), "Sorption and Flow of Gasses in Polyethylene", J. *Poly. Sc.*, 41, pp. 53-71.

Michaels, A.S., and Bixler, J.H. (1961), "Flow of Gases Through Polyethylene", *J. Poly. Sc.*, Vol. 50, PP. 413-439.

Michaels, A.S., Vieth, W.R., and Barrie, J.A. (1963), "Diffusion of Gases in Polyethylene Terephthalate", *J. Appl. Phy.*, Vol. 34, No. 1, pp. 13-20.

Onsagar, L., (1931) *Phys. Rev.*, 37, p405.

Rand, P.B., and Kraynik, A.M. (1983), Drainage of Aqueous Foams: Generation - Pressure and Cell-Size Effects", *Society of Petroleum Engineers Journal*, pp. 152-154, Feb, 1983.

Rinderle, J.R., and Suh, N.P. (1982), "Measure of Functional Coupling in Design," *ASME J. Eng. Ind.*, Vol. 104, Nov. 1982, p. 383-388.

Russell. K.C. (1980), "Nucleation in Solids: Induction and Steady State Effects", *Advances in Colloid and Interface Science,* 13, pp. 205 - 318.

Saunders, J.H. and Hansen, R. (1972), "The Mechanism of Foam Formation," *Plastic Foams*, K.C. Fritsch and J.H. Saunders, Ed., Marcel Dekker, p. 39.

Scriven, L.E. (1959), "On the Dynamics of Phase Growth," *Chem. Eng. Sci.*, vol. 10, no. 1/2, p. 1-13.

Su, K. (1980), "Void Nucleation in Particulate Filled Polymers and Its Implication on Friction and Wear Properties," Sc.D. Thesis, Department of Mechanical Engineering, MIT.

Su, K. and Suh, N. (1981), "Void Nucleation in Particulate-filled Polymeric Materials," *SPE ANTEC 1981*, p. 46.

Suh, N.P., Bell, A.C., and Gossard, D. (1978), "On an Axiomatic Approach to Optimization of Manufacturing and Manufacturing Systems", *J. Eng. Ind.*, ASME, Vol. 100, May 1978, pp. 127-130.

Suh, N.P. (1984), " Development of the Science Base for the Manufacturing field through the Axiomatic Approach", *Robotics and Computer Integrated Manufacturing*, Vol. 1, No. 3/4, pp. 397-415.

Suh, N.P. (1988), "Principles of Design", Oxford University Press, 1988 (To Appear).

Throne, J.L. (1975), "Structural Thermoplastic Foam - A Low Energy Processed Material", *Poly. Eng. and Sc.*, Vol. 15, No. 10, pp. 747-756.

Throne, James (1979), "Principles of Thermoplastic Structural Foam Molding: A Review," *Science and Technology of Polymer Process*, Nam P. Suh and Nak-Ho Sung, Ed., MIT Press, p, 77-131.

Underwood, E.E. (1970), "Quantitative Stereology", Addison-Wesley Publishing Company, Reading, Massachusetts.

Waldman, F.A. (1982) , "The Processing of Microcellular Foam," S.M. Thesis, Mech. Eng. Dept., MIT.

Wang, W.-C., Kramer, E.J., and Sachse, W.H. (1982), "Effects of High Pressure CO_2 on the Glass Transition Temperature and Mechanical Properties of Polystyrene," *J. Polym. Sci.*, Polymer Physics Edition, vol. 20, 1371-1384.

Wiedersich, H., and Katz, J.L. (1979), "The Nucleation of Voids and other Irradiation-Produced Defect Aggregates"; *Advances in Colloid and Interface Science*, 10, pp. 33-71.

Worthy, Ward (1978), "Versatile Microporous Polymers Developed," *C&NE*, Dec. 11, 1978, p. 23-24.

Youn, J.R. and Suh, N.P. (1985), "Processing of Microcellular Polyester Composites", *Polym. Compos.*, Vol. 6, No. 3, pp. 175-180.

Zeldovich, J.B. (1943), *Acta Physicochimica* U.R.S.S., 18, 1.